

DESIGNING AND OPTIMIZING
A BIOFILM EXPERIMENT
FOR SPACE FLIGHT

by

Starla G. Thornhill, B.S., M.S.

A dissertation submitted to the Graduate Council of
Texas State University in partial fulfillment
of the requirements for the degree of
Doctor of Philosophy
with a Major in Aquatic Resources and Integrative Biology
December 2020

Committee Members:

Robert J. C. McLean, Chair

Cheryl A. Nickerson

C. Mark Ott

David Rodriguez

Dana M. García

COPYRIGHT

by

Starla G. Thornhill

2020

FAIR USE AND AUTHOR'S PERMISSION STATEMENT

Fair Use

This work is protected by the Copyright Laws of the United States (Public Law 94-553, section 107). Consistent with fair use as defined in the Copyright Laws, brief quotations from this material are allowed with proper acknowledgement. Use of this material for financial gain without the author's express written permission is not allowed.

Duplication Permission

As the copyright holder of this work I, Starla G. Thornhill, refuse permission to copy in excess of the "Fair Use" exemption without my written permission.

ACKNOWLEDGEMENTS

First, I would like to thank my committee chair, Robert McLean, who brought me into his lab as a very timid undergraduate student and taught me how to be adventurous in my research (and tried very hard to teach me to be “diplomatic”). I would also like to thank Cheryl Nickerson for serving on my committee and always showing so much faith in my work. I would like to thank Mark Ott for serving on my committee and giving me very excellent advice for building my career after graduate school. I also thank David Rodriguez and Dana García for serving on my committee and offering great advice over the years.

The research presented in this dissertation is the result of a massively collaborative effort between Texas State University and Arizona State University. I would especially like to thank Jiseon Yang, whom I worked with extensively over the past four years while planning and optimizing the entire space flight experiment over countless emails, video chats, and phone calls. I would like to thank Sandhya Gangaraju for her help with confocal and scanning electron microscopy, as well as for her constant positivity and excellent job search advice. I would also like to thank Jenn Barrila for her advice in navigating the particulars of flight experiment planning (and NASA paperwork!) and Rich Davis for coordinating logistics.

For their work in producing the flight hardware, I would like to thank Louis Stodieck, Matt Vellone, and Shankini Doraisingam at BioServe Space Technologies (Boulder, CO), and Sid Gorti and Louise Strutzenberg at NASA MSFC (Huntsville, AL).

From Texas State University, I would like to thank Manish Kumar for his invaluable expertise in lambda red recombination. I would also like to thank Alissa Savage and Casey Smith for technical assistance with confocal microscopy and electron microscopy.

I extend my gratitude to the current, past, and honorary members of the Slime Gang. Julia Widmer, Shelbie Powers, and Calvin Tran: You guys have made the last year of my degree entirely too much fun. Quentin DiPasquale, Sahar Kianersi, and Kerri White, thank you for the many drinks, dinners, and hours of deep (and sometimes shallow) conversations. Thanks to Candace Longoria, Avry Howell, Sara Hall, and Mark Holliday, who were there at the beginning of my graduate school journey. I also want to thank Mara Cabungcal, Natalie Flygare, Erin Brown, Mark Faulkner, James McClellan, Eric Castro, Tian Lewis: Hailey Willey, Foster Ogu, and Isidoro Martinez.

From my cohort, I would like to thank Spandana Vemulapally, who was the best roommate I've ever had, Seif Tekaya, Trina Guerra, Stephanie Nordmeyer, Rebecca Kilgore, Phuong Le, Jared Hewitt, Emely Wiebe, Stephen Harding, and Carlos Baca.

This work was supported by NASA [Grant NNX17AC79G]. The confocal microscope was purchased with funds from NSF MRI grant DBI-0821252 awarded to Joseph R. Koke and Dana M. García (Texas State University). The Nanodrop 100 was purchased with funds from NSF grant IOB-0615762 awarded to Dana M. García and matching funds from the Department of Biology at Texas State University.

TABLE OF CONTENTS

	Page
ACKNOWLEDGEMENTS	iv
LIST OF TABLES	viii
LIST OF FIGURES	ix
LIST OF ABBREVIATIONS	xi
ABSTRACT	xiii
CHAPTER	
I. BACKGROUND.....	1
Biofilms in the Environment	1
Problems Associated with Biofilms in Water Systems	2
Life Support on ISS	3
Mechanosensing in Microgravity	4
Modeling Microgravity in a Full-Gravity Environment.....	9
Bacterial Growth, Gene Expression, and Biofilms in Microgravity and Modeled Microgravity	10
Investigating Biofilm Growth, Control, and Corrosion in Space Flight ...	13
II. OPTIMIZING THE IN-FLIGHT PARAMETERS OF THE SPACE FLIGHT EXPERIMENT.....	15
Culture Conditions.....	15
<i>E. coli</i> and <i>P. aeruginosa</i> Strains	16
<i>mCherry</i> Insertion.....	22
Media Selection	28
mAUM Optimization for Long-Term Stability	30
Silver Fluoride Bioavailability	35
Bacterial Cell Viability with Silver Fluoride.....	36
Frozen Inoculum Stability	41
Flight Hardware and 316L Stainless Steel Coupons	45
Fixation in Paraformaldehyde	52
RNA Preservation for Transcriptomics	54

Biofilm Matrix Staining	54
Experimental Timeline	57
Statistical Analysis and Graphing	59
Conclusion	60
III. GROUND-BASED BASELINE OF LONG-TERM DISINFECTION OF BIOFILMS BY SILVER FLUORIDE	62
Materials and Methods	64
Overview	64
Bacterial Culture in BioCells.....	64
E-SEM	65
Results and Discussion	66
Characterization of Long-Term Biofilm Growth in BioCells	66
Mixed Culture Biofilm Growth with Silver	72
IV. CORROSION.....	77
Materials and Methods	78
Sample Preparation.....	78
Coverage Analysis.....	78
Results and Discussion	79
V. EXPERIMENTAL VERIFICATION TEST AND CONCLUSIONS	87
REFERENCES	92

LIST OF TABLES

Table	Page
1. Summary of strains used in this study	18
2. Summary of characterization tests for each strain of <i>E. coli</i> and <i>P. aeruginosa</i> PAO1+ <i>gfp</i>	20
3. Summary of plasmids used to generate <i>E. coli</i> F11 $\Delta lacZ(453-660)::P_{proDmCherry-FRT}$	25
4. Primers used to produce <i>E. coli</i> F11 $\Delta lacZ(453-660)::P_{proDmCherry-FRT}$	26
5. mAUM formulation (34) and comparison to astronaut urine ersatz formulation	29
6. mAUM formulation	31
7. mAUM.v3 formulation and comparison to the NASA urine ersatz formulation	32
8. Linear regression of pH change over time in mAUM	34
9. Linear regression of corrosion measurements	86

LIST OF FIGURES

Figure	Page
1. The five stages of biofilm formation	1
2. Schematic of anodic and cathodic reactions in microbiologically influenced corrosion by biofilms.....	3
3. Catch-bond model for bacterial mechanosensing of shear forces	6
4. Proposed mechanisms for fluid shear detection by Gram-negative bacteria.....	8
5. Operation orientation of the RWV bioreactor system	9
6. Biofilm clogging on the ISS	12
7. Verification and optimization of selective antibiotic concentrations for isolation of individual species after mixed culture growth.....	19
8. <i>E. coli</i> survival in co-culture with <i>P. aeruginosa</i>	22
9. Insertion of <i>proD-mCherry</i> into the <i>E. coli</i> F11 chromosome	27
10. Growth analysis to determine pleiotropic effect of <i>mCherry</i> insertion.....	28
11. Stability of pH of different formulations of mAUM	33
12. Urea stability in mAUM.v3 for 96 days	35
13. Silver stability in mAUM	36
14. Effect of ionic silver on cell viability of mixed-culture planktonic and biofilm culture	40
15. Frozen inoculum stability after storage at -80°C	45
16. BioCell hardware.....	46
17. Stainless steel coupon geometry.....	48

18. Stainless steel coupon cleaning effectiveness	50
19. P-HAB and plate holder hardware	51
20. Fluorescence detection after fixing with PFA	53
21. Biofilm matrix staining.....	57
22. Biofilm survival on stainless steel in the BioCell	58
23. Inoculation and fixing timeline for the flight experiment	59
24. Post-flight analysis pathway.....	61
25. Mixed-culture biofilm growth in mAUM.....	68
26. <i>P. aeruginosa</i> (green) cell elongation was seen in P-HAB-incubated BioCells, but not in foil-wrapped BioCells	70
27. Mixed culture biofilm growth in mAUM with Ag ¹⁺	74
28. Effect of long-term treatment with 400 ppb AgF on phenotype	75
29. Corrosion on 316L stainless steel in A) inoculated and B) uninoculated mAUM.....	80
30. Corrosion on 316L stainless steel in A) inoculated and B) uninoculated mAUM with 400 ppb AgF disinfection treatment.....	81
31. BioCell temperatures	82
32. Coverage and quantity of corrosion spots on 316L stainless steel.....	85

LIST OF ABBREVIATIONS

Abbreviation	Description
ConA	Concanavalin A
D-PBS	Dulbecco's PBS
E-SEM	Environmental SEM
ECLSS	Environmental Control and Life Support System
ECM	Extracellular matrix
EDS	Electron dispersive spectroscopy
EMB	Eosin methylene blue agar
EPS	Extracellular polysaccharide
EVT	Experimental Verification Test
FEP	Fluorinated ethylene polypropylene
FM	Freezing media
FRT	Flp recombinase target
GFP	Green fluorescent protein
HFS	High fluid shear
ISS	International Space Station
KB	Kirby-Bauer
LB	Luria-Bertani
LFS	Low fluid shear

LMM	Light Microscopy Module
LSMMG	Low shear modeled microgravity
MAC	MacConkey's agar
mAUM	Modified artificial urine media
MIC	Microbiologically influenced corrosion
P-HAB	Plate Habitat
PBS	Phosphate buffered saline
PFA	Paraformaldehyde
ppb	Parts per billion
RPM	Rotations per minute
RWV	Rotating wall vessel
SEM	Scanning electron microscopy
SIM	Sulfide indole motility
SRV-K	Russian water recovery system
UTI	Urinary tract infection
WRS	Water recovery system

ABSTRACT

The International Space Station (ISS) is a built environment that has been continuously inhabited since November 2000. Living with the crew are the microorganisms carried to the ISS as normal astronaut flora and by accidental introduction in supplies. Microorganisms have established biofilms in the water recovery system (WRS) that recycles urine to provide drinking water to the ISS crew. Biofilms in the WRS can serve as a reservoir for opportunistic pathogens, including *Escherichia coli* and *Pseudomonas aeruginosa*, and can also induce clogs and corrosion damage on stainless-steel components. To investigate biofilm formation, silver disinfection susceptibility, and potential microbial corrosion in space flight, an experiment will be launched to the ISS on SpaceX-21 in December 2020. To model biofouling in the WRS, mixed-species biofilms of *E. coli* and *P. aeruginosa* will be cultured in artificial urine on 316L grade stainless-steel using a specialized BioCell apparatus. Flight samples will be compared to simultaneously tested ground (full gravity) controls. This research describes the design and optimization of the flight experiment, BioCell, ground-based silver disinfection capability, and data collection and analysis pathways for post-flight corrosion analysis. Analysis of pre-flight experiments shows a differential response to long-term silver disinfection treatment and suggests that corrosion on stainless steel could be the result of electrochemical processes, which may be exacerbated by silver fluoride treatment. Characterizing the microbial response to silver disinfection in flight will allow for a better understanding of the growth and treatment of biofilms on ISS.

I. BACKGROUND

Biofilms in the Environment

Bacterial cells in the environment are typically present as biofilms: surface-associated, mixed species communities of microbes surrounded by a “slimy” extracellular matrix (ECM) (1). The life cycle of a typical biofilm occurs in five stages (2). In the first stage, free-living planktonic cells discover and reversibly attach to a suitable surface. In the second phase, the bacterial cells produce attachment pili and begin to secrete extracellular polymeric substances (EPS). EPS is a mix of polysaccharides, extracellular DNA, secreted proteins, and other compounds that provide structural support and protection from environmental stressors. Stages three and four involve the development of the internal structure of the biofilm. The final phase is dispersion. Bacterial cells are released from the biofilm and begin to exhibit planktonic characteristics (2, 3). This information is summarized in **Figure 1** (2).

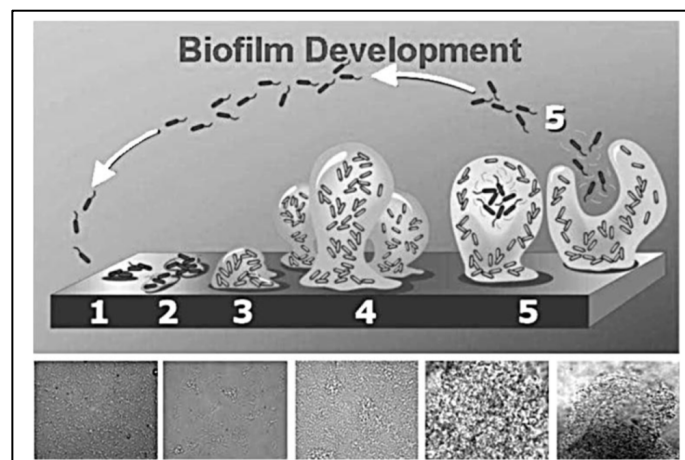


Figure 1. The five stages of biofilm formation. 1-Reversible attachment; 2-Irreversible attachment; 3-Maturation I; 4- Maturation II; 5- Release. Reprinted with permission from Stoodley et al. 2002, *Annu Rev Microbiol* 56:187-209.

Growth in a biofilm is beneficial to bacteria. Bacterial cells in a biofilm are extremely resistant to a multitude of environmental stressors, including pH extremes, treatment with disinfectants and surfactants, osmotic pressure, and heavy metals (3–7). Growth in biofilms also allows for sequestration of nutrients, which travel through the biofilm in structures called interstitial voids, or water channels (3, 8). These interstitial voids separate microcolonies, which are localized areas of bacterial replication within the biofilm (2, 8).

Problems Associated with Biofilms in Water Systems

Biofilms can cause microbially induced corrosion (MIC) (6, 9–13) even in metals that are considered to be corrosion resistant, such as stainless-steel or aluminum (9, 14). Acids secreted as a byproduct of normal microbial metabolism are trapped between the biofilm and the stainless-steel surface (9). Oxygen at the base of the biofilm is used up quickly, resulting in a difference in oxygen concentration between the anaerobic area beneath the biofilm and the surrounding environment (9). The difference in oxygen concentration creates a potential difference across the surface of the stainless steel, inducing movement of electrons in the stainless-steel surface from under the biofilm into the surrounding oxygen-exposed stainless steel (9). The movement of electrons allows positively charged metal ions to be dissolved into the biofilm, causing localized pitting in the steel beneath the biofilm (**Figure 2**) (9). Pitting increases bacterial adhesion, which in turn leads to a further increase in pitting (12). Leached metal ions, like iron, are utilized by bacteria in metabolic pathways (9, 10, 14).

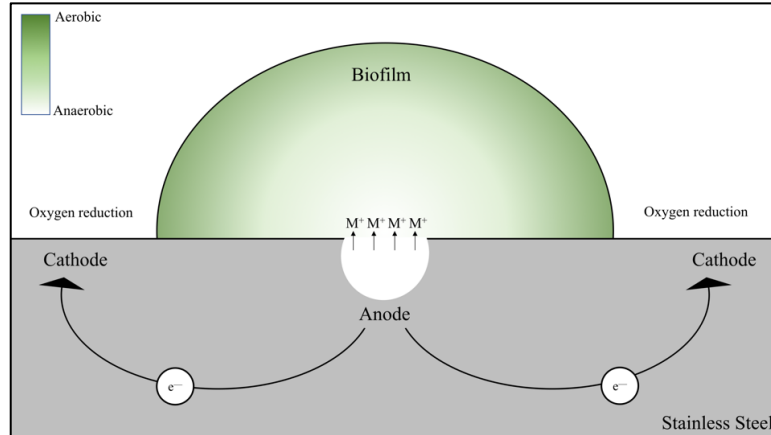


Figure 2. Schematic of anodic and cathodic reactions in microbiologically influenced corrosion by biofilms. Redrawn from Chaitra, 2017, Chapter 1, p. 5.

Life Support on the ISS

Transport of materials, including drinking water, to the International Space Station (ISS) is expensive, costing on average \$10,000 per pound of payload (15). The ISS is equipped with two water filtration systems that utilize physical and chemical purification methods to produce drinking water from astronaut-produced urine and ambient humidity waste products. The Russian water recovery system (SRV-K) is equipped on the Zvezda module, and the water recovery system (WRS) in the American Environmental Control and Life Support Systems (ECLSS) is equipped on the Tranquility module (16). In addition to purifying drinking water, ECLSS also controls temperature, humidity, maintains the atmosphere, and is equipped with a fire detection and suppression system (17). The SRV-K provides water for a crew of three, and currently serves as the back-up filtration system (16). ECLSS-WRS provides support for a crew of four (17).

In ECLSS-WRS, the physical methods of purification include filters and temperature changes (16, 18). Chemical methods include ion exchange chromatography,

catalytic oxidation, and iodine sterilization (17). While the current purification protocol is generally effective, the use of iodine poses a health risk to astronauts stationed on ISS, as prolonged exposure can induce hypothyroidism and sensitivity reactions (19). Therefore, additional steps to remove iodine are necessary (16). In the SRV-K, ionic silver is used to inhibit microbial growth (20). Of significance, a persistent biofilm has formed in the WRS (21–23). This necessitates a deeper understanding of biofilms in space, as well as an investigation into methods of biofilm sterilization that are safe for use in a semi-closed system. Since silver is already approved for use on the ISS, NASA has expressed interest in using silver-based disinfection in future long-term manned space flight missions (18, 24). Additionally, silver toxicity in humans is low (25, 26), with fewer adverse reactions than iodine, and silver has long been known to be effective as an antimicrobial (18, 26–29).

Mechanosensing in Microgravity

The ISS is a built environment that orbits Earth in the low Earth orbit (15), and therefore experiences 90% of the Earth’s gravitational pull. The low-gravity environment on ISS is the result of constant free fall at terminal velocity, which creates the perception of weightlessness, termed “microgravity.” In microgravity, fluid quiescence results in reduced mass diffusion, absence of particle settling, and low fluid shear (30). Low fluid shear (LFS) may be one cause of changes seen in the growth profile of several species of bacteria. Some species have shown a faster growth rate and increase in final cell density in space flight, including *E. coli* (31–33), *P. aeruginosa* (34, 35), and *Bacillus subtilis* (36), while others show reduced growth rate and final cell density, including *Staphylococcus epidermidis* (37), and *Bacillus cereus* (38).

Mechanosensing is the method by which organisms detect mechanical stimuli from the environment and translate it into a biological response. Bacteria use mechanosensing to regulate various functions, including osmoregulation (39–41), adhesion (42, 43), biofilm initiation (44) and matrix production (45). One force detected by mechanosensing is fluid shear, which is the friction generated when fluid flows over a surface or another fluid of a different density. As described earlier, LFS is seen in microgravity as a result of fluid quiescence, but it is also associated with laminar flow (46). Three models have been proposed to describe how bacteria may detect changes in shear forces (47). One model, called the “catch-bond” model, proposes that bacterial cells express surface molecules featuring hydrogen atoms that form hydrogen bonds when environmental shear forces are low (**Figure 3**). When the hydrogen bonds are intact, the cell signals LFS-associated pathway activation. High fluid shear (HFS) forces, such as those generated by turbulent flow, cause the hydrogen bond to break, initiating the signaling pathway that leads to HFS-associated pathway activation (42, 47).

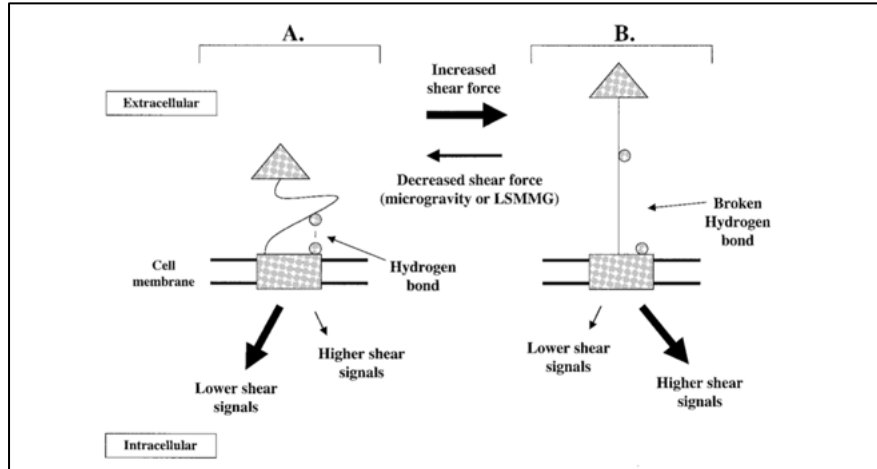


Figure 3. Catch-bond model for bacterial mechanosensing of shear forces. In LFS induced by microgravity or low shear modeled microgravity (LSMMG) (A), shear-sensing cell surface molecules are “folded”, with hydrogen bonds intact, which may trigger LFS associated signaling and pathways. In HFS (B), shear forces induce breakage of the hydrogen bond, signaling the activation of HFS-associated pathways. Reprinted with permission from Nickerson et al., 2004, *Microbiol Mol Biol Rev*, 68(2):345-361.

Other models of bacterial mechanosensing describe detection of changes in fluid shear forces by tension and deformations in the cellular membrane using two mechanisms: mechanically gated channel proteins (48, 49) and cytoskeletal stretching (47, 50). There are two families of mechanically gated channel proteins, MscL and MscS, which are found in bacteria as well as eukaryotes and archaea (51). These mechanosensitive ion channel (MSC) protein families have been shown to be controlled by tension, often induced by turgor pressure, and deformation in the lipid bilayer of the cellular membrane (52, 53), which may be induced by fluid shear stress (41, 54). In LFS conditions, the tension in the cellular membrane is below the tension threshold required to open the MSC proteins, thus they are closed (**Figure 4, (a)**) (41). In this condition, LFS-associated signaling pathways may be activated (**b**). When HFS force is applied, membrane tension, and possibly deformation, increases in the cellular membrane to

above the tension threshold **(c)** (41). Tension-induced pulling on the lipid bilayer around the MSC opens the channel **(d)** (52, 53), allowing non-specific transport of ions between the cell and the outside environment **(e)** (55), and may activate HFS-associated signaling pathways **(f)**. The activation of HFS-associated signaling pathways may be due to either the sudden change in the concentration of ions or due to energy released by the physical breaking of hydrogen bonds when the MSC is opened (56, 57).

The bacterial cytoskeleton may also play a role in sensing changes in fluid shear force. Eukaryotic cells have been shown to sense distortions in the cellular membrane by detecting changes in tension in the cytoskeleton and to respond to these changes by altering activation of signaling pathways, gene expression, and metabolic activity (50, 58). In bacteria, the cell is hypothesized to respond to cytoskeletal tension in the same way (47), although experimental evidence of such a response has not yet been reported in the literature. One of the major components of the eukaryotic cytoskeleton is actin. Many bacteria produce actin-like proteins, such as MreB (found in rod-shaped bacteria) (59–61) and FtsZ (62–64), which carry out functions attributed to the cytoskeleton, including determining bacterial cell shape (59, 65–67), spatially organizing the interior of the bacterial cell (68, 69), and playing key roles in bacterial cell division (60, 61, 65, 70, 71). **Figure 4** (right) illustrates a potential mechanism by which bacterial cytoskeletal tension may induce a response to external fluid shear forces. In LFS, the absence of fluid shear-induced tension and deformation on the bacterial cellular membrane may cause the cytoskeleton to only experience the tension required to maintain the bacterial cell shape (**Figure 4, (g)**) (41). In this state, the bacterial cell may activate LFS-associated pathways. In HFS, cellular membrane or wall tension or deformation **(h)** may cause

stretching of, or tension in, the cytoskeleton (i), although experimental evidence is not yet reported in the literature. The resulting tension in the cytoskeleton may activate HFS-associated pathways (j).

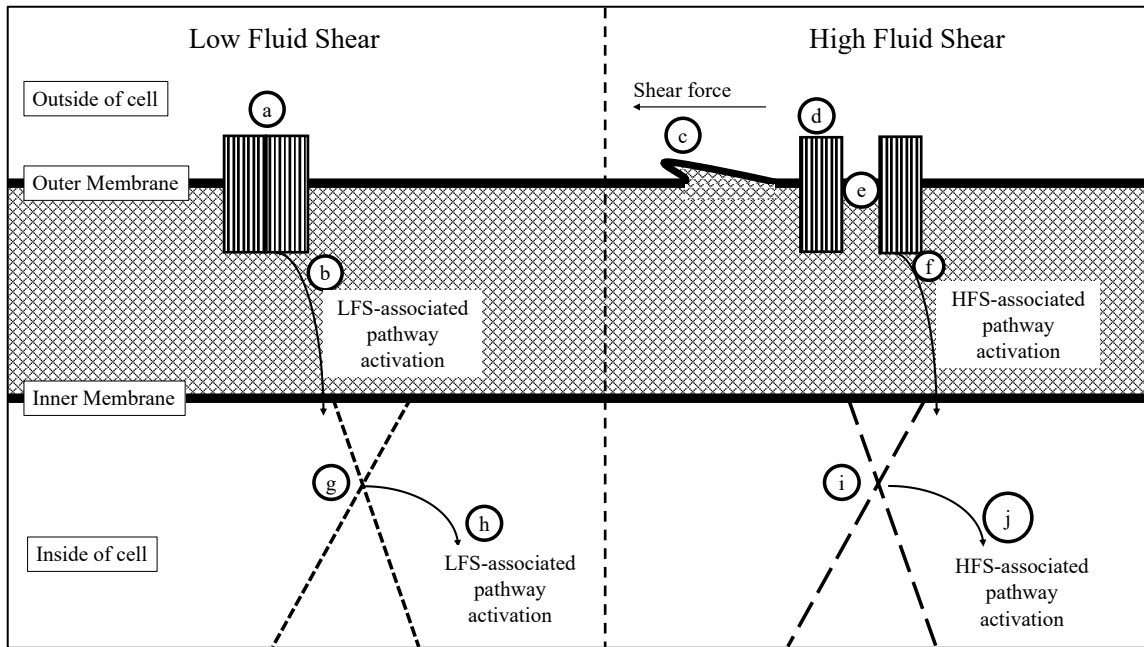


Figure 4. Proposed mechanisms for fluid shear detection by Gram-negative bacteria. MSC proteins (**top**) and cytoskeletal tension (**bottom**) may sense changes in external fluid shear forces. Top: In LFS (**left**), bacterial cell membrane tension is relatively low and MSC proteins are closed (**a**), which may lead to activation of LFS-associated pathways (**b**). In HFS (right), tension or deformation in the bacterial cellular membrane (**c**) can force MSC proteins open (**d**), allowing exchange of ions (**e**), which may activate HFS-associated pathways. Bottom: In LFS (**left**), the bacterial cytoskeleton is only experiencing the tension required to maintain the cell structure (**g**), which may result in LFS-associated pathway activation (**h**). In HFS (right), tension or deformation in the bacterial cellular membrane (**c**) may lead to increased tension in the bacterial cytoskeleton (**i**), activating HFS-associated pathways (**j**). The peptidoglycan-containing periplasmic space is indicated by cross hatch shading, the vertical line shading indicates MSC proteins, and the dashed lines indicate the cytoskeleton (small dashes indicate relaxed, long dashes indicate stretched).

Modeling Microgravity in a Full-Gravity Environment

To model the LFS environment present on the ISS, the Biotechnology Group at NASA Johnson Space Center developed a Rotating Wall Vessel (RWV) bioreactor system (46, 72, 73). The RWV models microgravity and establishes a low fluid shear environment by inducing laminar flow or near solid body rotation of the liquid inside the RWV when rotated at constant velocity in the low shear modeled microgravity (LSMMG) orientation (**Figure 5 Ai**) (46, 47, 74). To induce the LFS condition, the RWV must be filled completely (“zero airspace”) with culture media, as air bubbles can create turbulence and increase fluid shear (46).

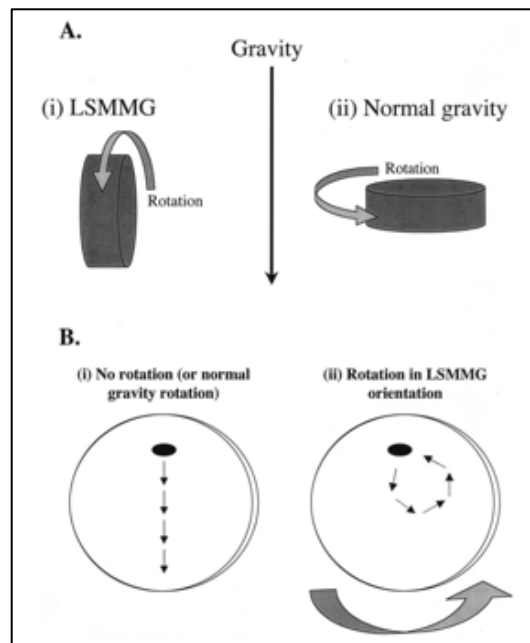


Figure 5. Operation orientation of the RWV bioreactor system. Rotation in LSMMG orientation (**Ai**) perpendicular to the direction of gravity establishes laminar flow within the bioreactor, allowing cells to reach terminal velocity as they fall through the liquid media (**Bii**). Rotation in the normal gravity orientation parallel to the direction of gravity (**Aii**) allows cells to sediment to the bottom of the bioreactor, which also occurs when the bioreactor in the LSMMG orientation is stopped (**Bi**). Reprinted with permission from Nickerson et al., 2004, *Microbiol Mol Rev* 68(2):345-361.

The RWV simulates microgravity when rotated in the LSMMG orientation (**Figure 5**). As the RWV rotates around an axis perpendicular to gravity (**Figure 5 Ai**), the gravitational vector inside the RWV is constantly being reoriented so that the time-averaged net gravitational vector on the cells is near to zero, preventing cell sedimentation (**Figure 5 Bii**) (74). Cells suspended in the RWV are in constant fall at terminal velocity and experience functional weightlessness, where there is a perception of the absence of gravity, although the entire RWV is still experiencing normal gravity (74, 75). The rate of rotation that is required to suspend objects in LSMMG is related to the size and density of the particles inside the RWV (72). The density of particles in the RWV must be equal, or nearly equal, to the density of the liquid media in order to prevent sedimentation of cells (46).

Changing the axis around which the RWV rotates to be parallel to the gravitational vector, or stopping the rotation while keeping the RWV in the LSMMG orientation, can be used as a normal gravity control (**Figure 5 Bii**) (47). The normal gravity control allows cells to sediment on the lowest point of the RWV in the direction of the gravitational vector (47, 75).

Bacterial Growth, Gene Expression, and Biofilms in Microgravity and Modeled

Microgravity

Bacterial growth in LFS has been associated with changes to secondary metabolite production (76–78), growth kinetics (32, 35, 36, 79–82), and gene expression profiles (79–87). Changes to bacterial growth kinetics in space flight and LSMMG vary by species. As described earlier, some species have shown a faster growth rate and increase in final cell density in space flight, including *E. coli* (31–33), *P. aeruginosa* (34,

35), while others show reduced growth rate and final cell density, including *Staphylococcus epidermidis* (37), *Bacillus cereus* (38), and *Staphylococcus aureus* (88). One study found that *P. aeruginosa* final cell density in space flight, but not on Earth, was increased when phosphate and oxygen availability were reduced, suggesting that fluid quiescence may improve *P. aeruginosa* growth in nutrient-limited environments (35). Another phenotype altered in space flight or in LSMMG included a change in virulence, which has been shown to be increased in *Salmonella enterica* serovar Typhimurium (82, 89, 90) and decreased in *S. aureus* (88, 91), *Listeria monocytogenes* (91), and *E. faecalis* (91). Increased antibiotic resistance has also been observed in some species (33, 85), but not in others (81, 92, 93).

Sigma factor AlgU, which regulates expression of genes related to motility, chemotaxis, and stress response genes in *Pseudomonas aeruginosa*, was found to be upregulated when *P. aeruginosa* was cultured in both in space flight and in LSMMG (94). Also seen with upregulation of AlgU is an upregulation of genes controlled by AlgU (94). In *S. Typhimurium*, the global regulator *hfq* is downregulated in space flight and LSMMG conditions as compared to appropriate controls; *hfq* is a regulator protein for approximately 32% of genes found to be differentially expressed in space flight, including genes involved in stress response, biofilm formation, and iron storage and utilization (82). The *hfq* gene is also differentially expressed in *P. aeruginosa* in space flight (94), and in *Staphylococcus aureus* (88) and *Vibrio fischerii* (95) in LSMMG. A meta-analysis of transcriptome profiles of *P. aeruginosa* (83, 94) and *S. Typhimurium* (82, 96) has shown that multiple pathways involved in metabolism and cellular processes are differentially expressed in both space flight and LSMMG (97).

Previous research has shown that biofilms form in space flight and in LSMMG (34, 82, 88, 98, 99). Additionally, genes involved in biofilm formation in *E. coli* (80), *Klebsiella pneumoniae* (100), *S. Typhimurium* (82), and *B. subtilis* (101) are also upregulated in space flight. *P. aeruginosa* biofilms cultured in an artificial urine media in space flight have been shown to display column-and-canopy structures that are not seen in control biofilms which were grown on Earth (34). *E. coli* biofilms grown on glass beads in LSMMG are thicker and show increased resistance to salt stress, ethanol disinfection, and antibiotic resistance when compared to normal gravity controls (99).

Biofilms are problematic on the ISS. Bacterial cells growing in a biofilm are released as part of the normal biofilm cycle (**Figure 1**) (3). Biofilms also produce clogging of piping and pathways in both SRV-K (**Figure 6 A**) and WRS (**Figure 6 B**) on the ISS (102). As clean water moves through ECLSS, bacterial cells are released from the persistent biofilm and are consumed by astronauts who already have a reduced immune response (82). Combined with the reduced immune response in astronauts, calcium loss in bones from space flight (15) may increase risk of urinary tract infection (UTI).

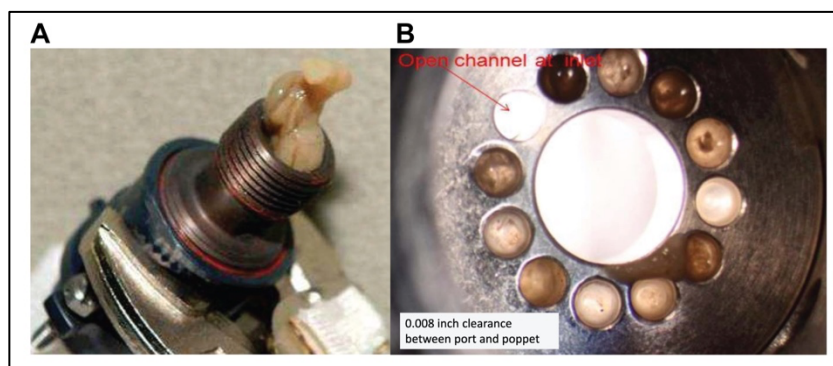


Figure 6. Biofilm clogging on the ISS. A) A biofilm which has clogged a hose in SRV-K. B) A biofilm which has clogged the inlet valve of the Mostly Liquid Separator of WRS. Both images reprinted from Carter, 2017, NASA Report M17-6276.

Investigating Biofilm Growth, Control, and Corrosion in Space Flight

To investigate biofilm growth, efficacy of silver-based disinfection in treating biofilms, and associated microbially-induced corrosion of 316L grade stainless steel in space flight, an experiment will be launched to the ISS on SpaceX 21, a 35-day mission which is currently scheduled to launch in December 2020. In this experiment, mixed-species biofilms of *E. coli* and *P. aeruginosa* will be cultured in an artificial urine growth medium with 316L grade stainless steel as a biofilm attachment substrate. We have chosen 316L stainless steel with a 2B brushed finish as this is the grade which is used in stainless steel components of WRS on the ISS (16, 103). Artificial urine, which is formulated to match astronaut urine in wastewater streams on the ISS (104), will be used as growth medium. The flight experiment aims to 1) characterize *E. coli* and *P. aeruginosa* mixed-species biofilm growth on stainless steel in space flight; 2) characterize the mixed-species biofilm response to long-term silver disinfection in space flight; and 3) characterize microbially-induced corrosion on 316L stainless steel in space flight.

It is a rare opportunity to be able to send an experiment to the ISS. Extensive planning is required to ensure a successful experiment, since repeated attempts are unlikely to be approved, especially when a failed experiment is the result of poor planning. In this case, a well-planned experiment utilizes growth media and reagents which are stable for at least 45 days (35 days for the SpaceX 21 mission plus at least 10 days to accommodate sample launch and potential delays in the launch date), produces samples which are stable after fixing until they are returned and able to be processed, and minimizes the time spent needed for post-flight sample handling to prevent sample

degradation before all necessary data are collected. The research presented in this dissertation aims to meet those success requirements by 1) investigating and optimizing the key experimental parameters in ground-based pre-flight studies that need to be controlled in-flight; 2) identifying baselines for biofilm growth, disinfection, and corrosion; and 3) designing post-flight data collection and analysis methods to efficiently process time-sensitive samples.

II. OPTIMIZING THE IN-FLIGHT PARAMETERS OF THE SPACE FLIGHT EXPERIMENT

Resources for space flight experiments on the ISS are limited. The cost to send an experiment to space is high, and stowage space and crew time are valuable resources that must be considered; experiments cannot be repeated multiple times due to procedural or design errors. Many experiments on the ISS are performed by astronauts with varying backgrounds; therefore, methods must be clearly described and simple enough to be performed by someone who may not have expertise in biology. Designing an experiment for flight necessitates validating every reagent and experimental parameter on Earth before sending the experiment to space, as well as optimizing hardware compatibility and design, and incorporating engineering and safety considerations. As such, designing an experiment for space flight is necessarily interdisciplinary and requires extensive collaboration between a large team of scientists to achieve.

Culture Conditions

The strains used in this study were stored as freezer stocks at -80°C in 12.5% (v/v) glycerol, prepared by adding sterile glycerol to overnight broth culture of each strain. Prior to each experiment, the appropriate organism was pulled from -80°C storage and streaked onto LB agar plates, then incubated at 37°C for 24 hours. Starter cultures were inoculated from LB agar plates to modified artificial urine media (mAUM) and incubated at ambient temperature ($22-24^{\circ}\text{C}$) with gentle shaking in an orbital shaking platform (100 RPM) for 24-72h, until the culture reached stationary phase, unless otherwise indicated. Experimental cultures were inoculated from overnight cultures with a 1:100 dilution of overnight culture to mAUM unless otherwise specified.

E. coli and *P. aeruginosa* Strains

Pathogenic strains of *E. coli* and *P. aeruginosa* are known to cause UTIs (83, 105–107). In particular, *P. aeruginosa* has been identified as the source of a UTI contracted by an astronaut on Apollo 13 (108–110). Additionally, mixed culture interactions between *E. coli* and *P. aeruginosa* have been previously studied. *E. coli* produces indole, a tryptophan derivative that serves a variety of functions including reducing biofilm formation (111) and providing a competitive advantage in mixed culture with *P. aeruginosa* (112). Indole secreted by *E. coli* in co-culture with *P. aeruginosa* has been reported to inhibit *P. aeruginosa* quorum signaling, reducing production of the antimicrobial pyocyanin. When less pyocyanin is present in the environment, *E. coli* survival in mixed culture is enhanced (112).

P. aeruginosa PAO1 was selected because it is a common strain that has been previously studied in pure culture in LSMMG and in space flight (83, 94, 98). *P. aeruginosa* PAO1 was derived from an opportunistic pathogen, PAO, which was isolated from a wound in an Australian patient (113) and has since been used in laboratories worldwide to study a variety of infections, including UTIs (114, 115), wound infections (116–118), and lung infections (119–121). Additionally, a strain of *P. aeruginosa* PAO1 containing a random chromosomal insert of constitutively expressed *gfp* was available; the modified strain was found to have no change in biofilm formation as a result of the *gfp* insertion (122). GFP-tagging allows for detection of *P. aeruginosa* with confocal and epifluorescence microscopes using EGFP filter sets (488 nm excitation). The selected *E. coli* strain (discussed below) was transformed to express *mCherry* from a chromosomal insert. mCherry can be detected using Texas Red filter sets (559 nm excitation) and

allows for detection of *E. coli* as well as differentiation from GFP-tagged *P. aeruginosa*.

Ten clinical UTI isolates were assessed to determine which strain would be optimal to investigate in mixed culture with *P. aeruginosa* PAO1 (**Table 1**). Since some of the available *E. coli* strains were clinical isolates that have not been published, a simple characterization of all of the strains was performed. Indole production was tested using sulfide indole motility (SIM) agar and Kovac's reagent, and lactose metabolism was tested using MacConkey agar (MAC) and eosin methylene blue agar (EMB). To enable separation and quantification *E. coli* and *P. aeruginosa* after mixed culture growth, antibiotic susceptibility was tested using Kirby-Bauer (KB) antibiotic testing on Mueller-Hinton (MH) agar using pre-made antibiotic disks (BD BBL Sensi-Disc test discs). Antibiotic susceptibility was also tested by streaking each strain onto a LB agar with various antibiotics. The results of these tests are summarized in **Table 2**. The optimal antibiotics for strain isolation were cefsulodin (112), to which all *E. coli* strains were resistant, and nalidixic acid, to which *P. aeruginosa* is resistant (**Table 2**). The standard cefsulodin concentration of 25 µg/mL (112) was shown to inhibit *P. aeruginosa* without killing *E. coli* (**Figure 7 A**). The nalidixic acid concentration was optimized to 10 µg/mL, which is the concentration that allowed *P. aeruginosa* growth (**Figure 7 B**), but inhibited *E. coli* (**Figure 7 C**). Additionally, since future experiments will involve gene insertion and transcriptomic analysis, sequence availability for each strain was determined. Moving forward, only strains that were fully sequenced (536, CFT073, and F11) were considered.

Table 1. Summary of strains used in this study.

Strain	Characteristic(s)	Reference
<i>E. coli</i>		
GR-12 ¹	Clinical UTI isolate, pyelonephritis	(123)
HU968-63 ¹	Clinical UTI isolate	
HU968-149 ¹	Clinical UTI isolate	
HU968-206 ¹	Clinical UTI isolate	
HU968-214 ¹	Clinical UTI isolate	
HU968-357 ¹	Clinical UTI isolate	(124)
J96 ¹	Clinical UTI isolate, pyelonephritis	(107)
F11 ²	Clinical UTI isolate, cystitis with bacteriuria	(125)
CFT073 ²	Clinical UTI isolate, pyelonephritis and sepsis	(126)
536 ²	Clinical UTI isolate, pyelonephritis	(127)
BW25141/pKD3 ³	Lambda Red Recombination genes <i>exo</i> , <i>bet</i> , <i>gam</i> on the pKD3 plasmid	(128)
MG1655/pDK46 ⁴	<i>cat</i> cassette on the pKD46 plasmid	(128)
MG1655/pCP20 ⁵	FLP recombinase on the pCP20 plasmid	(128)
Top10/pBT1-proD-mCherry ⁶	<i>mCherry</i> under control of an <i>E. coli</i> artificial constitutive promoter	
F11+mcherry	<i>mCherry</i> constitutive expression from the chromosome	This study
<i>P. aeruginosa</i>		
PAO1+gfp ⁷	<i>gfp</i> constitutive expression from the chromosome	(122)
<i>P. mirabilis</i>		
2573 (ATCC 49565)	Urea-metabolizing	(129)

¹Gift from R. Hull and S. I. Hull at Baylor College of Medicine; ²Gift from H. L. T. Mobley at University of Michigan. ³Obtained from the *E. coli* Genetic Stock Center. ⁴Gift from M. Whiteley at Georgia Institute of Technology. ⁵Gift from D. Siegele at Texas A&M University. ⁶Gift from M. Lynch (Addgene plasmid # 65823). ⁷Gift from M. Parsek at University of Washington.

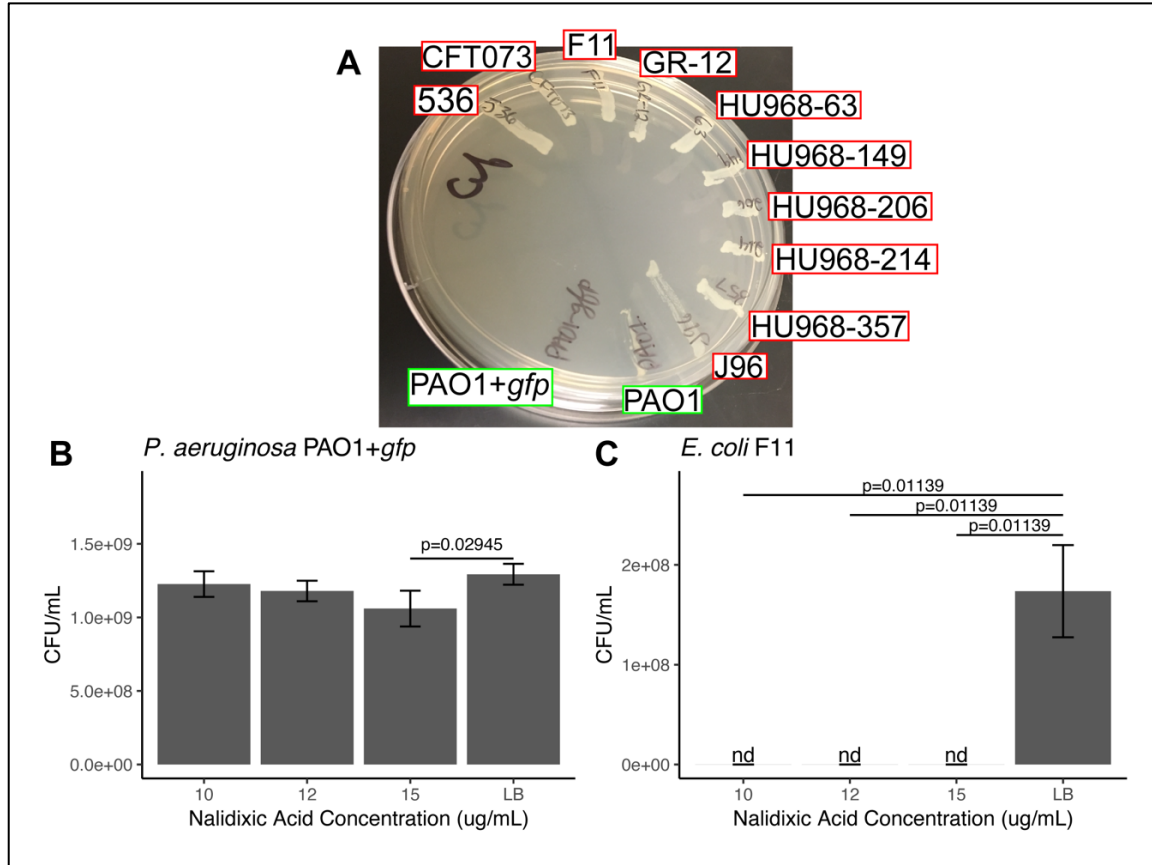


Figure 7. Verification and optimization of selective antibiotic concentrations for isolation of individual species after mixed culture growth. A) Growth of all strains of *E. coli* was permitted on LB+cefsulodin (25 $\mu\text{g}/\text{mL}$), but growth of *P. aeruginosa* PAO1+gfp was inhibited. B) *P. aeruginosa* survival was significantly reduced when plated on LB with 15 $\mu\text{g}/\text{mL}$ nalidixic acid (15 $\mu\text{g}/\text{mL}$: $p = 0.02945$, $n=3$), but not when plated on LB with 12 $\mu\text{g}/\text{mL}$ or 10 $\mu\text{g}/\text{mL}$ nalidixic acid. C) *E. coli* growth was inhibited on LB with all concentrations of nalidixic acid ($p < 0.05$, $n = 3$). Error bars represent standard deviation. Welch's T-Test, 95% confidence interval.

Table 2. Summary of characterization tests for each strain of *E. coli* and *P. aeruginosa* PAO1+gfp. Metabolism tests: + indicates a positive reaction, ++ indicates a strong positive reaction on EMB, determined by a metallic green color change, and — indicates a negative reaction. Kirby-Bauer tests: TE30-tetracycline (38 µg); P10-penicillin (10 units); K30-kanamycin (30 µg); C30-chloramphenicol (30 µg); S10-streptomycin (10 µg); B10-bacitracin (10 units); AM10-ampicillin (10 µg). NS indicates not susceptible. Antibiotic streak tests: All antibiotics present in the indicated concentrations in LB agar. Nal-nalidixic acid; Cm-chloramphenicol; Cef-cefsulodin; Amp-ampicillin; Sm-streptomycin; Km-kanamycin. + indicates growth on the antibiotic, — indicates no growth. ** indicates optimal antibiotic selection for isolation of any *E. coli* strain and *P. aeruginosa* PAO1+gfp.

Strain	Sequence available	Metabolism			Kirby-Bauer							Antibiotic streak					
		Indole	Mac	EMB	TE30	P10	K30	C30	S10	B10	AM10	Nal (15 µg/mL) **	Cm (25 µg/mL)	Cef (20 µg/mL) **	Amp (100 µg/mL)	Sm (50 µg/mL)	Km (30 µg/mL)
536	Yes	+	+	+	18	NS	20	25	NS	NS	15	—	—	+	+	+	—
CFT073	Yes	+	+	+	17	NS	19	22	18	NS	18	—	—	+	+	~	—
F11	Yes	+	+	++	15	NS	19	20	NS	NS	9	—	—	+	+	—	—
GR-12	No	+	+	+	18	NS	20	23	8	NS	NS	—	—	+	+	—	—
HU968-63	No	+	—	+	17	NS	19	26	20	NS	15	—	—	+	+	—	—
HU968-149	No	+	—	—	17	NS	19	19	15	NS	15	—	—	+	—	—	—
HU968-206	No	+	+	+	NS	NS	18	NS	8	NS	NS	—	+	+	+	—	—
HU968-214	No	+	+	+	NS	NS	15	NS	10	NS	NS	—	+	+	+	—	—
HU968-357	No	+	+	+	17.5	NS	18	23	11	NS	18	—	—	+	—	—	—
J96	No	+	—	+	20	NS	26	20	19	NS	16	—	—	+	—	—	—
<i>P. aeruginosa</i> PAO1+gfp	No	—	—	—	16	NS	10	NS	17	NS	NS	+	+	—	+	—	—

To determine the survivability of each sequenced *E. coli* strain against *P. aeruginosa* PAO1+*gfp*, 1×10^8 CFU/mL of each species was inoculated in co-culture in 50 mL LB or an artificial urine medium, then incubated at 37°C (LB) or 25°C (artificial urine) with shaking at 150 RPM for 24 hours. LB was used to determine survival at the optimal growth temperature for each species in a rich medium, and artificial urine was tested at 25°C, since this is the condition which will be used in the flight experiment. Bacterial cells were quantified by viable cell counting using serial dilution in phosphate buffered saline (PBS) (137 mM NaCl, 2.7 mM KCl, 10 mM Na₂HPO₄, 1.8 mM KH₂PO₄; pH 7.4), followed by spread plating onto LB and LB with selective antibiotics. *E. coli* was isolated using LB with cefsulodin (25 µg/mL), and *P. aeruginosa* was isolated using LB with nalidixic acid (10 µg/mL). Briefly, nalidixic acid antibiotic stocks were made at 100 mg/mL in 0.3 M NaOH, then filter sterilized, aliquoted, and stored at -20°C for a maximum of 3 months. Cefsulodin antibiotic stocks were made at 100 mg/mL in deionized water, then filter sterilized, aliquoted and stored in the dark in a non-frost-free freezer at -20°C for up to 6 months.

E. coli F11 showed the best survivability against *P. aeruginosa* PAO1+*gfp* (**Figure 8 A**) at 37°C in LB, as well as the highest reproducibility (**Figure 8 A, B**) in both LB (37°C) and mAUM (25°C). Therefore, *E. coli* F11 was selected as the strain to use in all subsequent experiments.

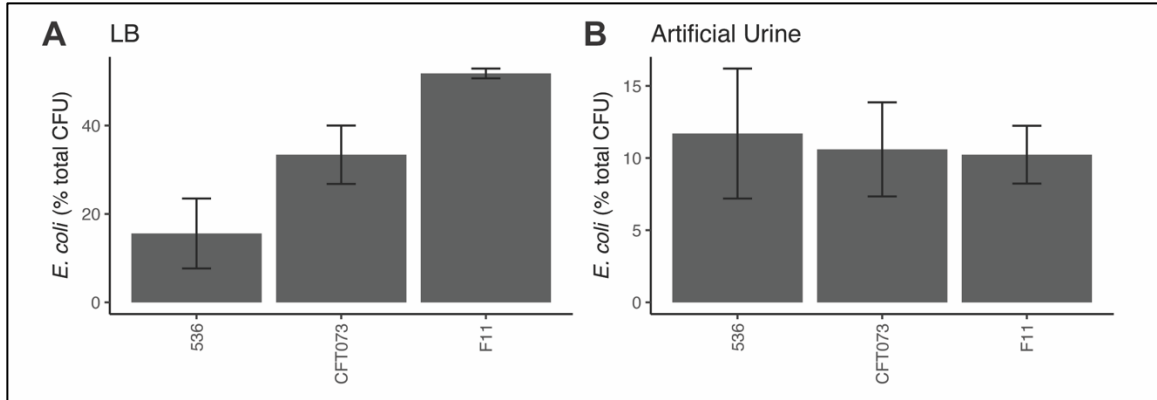


Figure 8. *E. coli* survival in co-culture with *P. aeruginosa*. A) Percentage of the total CFU in each culture that is *E. coli* at 24h of growth in LB at 37°C. B) Percentage of *E. coli* that comprises the total CFU/mL of cocultures grown in mAUM at 25°C, at 24h of growth. n=3, error bars represent standard deviation.

mCherry Insertion

To allow detection of, and differentiation from, *P. aeruginosa* under fluorescence light microscopy, *E. coli* F11 was transformed to express *mCherry* constitutively from a chromosomal insert. *mCherry*, under control of the *proD* promoter was inserted into *lacZ* on the *E. coli* F11 chromosome using lambda Red recombination (128). *proD* is an artificial *E. coli* promoter that enables constitutive expression (130). Chromosomal insertion of *mCherry* allows for retention of the *mCherry* gene without requiring selective pressure. Using *lacZ* as the insertion site allowed easy detection of proper transformants using blue/white screening.

The strains which carried the plasmids used here are described in **Table 1**. All plasmids (**Table 3**) were isolated using GeneJet Plasmid Miniprep Kit (Invitrogen K0503). All nucleic acid extractions were quantified using a Nanodrop 100 spectrophotometer (Thermo Fisher Scientific). All transformations were performed using electroporation. The chloramphenicol cassette was amplified from pKD3 using Phusion High-Fidelity DNA Polymerase (Thermo Fisher Scientific F530L) and primers that each

contained SacII restriction sites (**Figure 9 A, Table 4**). The PCR reaction was cleaned using GeneJet PCR purification kit (Thermo Scientific K0701). The chloramphenicol cassette PCR amplicon and extracted pBT1-*proD-mCherry* (1 µg each) were treated with SacII (New England BioLabs R0157S), then the chloramphenicol cassette was ligated into pBT1-*proD-mCherry* using T4 ligase with a 1:3 ratio of insert to vector. The resulting plasmid, pBT1-*proD-mCherry-FRT-cat-FRT* (**Figure 9 A**) was inserted to *E. coli* DH5α for amplification, then *proD-mcherry-FRT-cat-FRT* was amplified from *E. coli* DH5α using the Phusion High-Fidelity PCR Kit described above. *E. coli* F11 was transformed to carry pKD46, which provided the lambda Red recombination genes *exo*, *bet*, and *gam*. *E. coli* F11-pKD46 was grown in LB broth to an OD600 value of approximately 0.2. L-arabinose (2% w/v) was added to induce expression of lambda Red recombination genes, then the culture was grown to an OD600 of approximately 0.4. The resulting culture was induced for electroporation competency using 1% (v/v) glycerol. The *proD-mCherry-FRT-cat-FRT* PCR amplicon was inserted into *E. coli* F11+pKD46 using electroporation. The transformants were plated onto LB agar + chloramphenicol (25 µg/mL) + X-gal (20 µg/mL) to select for recombinants. Colonies that grew white on X-gal with chloramphenicol were imaged using confocal microscopy to confirm expression of mCherry, which was seen in the transformed strain (**Figure 9 B, right**), but not the parent strain (**Figure 9 B, left**).

pCP20, which contained FLP recombinase, was transformed into *E. coli* F11 *lacZ*/*mCherry-cat*⁺ to induce recombination of the FRT sites, removing *cat* and leaving a small FRT scar (**Figure 9 A**). PCR using primers targeting regions of *lacZ* which flanked the insertion site (**Table 4, Figure 9 A**) was used to confirm correct insertion of *mCherry*

and subsequent removal of *cat*. Gel electrophoresis showed that the size of the PCR amplicon had increased from 381 bp to 1712 bp, which was consistent with *mCherry* insertion into the *lacZ* gene (**Figure 9 C**).

To check for pleiotropic effect, growth of *E. coli* F11 *lacZ/mCherry*⁺ was compared to the parent strain by generating growth curves in LB broth and mAUM (Figure 10) as previously described (131). Wells of a 96-well microtiter plate were filled with 198 μ L LB broth or mAUM, inoculated with 2 μ L of overnight culture, then incubated in a Biotek Powerwave-X2 plate reader at 37°C for 72 hours, with OD600 reads every 15 minutes. Both *E. coli* F11 (filled) and *E. coli* F11 *lacZ/mCherry*⁺ (empty) reached stationary phase at the same time and at the same optical density in both LB (black) and mAUM (red), indicating that there was no change in optical cell density as a result of the *mCherry* insertion (**Figure 10**). *E. coli* F11 *lacZ/mCherry*⁺ in mAUM shows a series of optical density readings of zero in the first several hours of growth. Failure to detect growth at early time points is sometimes seen when condensation forms on the lid of the microtiter dish during incubation, which causing similar readings between inoculated and uninoculated wells. When plotting OD600 generated growth curves, the optical density of uninoculated wells was subtracted from inoculated wells to control for optical density of the plastic and the medium. Condensation on the lid of the microtiter dish may have increased optical density readings, and since condensation on the lid is usually seen above all filled wells, subtracting the optical density of uninoculated wells from inoculated wells could have obscured changes in optical density which were related to bacterial cell growth. Thus, the zero readings at the early stages of the growth curve may represent an artifact of using OD600 readings as a measurement for cell growth.

Viable cell density of stationary phase *E. coli* F11 *lacZ/mCherry*⁺ in mAUM was also compared to the parent strain. Pure cultures of *E. coli* F11 (wt) and *E. coli* F11 *lacZ/mCherry*⁺ were inoculated into mAUM and incubated for 3 days at ambient temperature with gentle shaking (100 RPM). Viable cells were then enumerated using viable cell counting by serial dilution plating. *E. coli* F11 *lacZ/mCherry*⁺ (5.63 x 10⁸ CFU/mL; standard deviation: 0.758 x 10⁸ CFU/mL) showed no significant difference in viability from the parent strain (5.60 x 10⁸ CFU/mL; standard deviation: 0.930 x 10⁸ CFU/mL) (p = 0.9471, Welch's T-Test, n=6).

Table 3. Summary of plasmids used to generate *E. coli* F11 Δ *lacZ*(453-660)::*P_{proD}mCherry-FRT*.

Plasmid	Characteristic(s)	Source
pKD3	Chloramphenicol resistance gene flanked by FRT recombination sites, SacII restriction site	Datsenko and Wanner, 2000
pKD46	<i>exo</i> , <i>bet</i> , <i>gam</i> (lambda Red recombinase genes) under control of <i>araC</i> promoter, ampicillin resistance	Datsenko and Wanner, 2000
pCP20	Flp recombinase under control of heat inducible promoter, ampicillin resistance	Datsenko and Wanner, 2000
pBT1-proD-mCherry	proD constitutive promoter, mCherry insert, ampicillin resistance	Gift from Michael Lynch (Addgene plasmid # 65823)

Table 4. Primers used to produce *E. coli* F11 $\Delta lacZ(453-660)::P_{proDmCherry-FRT}$. Inserted SacII sequences are underlined, *lacZ* targeting recombination sequences are in bold.

Primer		Sequence (5' to 3')	Annealing Temperature (°C)	Size (bp)
<i>cat</i> cassette	Forward	GCT GAC ATG GGA ATT AGC <u>CGC</u> <u>GGT</u> CCA TA	65.5	1329
	Reverse	<u>ATG</u> CGA GAC <u>CGC</u> <u>GGA</u> ACT GCC A		
<i>mCherry</i> with <i>cat</i> cassette and flanking <i>FRT</i> regions	Forward	GGC AGG TCA GGC CAA TCC GCG CCG GAT GCG GTG TAT CGC TCG CTG AGA TAG GTG CCT CAC	56.6	2587
	Reverse	CGA CAT TGG CGT AAG TGA AGC GAC CCG CAT TGA CCC TAA CCT GTC CAT CAG CTT GTC CAG		
Flanking regions of the <i>lacZ</i> insertion site	Forward	CAG TTT ACC CGC TCT GAG ACC T	58.6	1217
	Reverse	TCA CAG ATG TGG ATT GGC GAT GAA A		

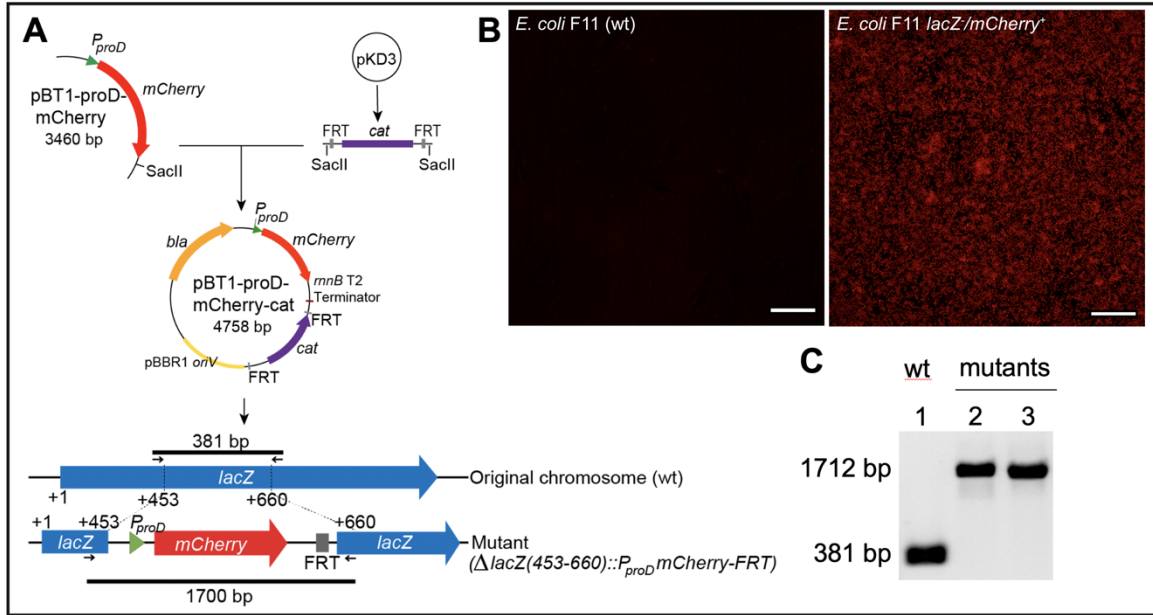


Figure 9. Insertion of *proD-mCherry* into the *E. coli* F11 chromosome. **A)** The schematic of lambda Red recombination to produce *E. coli* F11+*mCherry*. The *cat* cassette from pKD3 was inserted to pBT1-*proD-mCherry* using the unique *SacII* site downstream of the *mCherry* gene. *P_{proD}* with *mCherry* and the *cat* cassette were amplified from the plasmid using high fidelity PCR and inserted to the *E. coli* F11 *lacZ* gene in the bacterial chromosome. The *cat* cassette was removed from the bacterial chromosome using FLP recombinase. **B)** mCherry produced by *E. coli* F11 *lacZ/mCherry*⁺ was detected by confocal microscopy using a 559 nm laser but was not detected in the parent strain (left). Scale bars = 30 μm. **C)** Agarose gel electrophoresis in 0.8% agarose gel of whole cell PCR products obtained using primers targeting the flanking regions of *lacZ* showed insertion of *proD-mCherry* into the bacterial chromosome. Lane 1: *E. coli* F11 wild-type (WT) PCR product of 381 bp, indicating *lacZ* is intact. Lanes 2 and 3: the isogenic mutants of *E. coli* F11 *lacZ/mCherry*⁺. The band size of 1712 bp showed that *lacZ* had been disrupted.

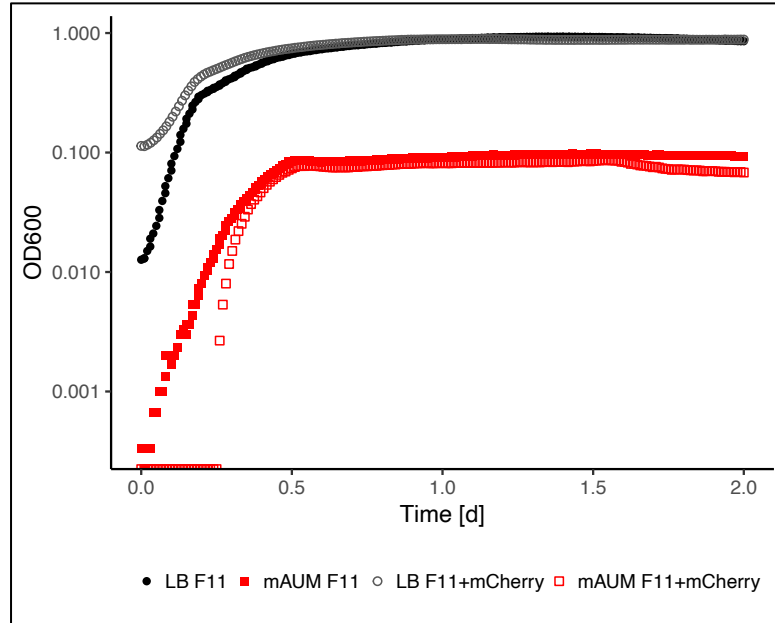


Figure 10. Growth analysis to determine pleiotropic effect of *mCherry* insertion. Growth in LB (circles, black) and mAUM (squares, red) of WT (filled) and transformed (empty) *E. coli* F11 reached stationary phase at the same time and at the same optical density when cultured in the same media.

Media Selection

In this research, *E. coli* and *P. aeruginosa* biofilms were cultured in mAUM, which was previously used by Kim *et al.* to investigate biofilm formation by *P. aeruginosa* in space flight (34). mAUM was selected for the flight experiment to model biofilm growth of pathogens in the WRS on ISS, which purifies astronaut waste, including urine, into potable water (16). Verostko *et al.* have described ersatz recipes which are designed to model various stages of the waste water stream as the water is purified in the WRS on ISS, including astronaut urine (104, 132). mAUM was compared to the urine ersatz formulation to ensure that mAUM is a reasonable model of astronaut urine (Table 5).

Table 5. mAUM formulation (34) and comparison to astronaut urine ersatz formulation (104).

Component	mAUM Formulation (mg/L)	Urine Ersatz Formulation (mg/L)
Ammonium ⁺⁺	452	50-631
Bicarbonate ⁻	1525	41-757
Calcium ⁺⁺	13.3	34-185
Chloride ⁻	3963	774-8301
Iron ⁺⁺	0.511	NA
Magnesium ⁺⁺	48.6	14-127
Nitrate ⁻	302.01	NA
Phosphate	347	155-4312
Potassium ⁺	211	238-2347
Sodium ⁺	4630	432-4002
Sulfate ⁻	1632	119-2111
Citric acid	420	77-679
Arginine	200	NA
Asparagine	57	45-132
Aspartic acid	20	NA
Cystine	50	2-6
Glutamic acid	20	40-155
Glycine	10	563-1802
Histidine	15	776-2327
Proline	40	NA
Isoleucine	50	NA
Leucine	50	26-101
Lysine	40	47-424
Methionine	15	NA
Phenylalanine	15	NA
Serine	30	210-730
Threonine	20	95-381
Tryptophan	5	NA
Tyrosine	23	NA
Valine	20	22-87
Urea	10220	10000-22857
Uric acid	67.2	NA
Creatine	918	NA
Creatinine	NA	533-1333
Taurine	NA	334-1614
L-Glutamine	293	438-1520
Alanine	NA	143-615
Carnosine	NA	36-283
D-glucuronic acid	NA	12-125
Phenol	NA	3-12
Citrulline	NA	<1-19
Bilirubin	NA	<1-30

mAUM Optimization for Long-Term Stability

mAUM was optimized to extend the shelf-life and allow for longer storage before inoculation. mAUM must be stable for at least 45 days (35 days for the SpaceX 21 mission plus 10 days to accommodate sample transit and potential launch delays). The buffer capacity of mAUM was increased by increasing the concentration of the phosphate buffer components, KH_2PO_4 and K_2HPO_4 , to 10 times their original concentration (**Table 6**). Other changes to the mAUM composition arose from a mistake in the recipe calculation that was discovered too late to be corrected. Longer media shelf-life increases flexibility for flight scheduling and on-board inoculations. The updated mAUM recipe, mAUM.v3, is reported in Table 6 (mAUM.v2 refers to a version of mAUM (34) from which L-glutamine was accidentally excluded). **Table 7** compares mAUM.v3 to NASA's urine ersatz formulation (104). In mAUM.v4, the amino acids from mAUM.v3 were removed to be used as a freezing buffer for the space flight bacterial inoculum. This change will be discussed in detail in the next section.

Table 6. mAUM formulation. mAUM describes the formulation as originally published (34). mAUM.v3 had been optimized for long-term stability, and mAUM.v4 is mAUM.v3 with the amino acids removed to be used as a freezing buffer for cryopreserving the flight bacterial inoculum.

Component	mAUM	mAUM.v3	mAUM.v4
Citric acid	2 mM	0.5 mM	0.52 mM
Lactic acid	1.1 mM	1.1 mM	1.13 mM
Sodium chloride	90 mM	45 mM	46.39 mM
Ammonium chloride	25 mM	12.5 mM	12.89 mM
RPMI 1640 amino acids	20 ml/L	20 ml/L	0 mM
Urea	170 mM	170 mM	175.26 mM
Uric acid	0.4 mM	0.4 mM	0.412 mM
Creatine	7 mM	3.5 mM	3.61 mM
Calcium chloride	0.25 mM	0.03125 mM	0.03222 mM
Magnesium sulfate	2 mM	0.5 mM	0.515 mM
Sodium sulfate	10 mM	2.5 mM	2.577 mM
Sodium bicarbonate	25 mM	6.25 mM	6.443 mM
Sodium nitrite	6 mM	1.5 mM	1.546 mM
Ferrous sulfate	0.005 mM	0.005 mM	0.00515 mM
Monopotassium phosphate	1.8 mM	18 mM	18.56 mM
Dipotassium phosphate	1.8 mM	18 mM	18.56 mM
L- Glutamine	2 mM	2 mM	0 mM

Table 7. mAUM.v3 formulation and comparison to the NASA urine ersatz formulation. Urine ersatz formulation describes the formulation described by NASA to model astronaut urine (104, 132).

Component	mAUM.v3 Formulation (mg/L)	Urine Ersatz Formulation (mg/L)
Ammonium ⁺⁺	226	50-631
Bicarbonate ⁻	381	41-757
Calcium ⁺⁺	1.25	34-185
Chloride ⁻	2041	774-8301
Iron ⁺⁺	0.36	NA
Magnesium ⁺⁺	12.14	14-127
Nitrate ⁻	93	NA
Phosphate	3419	155-4312
Potassium ⁺	2111	238-2347
Sodium ⁺	1153	432-4002
Sulfate ⁻	275	119-2111
Citric acid	96	77-679
Arginine*	200	NA
Asparagine*	57	45-132
Aspartic acid*	20	NA
Cystine*	50	2-6
Glutamic acid*	20	40-155
Glycine*	10	563-1802
Histidine*	15	776-2327
Proline*	40	NA
Isoleucine*	50	NA
Leucine*	50	26-101
Lysine*	40	47-424
Methionine*	15	NA
Phenylalanine*	15	NA
Serine*	30	210-730
Threonine*	20	95-381
Tryptophan*	5	NA
Tyrosine*	23	NA
Valine*	20	22-87
Urea	10220	10000-22857
Uric acid	67.2	NA
Creatine	588.386	NA
Creatinine	NA	533-1333
Taurine	NA	334-1614
L-Glutamine	293	438-1520
Alanine	NA	143-615
Carnosine	NA	36-283
D-Glucuronic acid	NA	12-125
Phenol	NA	3-12
Citrulline	NA	<1-19
Bilirubin	NA	<1-30

The pH of mAUM (34) (hereafter referred to as mAUM.v1) was compared to mAUM.v3 and mAUM.v4 with and without AgF, which is the disinfectant to be tested in this study. Briefly, multiple batches of media were made and stored at 4°C for varying amounts of time. The pH of each batch was read at the time of preparation and after storage. The change in pH over time was calculated using linear regression analysis. The pH of mAUM.v3 (blue triangles) showed increased pH stability relative to mAUM.v1 (red circles) (**Figure 11, Table 8**). The pH of mAUM.v4 (green squares), which is the formulation which will be loaded into the flight hardware, trended toward further increased stability, which was maintained in the presence of 400 ppb (parts per billion) AgF (**Figure 11, Table 8**). It must be noted that due to the small sample sizes of mAUM.v4 and mAUM.v4 with 400 ppb AgF, the statistical power of the regression analysis for those media are low.

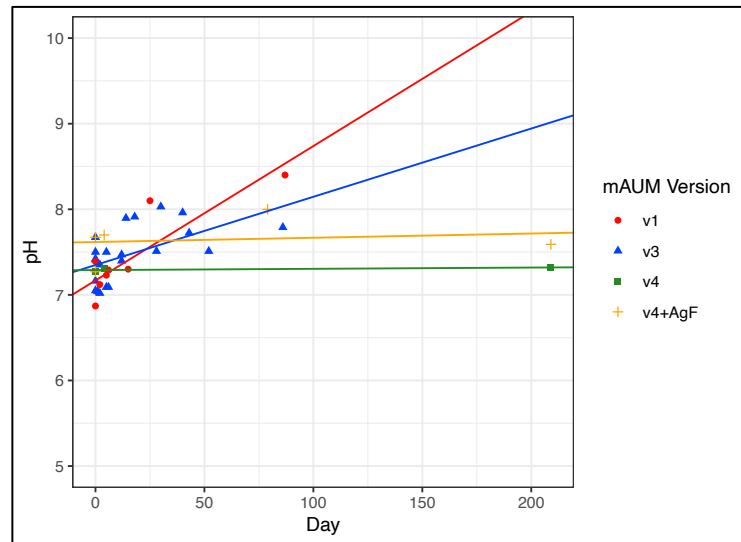


Figure 11. Stability of pH of different formulations of mAUM. The pH of mAUM.v1 (red) increased more rapidly ($y = 7.1685 + 0.0157x$, $R^2 = 0.7599$) than mAUM.v3 (blue) ($y = 7.349 + 0.0080x$, $R^2 = 0.3118$). mAUM.v4 (green) ($y = 7.2895 + 0.0001x$, $R^2 = 0.4452$) and mAUM.v4 with 400 ppb AgF trended towards pH stability (yellow) ($y = 7.6175 + 0.0005x$, $R^2 = 0.0297$).

Table 8. Linear regression of pH change over time in mAUM. β_1 describes the change in pH per day. mAUM.v3 and mAUM.v4 showed increased stability during storage relative to mAUM.v1. mAUM.v4 stability was maintained with the addition of 400 ppb Ag. ($H_0: \beta_1 = 0$; * $p < 0.05$, ** $p < 0.01$, *** $p < 0.001$).

<i>Media</i>	Coefficients		<i>DF</i>	<i>R</i> ²
	β_1	<i>St. Error</i>		
mAUM.v1	0.0157*	0.0033	7	0.760
mAUM.v3	0.0080***	0.0026	20	0.312
mAUM.v4	0.0001	0.0002	1	0.802
mAUM.v4-AgF	0.0005	0.0016	3	0.030

Urea is known to be unstable in aqueous solution (133). Urea decomposition in aqueous solution produces ammonium cyanate (133), which is toxic to many bacteria at concentrations as low as 200 ppm (134). Additionally, urea is the primary source of carbon in mAUM.v3 (hereafter referred to as mAUM) that is not in an amino acid, so stability of urea during long-term storage is critical to extending mAUM shelf life. Urea stability was assayed using a modified urease test (135, 136). Briefly, batches of mAUM were prepared and stored at 4°C for up to 96 days. After storage, 5 mL from each batch were inoculated with overnight culture of *Proteus mirabilis* 2573 (ATCC 49565) (Table 1), which had been cultured in LB broth at 37°C with shaking at 150 RPM. *P. mirabilis* produces the enzyme, urease, that metabolizes urea to ammonia (135). Ammonia concentration was then assayed using a phenol-hypochlorite reaction (136), which produces a blue color in the presence of ammonia that can be read using a spectrophotometer at 625 nm. Control reactions were also carried out using uninoculated mAUM to account for ammonia already present in mAUM. Released ammonia was calculated as described in Equation 1:

$$\text{Released ammonia} = A_{625(\text{inoculated})} - A_{625(\text{control})} \quad (1)$$

Over a period of 3 months, urea concentration was stable (Figure 12). Slight changes in

urea concentration can be attributed to batch-to-batch variation.

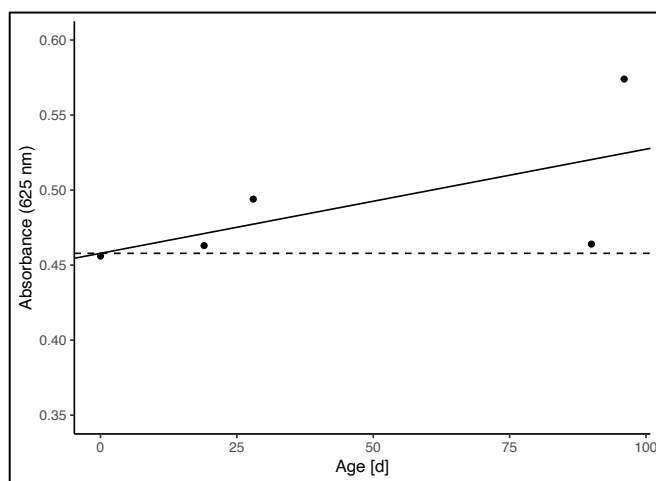


Figure 12. Urea stability in mAUM.v3 for 96 days. Over 96 days, urea concentration remained stable in mAUM ($H_0: \beta_1 = 0$, $p = 0.268$, Student's T-test). Solid line indicates linear regression of released ammonia over time; dashed line indicates $\beta_1 = 0$.

Silver Fluoride Bioavailability

Silver binds readily to organic molecules (137), forming complexes which may reduce the antimicrobial activity of ionic silver in mAUM. To ensure that the antimicrobial activity of silver fluoride was stable after long term storage, silver fluoride antimicrobial activity after storage in mAUM was assessed.

Batches of mAUM were mixed with 0, 400, 800, and 1600 ppb AgF and stored for 3 days ("Fresh") or 5.5 weeks at 4°C. Five mL of each batch was inoculated at 1×10^5 CFU/mL, incubated for 24 hours at room temperature in static culture, and serially diluted and plated for viable cell counts to determine bioactivity of AgF. No difference in cell viability between fresh and 5.5-week-old mAUM was observed, indicating that AgF antimicrobial activity was stable after long-term storage (Figure 13).

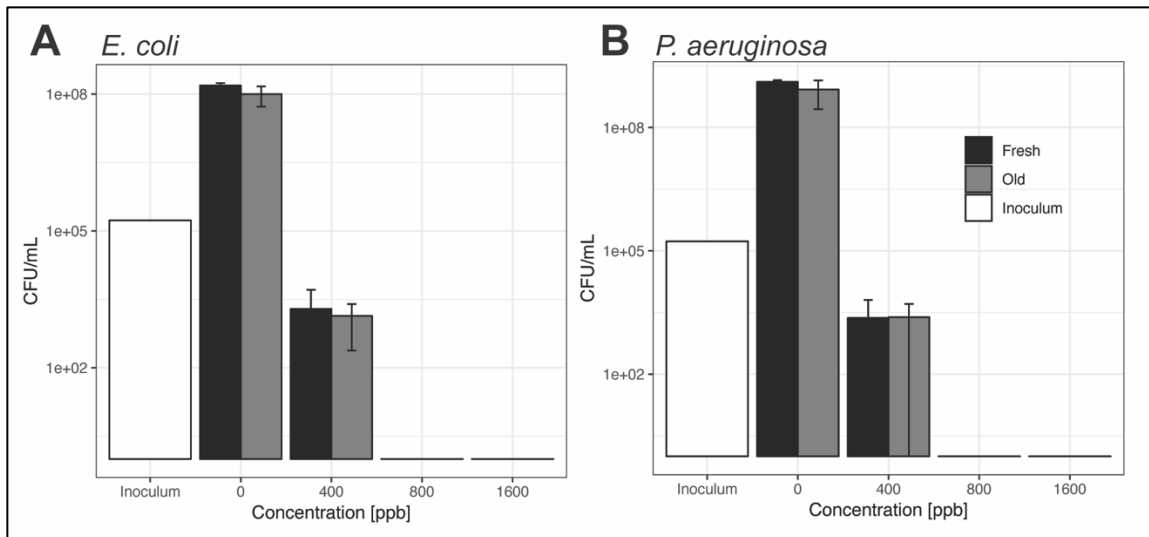


Figure 13. Silver stability in mAUM. AgF which had been stored with mAUM for 5.5 weeks (gray bars) and 3 days (black bars, “Fresh”) showed the same amount of killing against **A)** *E. coli* and **B)** *P. aeruginosa*, indicating that silver activity is stable even after long-term storage at 4°C. The inoculation concentration is shown as white bars. No significant difference was found between any fresh and 5.5-week media at any AgF concentration (Welch’s T-test). Error bars indicate standard deviation.

Bacterial Cell Viability with Silver Fluoride

To determine the optimal concentration of AgF treatment for the flight experiment, Ag⁺ disinfection against cell viability was assayed in 125 mL Erlenmeyer flasks containing 25 mL mAUM.v3 and a stainless-steel coupon. A stock solution of silver (I) fluoride (Matrix Scientific 101775) was made at 1000 ppm in high resistance (18 MΩ) water, then sterilized by passing through a 0.2 μm pore filter. A 100-ppm working solution was made by diluting the stock solution 1:10 in high resistance (18 MΩ) water; the final solution was filter sterilized. Both the stock and working solutions were stored at 4°C in the dark in containers wrapped in foil. Silver fluoride was added to mAUM.v3 at concentrations ranging from 0 ppb to 3200 ppb, then the flasks were inoculated with *P. aeruginosa* PAO1 and *E. coli* F11 in mixed culture and incubated at

ambient temperature in the dark for 24 hours to check for the short-term response or 1 week to check for the long-term response to silver disinfection. It must be noted that the amount of oxygen in the batch culture may have been different in the batch culture as compared to BioCell cultures, so the flasks were incubated statically rather than shaking, to reduce the amount of oxygen introduced to the media. *P. aeruginosa* has been shown to be more resistant to silver nanoparticles in aerobic growth than in anerobic growth, which may have caused silver resistance to be higher in batch culture than in the BioCell (138).

After incubation, mAUM broth was sampled directly for viable cell counting of planktonic cells. To count viable bacterial cells in the biofilm, the stainless-steel coupon was removed from the flask, gently rinsed once in sterile D-PBS, then submerged in 2 mL D-PBS and sonicated in a sonication bath (Fisher Scientific FS20) for 10 minutes to release the bacterial cells. The sonicate was vortexed for 15 seconds to break up cell clumps, then serially diluted and assayed for viable cell count. Biofilm viable cells are presented as the density of surface coverage, which was calculated as described in Equation 2:

$$\frac{CFU * 2 \text{ mL}}{2(10 \text{ mm} * 10 \text{ mm}) + 4(10 \text{ mm} * 1 \text{ mm})} \quad (2)$$

E. coli and *P. aeruginosa* in mixed culture resulted in higher numbers of viable cells, showing higher resistance to Ag¹⁺ in long exposure (**Figure 14 B,D**) than in short exposure (**Figure 14 A,C**). Similar trends were seen between planktonic bacterial cells (**Figure 14 A,B**) and bacterial cells in biofilms (**Figure 14 C,D**) at the same exposure times. Interestingly, *E. coli* resistance to silver disinfection was lower when both biofilms

and planktonic bacterial cells were exposed to 1600 ppb Ag^{1+} than when exposed to 3200 ppb Ag^{1+} for 1 day, and *P. aeruginosa* appeared equally susceptible after 1 day when comparing 1600 and 3200 ppb Ag^{1+} treatments (**Figure 14 A,C**). However, at 1-week exposure, both planktonic and biofilm-associated *E. coli* and *P. aeruginosa* developed resistance to 1600 ppb Ag^{1+} but were unable to grow when treated with 3200 ppb Ag^{1+} . *P. aeruginosa* produces pyocyanin, a blue-green pigmented phenazine that acts as an antimicrobial against other bacterial species by inducing oxidative stress by the formation of reactive oxygen species (139). Previous studies have shown that pyocyanin can neutralize Ag^{1+} ions by reducing ionic silver to the elemental form, Ag^0 (140). Pyocyanin-mediated reduction of Ag^{1+} can also be carried out by *E. coli* (141). Pyocyanin production in *P. aeruginosa* is inversely correlated to the rate of cell growth (142). Whooley and Laughlin were able to induce production of pyocyanin by reducing the growth rate of log-phase *P. aeruginosa* (142). Pyocyanin production has also been shown to be reduced in the presence of urea at 200 mM (the concentration of urea in mAUM is 180 mM) (143). I hypothesize that early inhibition of *P. aeruginosa* growth in the presence of Ag^{1+} (138) may have allowed the production of pyocyanin (142), but the presence of urea, combined with low *P. aeruginosa* cell number might have caused the rate of pyocyanin production to be low (143). Thus, the amount of time it may have taken to neutralize Ag^{1+} could have been dependent on the concentration of Ag^{1+} , which may have caused a delay in the initiation of growth. This effect might not have been seen in cultures which were treated with weaker concentrations of Ag^{1+} , since the lower concentration could have been neutralized more quickly. If the rate of Ag^{1+} neutralization was slow enough that it took more than 24 hours to neutralize enough silver to allow *P.*

aeruginosa and *E. coli* growth, I would expect to see the pattern shown here. Eventually, the silver could have been neutralized, which might have allowed both *P. aeruginosa* and *E. coli* to enter log-phase growth. Additionally, *E. coli* has been shown to be susceptible to pyocyanin (144), which may have contributed to the decrease in *E. coli* cell density seen in 1600 ppb AgF treatment after 1 day. The toxicity of pyocyanin-produced reactive oxygen species as a result of silver neutralization, combined with the toxicity of ionic silver, may have caused an additional decrease in cell number. At 3200 ppb, it is possible that the amount of silver bound to the bacterial cell membrane, proteins, and DNA (145) may have been too strong to overcome, which might be why we did not see the population rebound after 1 week incubation. An experiment investigating various concentrations of pyocyanin against biofilm growth in the presence of AgF may support this hypothesis.

After one day, planktonic and biofilm-associated *E. coli* and *P. aeruginosa* treated with 400 ppb AgF, which is the maximum concentration identified by NASA for use as a water disinfectant (146), were present in lower density than the same cells which were untreated. At one week, planktonic cells and biofilms treated with 400 ppb AgF were recovered, and increased numbers of *P. aeruginosa* planktonic cells were seen as compared to the untreated (0 ppb) control, while *E. coli* planktonic cell numbers were reduced (**Figure 14 B**). This data, combined with interesting results seen by confocal microscopy which will be discussed in Chapter 3, led to the selection of 400 ppb as the treatment concentration for the flight experiment.

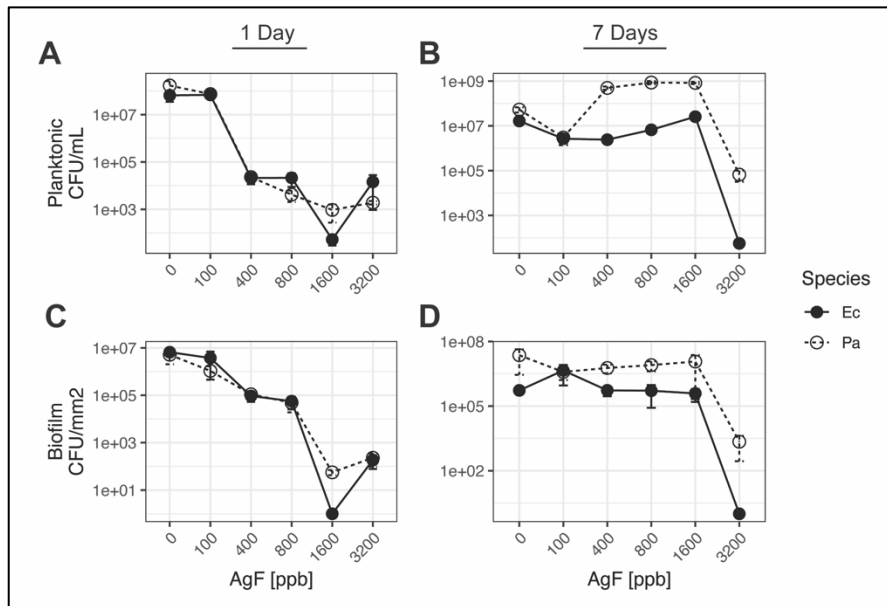


Figure 14. Effect of ionic silver on cell viability of mixed-culture planktonic and biofilm culture. Silver exposure for 1 day (A,C) or 7 days (B,D) to mixed-culture planktonic (A,B) or biofilm (C,D) growth showed that after long-term exposure, both *E. coli* and *P. aeruginosa* were more resistant to silver fluoride treatment. Error bars indicate standard deviation.

The effect of fluoride was not investigated here. Previous research shows that fluoride ions have antimicrobial activity (147); however antimicrobial effect is typically found at concentrations much higher than those used here. The antimicrobial effect of fluoride ions has been investigated primarily in gram positive bacteria which are found in the human oral cavity (147), but some studies investigating ionic fluoride susceptibility in *E. coli* have been described. In one study, *E. coli* BW25113, a common lab strain, was exposed to ionic fluoride (as a sodium salt) for 6 hours and no antimicrobial effect was observed even at concentrations as high as 500 μM in rich media (LB) (148), or 20X the concentration of AgF used in this study (the highest concentration of AgF used in this study is 3,200 ppb, or 0.025 mM). In another study, Baker *et al.* found that *E. coli* BW25113 growth was reduced after incubation for 16 hours at 30 mM NaF and inhibited

at 200 mM NaF in rich media (LB) (149) – concentrations 1,200X and 800X the concentration of fluoride used here, respectively. Only one study could be found investigating the susceptibility of *P. aeruginosa* to fluoride, although they did not report the *P. aeruginosa* strain studied (150). The minimum inhibitory concentration of fluoride against *P. aeruginosa* was reported to be 0.6 mg/mL in rich media (LB broth) (150), or 187.5X the highest concentration of fluoride (3,200 ppb = 0.0032 mg/mL) used in this study. Considering the extremely low dose of fluoride ions used in this research when compared to inhibitory concentrations reported in the literature, I attribute the antimicrobial effect of AgF seen in this study to the action of ionic silver.

Frozen Inoculum Stability

To minimize crew risk and time requirements, single-dose syringes containing pre-mixed *E. coli* and *P. aeruginosa* frozen inoculum will be sent to the ISS to be mixed directly into the sample well in flight. As such, the freezing buffer will be added to the sample well with the bacterial cells. Glycerol, a common freezing medium used for cryopreservation of bacteria, can be metabolized by both *P. aeruginosa* (151–155) and *E. coli* (156–160). In *P. aeruginosa*, glycerol is known to increase pyocyanin production (151–155). As discussed previously, pyocyanin produced by *P. aeruginosa* can act as an antimicrobial against other species in mixed culture to enhance *P. aeruginosa* competition (112). As a carbon source, glycerol is energy-poor (161). *E. coli* has been shown to activate stress-response pathways when metabolizing low-energy carbon in minimal media, such as mAUM (162–164). Thus, it has been postulated that glycerol metabolism may induce a stress response in *E. coli*, although this has not been studied (161). It is possible that using glycerol as the freezing buffer for the frozen inoculum

could confer a competitive advantage to *P. aeruginosa* when incubated in mAUM as a mixed culture with *E. coli*. Glycerol is also not described in the urine ersatz formulation discussed earlier (104, 132). Thus, glycerol is not suitable for use as a freezing buffer for the flight experiment.

Considering the wide range of time points which will be used for the flight experiment, the inoculum dose must be stable for a minimum of 45 days. Previous research suggests that concentrated solutions of amino acids may be used as a bacterial freezing buffer (165–168), although this has not been extensively investigated. Considering the need to avoid introducing glycerol to the sample well, we investigated whether this approach could be used for the flight experiment. mAUM includes two concentrated, commercially available amino acid solutions: 50X RPMI 1640 Amino Acids (Sigma-Aldrich R7131) and 100X L-glutamine (VWR L0131), which could potentially be used as a freezing buffer. We hypothesized that we could withhold the amino acid solutions from mAUM which was loaded into the BioCell wells, and instead combine them for use as a freezing buffer to stabilize the single-dose frozen inoculum. When the BioCells are inoculated in flight, the mixing of the freezing buffer into mAUM without amino acids (mAUM.v4) will produce mAUM.v3, the intended experimental medium, without introduction of an additional cryopreservative.

This work was completed by collaborators at Arizona State University. Briefly, 1 mL of stationary phase, 3 day broth cultures of *E. coli* (1.50×10^7 CFU) and *P. aeruginosa* (1.75×10^7 CFU) in mAUM were centrifuged at 7000 R.P.M. for 7 minutes. We selected a 1:1 ratio of *E. coli* to *P. aeruginosa* as our inoculum to avoid introducing a competitive advantage to one species based on bacterial cell number in the inoculum

dose. The supernatant was removed, and the cell pellet was resuspended in a volume equal to the supernatant of freezing media (FM): 25X RPMI 1640 amino acid solution (Sigma R7131) with 25X L-glutamine (VWR 02-0131-0100). The entire 1 mL volumes of *E. coli* and *P. aeruginosa* were each diluted 1:10 into 9 mL FM, and then combined to produce a 1:20 dilution of each strain in FM. The resulting inoculum was aliquoted as 68 μ L aliquots into 1 cc needleless syringes, capped with Luer-lock caps, and stored at -80°C in batches of 10 syringes for 3 to 6 days, approximately 1 month, 2 months, and 3 months. The syringes were removed from the freezer and thawed to room temperature, then quantified using serial dilution plating onto LB with either nalidixic acid (10 μ g/mL) to select for *P. aeruginosa* or cefsulodin (25 μ g/mL) to select for *E. coli*. The resulting plates were evaluated to determine cell viability after storage. As a control, the starting cell concentration of the inoculum was also measured by serial dilution plating prior to freezing.

Over three months of storage, there was no statistically significant decrease in *E. coli* or *P. aeruginosa* cell viability as measured by viable cell counting (**Figure 15 A, C**). A significant decrease in viable cell number was seen in *E. coli* after three months storage at -80°C when compared to the samples which were stored for two months; however, statistical analysis shows that there was no difference in bacterial cell recovery when comparing 3 months to 3-5 days or to 1 month, indicating that the difference in recovery between two and three months storage may have arisen from an increase in *E. coli* recovery at 2 months, rather than a decrease in cell recovery at 3 months (**Figure 13 B**). Indeed, percent survival of *E. coli*, calculated as the concentration of bacterial cells which were recovered after freezing divided by the concentration of bacterial cells in FM before

freezing, showed an increase in *E. coli* recovery at two months when compared to percent recovery at all other storage times (**Figure 13 D**). This may have been the result of an experimental error. If the two-month frozen inoculum was left to thaw for an extended time, *E. coli* in the freezing buffer may have begun to metabolize the amino acids and begun to replicate, leading to an increase in bacterial cell number at two months.

Alternatively, the two-month stored inoculum may have been placed in a warmer location during thawing, which would have increased the thawing rate. Importantly, there was no decrease in the concentration or percentage of *E. coli* or *P. aeruginosa* cells after one, two, or three months storage at -80°C when compared to the inoculum which was stored for 3-6 days, which exceeded the requirement for inoculum stability for 45 days, indicating that FM is an acceptable freezing buffer for use in the flight experiment.

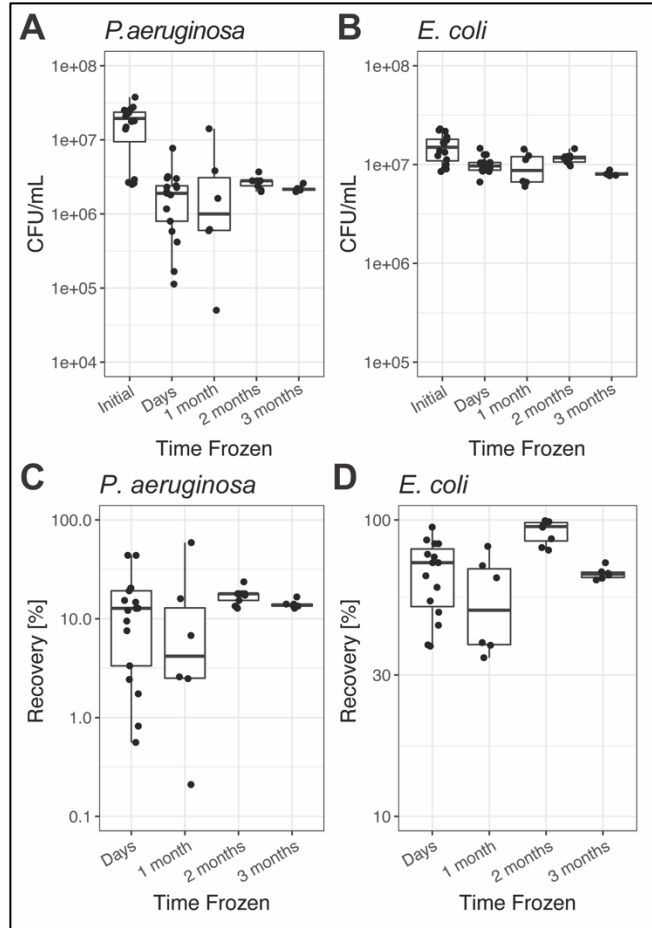


Figure 15. Frozen inoculum stability after storage at -80°C. Top: Stability of mixed-species inoculum as measured by viable cell counting. **A)** *P. aeruginosa* PAO1 showed no loss in viability as storage time at -80°C increases when compared to the short-term (days) storage time. **B)** *E. coli* F11 also showed no loss viability over one, two, and three months at -80°C when compared to the short-term (days) storage time. Bottom: Stability as determined by percent survival. Percent survival was calculated as the number of bacterial cells surviving divided by the number of bacterial cells mixed into the inoculum. **C)** *P. aeruginosa* showed no change in recovery. **D)** *E. coli* showed no decrease in recovery at after one, two, or three months when compared to the short-term (days) storage time. *E. coli* showed an increase in recovery at 2 months, which may have been the result of an experimental error. Statistics: Tukey's HSD, 95% confidence interval. N: Days = 15; 1 month = 6; 2 months = 8; 3 months = 6.

Flight Hardware and 316L Stainless Steel Coupons

BioCells (BioServe Space Technologies, Boulder CO) were selected as the culturing vessel for the flight experiment. BioCells are 12-well plates that are easily

customizable, and the general design has already been approved by NASA for flight. The BioCell is covered with a flexible, optically pure, gas permeable, fluorinated ethylene propylene (FEP) Teflon membrane. The optically pure membrane allows imaging of the biofilm in the growth configuration, without the need to remove the stainless-steel coupons or membrane. The stainless-steel grade and finish were selected to match materials used in the ISS WRS. For this research, we used 1 (+/-0.1) cm² 316L grade stainless steel coupons with a 2B brushed finish, which were affixed to a pedestal inside each well of the BioCell, to act as a biofilm attachment surface (**Figure 16 A**). The pedestal raised the coupon to sit 2 mm below the FEP Teflon membrane (**Figure 11 B**), so that it could be imaged using a microscope lens with a working distance of at least 2 mm, without the need to remove the FEP Teflon membrane.

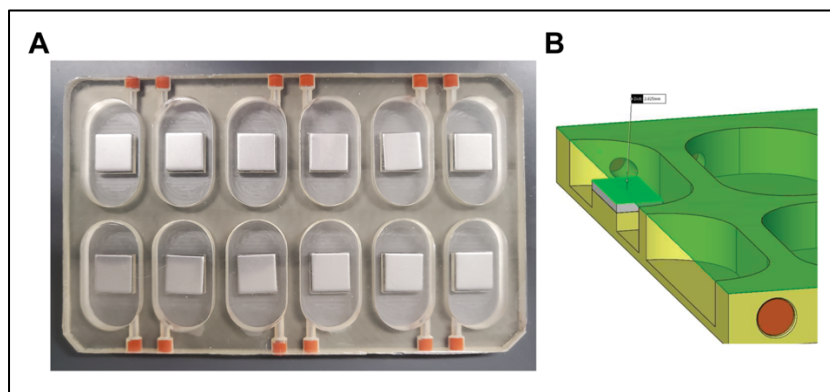


Figure 16. BioCell hardware. **A)** A 12-well BioCell that has been adapted for this experiment with a pedestal to which a 316L stainless steel coupon has been affixed. **B)** Schematic of the interior of the well showing the pedestal height as the 2 mm distance between the surface of the coupon (green, opaque) and the FEP Teflon membrane (green, transparent). Figure B was provided by BioServe Space Technologies.

Biofilms in the ISS WRS have been observed on components which are composed of 316L stainless steel (16, 103, 169). Thus, coupons composed of 316L

stainless steel with a brushed finished were selected as the attachment surface for biofilm growth. Two cutting methods, punch-cutting and diamond-wire saw cutting, were considered with respect to stainless steel coupon geometry and damage to the cut edge to determine the best method of preparation.

Punch-cutting resulted in coupons that were flat on the top surface, but rounded on the bottom (Figure 17A), which prevented complete adherence to the BioCell pedestal, resulting in the coupons detaching from the BioCell during autoclaving (Figure 17B). Diamond-wire saw cutting produced coupons which were completely flat on both sides (Figure 17C). Scanning electron microscopy (SEM) showed distinct differences in the coupon edge between these two cutting methods. Punched coupon edges were more damaged and irregular and had rough edges (Figure 17D, top). Coupon edge uniformity was preferred as rough edges can increase microbial access to the stainless steel, which may affect the amount of corrosion seen at the coupon edge. Diamond-wire saw cut coupons had edges that were even and regular (Figure 17D, bottom). Based on increased flatness and edge uniformity, diamond-wire saw cutting was selected as the method of coupon preparation.

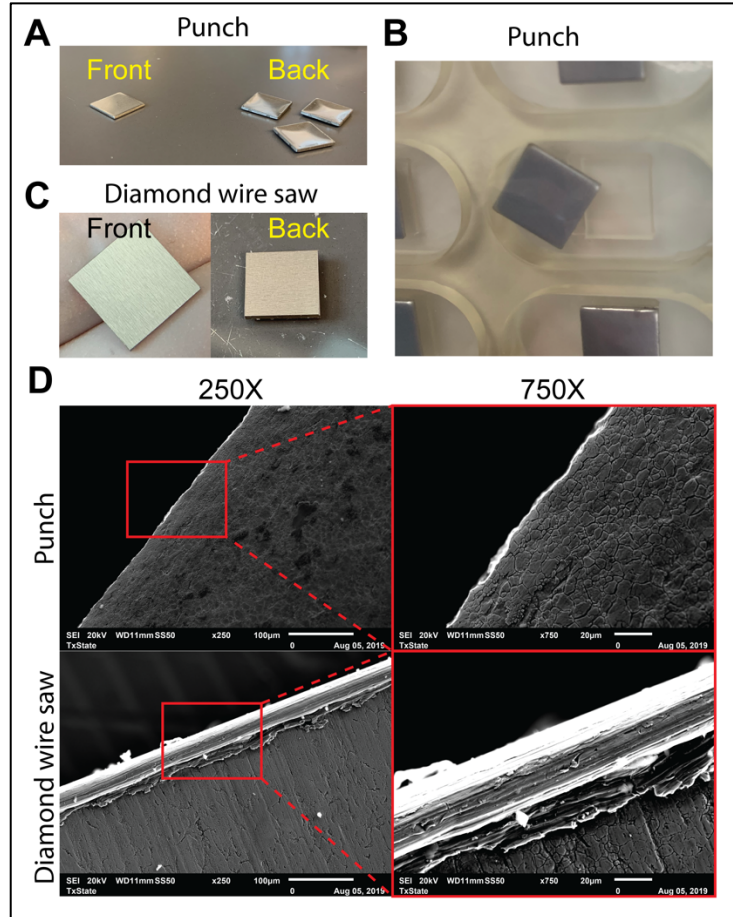


Figure 17. Stainless steel coupon geometry. A) Punched coupons showed curving on the back surface (**right**) but not the front (**left**). B) Punched coupons detached from the BioCell pedestal during autoclaving. C) Diamond-wire saw cut coupons were completely flat on the front (**left**) and back (**right**). D) SEM of the coupon edge shows that the cut edge (**bottom panels**) was more uniform than the punched edge (**top panels**). Red boxes on the left panels indicate differences in the coupon edge between the two cutting methods and are lower magnification images of the right panels.

To ensure that the stainless-steel coupons did not contaminate the BioCell with any residues from the manufacturing or cutting process which could have potentially impacted biofilm formation, a cleaning protocol was developed. All stainless-steel coupons were cleaned by soaking in 1% (w/v) Tergazyme (Alconox 1304-1) for 1 hour with gentle shaking (100 RPM) on a rotary platform. Coupons were rinsed 5 times for 5 minutes each in a sterile deionized water bath with gentle shaking (100 RPM), then 5

times for 5 minutes each in a sterile high-resistance (18 M Ω ; “MilliQ”) water bath with gentle shaking (100 RPM). The coupons were then air dried and autoclaved using standard autoclave conditions with fast exhaust to promote evaporation of any condensed steam. Coupon cleaning effectiveness was measured using Electron Dispersive Spectroscopy (EDS) and compared to the metallurgical report provided by the stainless-steel manufacturer. Electron dispersive spectroscopy (EDS) analysis was performed on a JEOL JSM-6010 PLUS/LA SEM using the JEOL EDS System. Both mapping and spot analysis were performed.

EDS analysis showed that cleaning with 1% (w/v) Tergazyme was effective at removing contaminating carbon and aluminum (**Figure 18**). Carbon and aluminum were possibly residues that accumulated during storage or the cutting process. Oxygen was detected on both the cleaned and uncleaned coupons but was not noted on the manufacturer’s metallurgical report. It is possible that the buildup of oxygen was the result of oxidation during storage and could not be avoided.

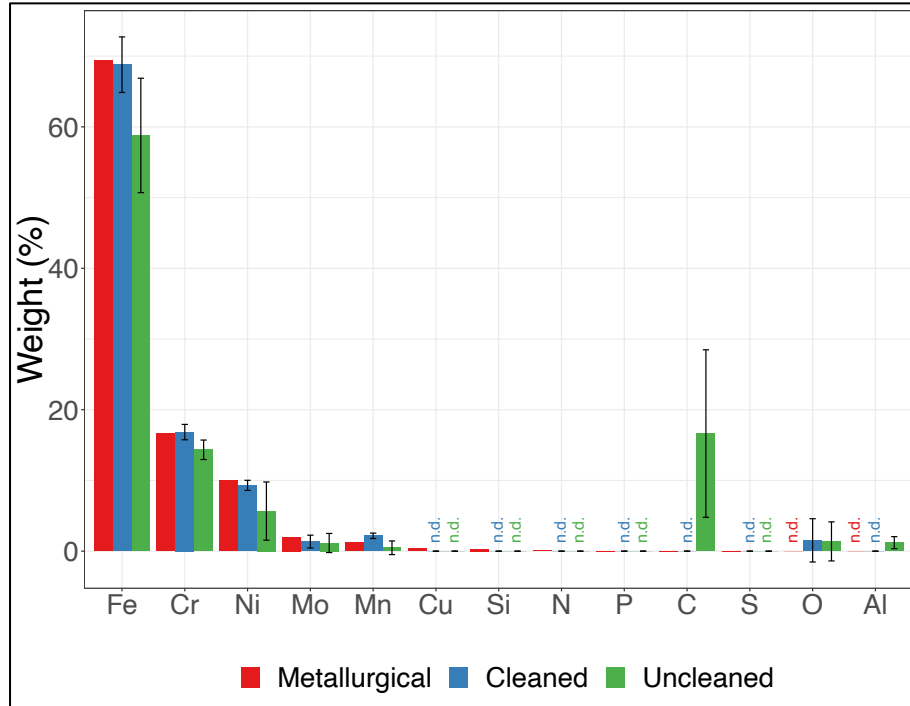


Figure 18. Stainless steel coupon cleaning effectiveness. EDS spectroscopy of cleaned (blue) and uncleaned (green) coupons showed that cleaning with Tergazyme was effective at removing contaminating carbon and aluminum. Metallurgical (red) bars show the percentage of each component as reported in the metallurgical report which was supplied by the stainless steel manufacturer.

During launch, in-flight incubation, and sample return, the BioCells will be loaded into Plate Habitats (P-HABs, BioServe Space Technologies, Boulder CO). The P-HAB (**Figure 19 A**) is a closed box which serves as an incubation chamber and provides the additional level of containment that is necessary to keep flight crew safe in the event of a BioCell failure during incubation. There are two vents (**Figure 19 A**, arrows), which allow air flow into the P-HAB, and the interior is fitted with slots that fit multiple BioCells (**Figure 19 B**).

In flight, the BioCell will be removed from the P-HAB and loaded into a plate holder (**Figure 19 C, D**), which has a slot to hold one BioCell, and a thick plastic protective cover to prevent rupture of the FEP Teflon membrane during mixing (**Figure**

19 C). The plate holder allows for inoculation, fixation, and mixing of the samples using a syringe (Figure 19 D).

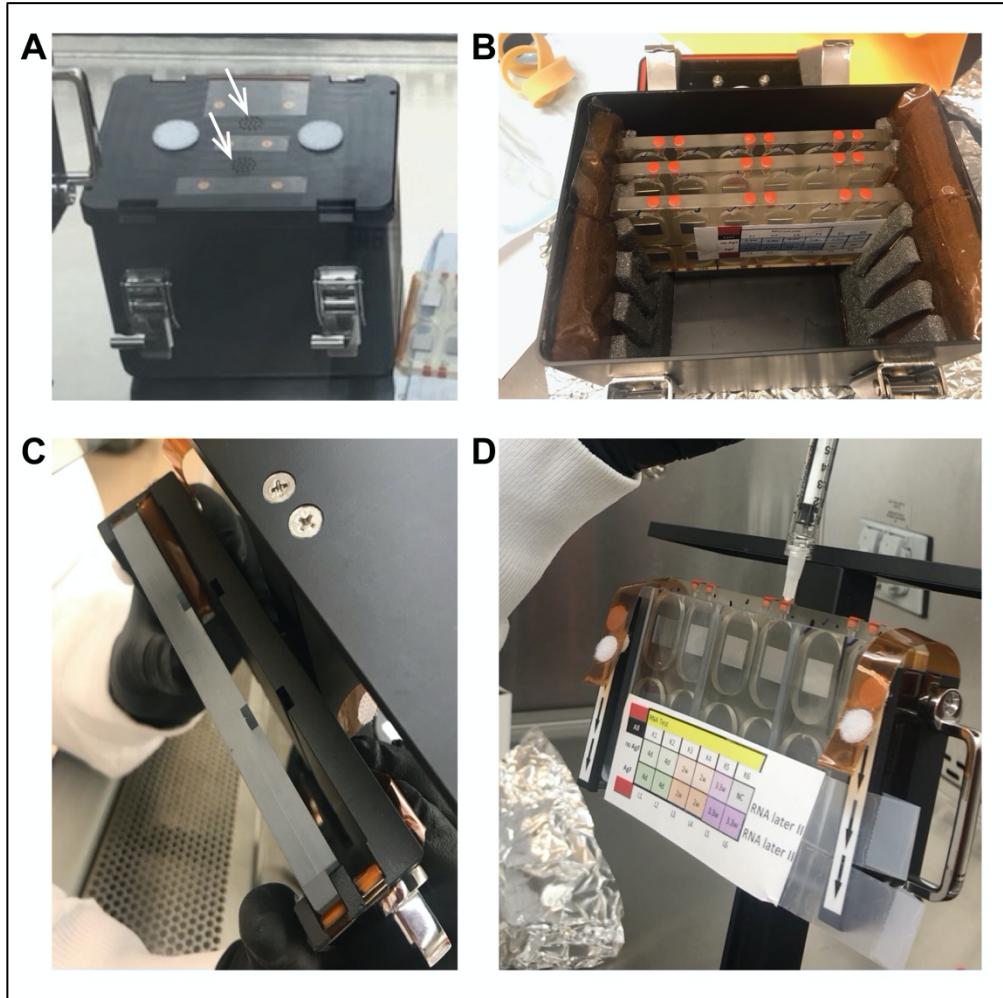


Figure 19. P-HAB and plate holder hardware. **A)** The P-HAB, when closed, serves as both an incubation chamber and as a secondary level of containment. The lid is equipped with two vents (arrows). **B)** The interior of the P-HAB can hold several plates. **C)** The plate holder has a slot that can hold and stabilize one BioCell for inoculation or addition of fixative. **D)** A BioCell is inoculated while in the plate holder.

Fixation in Paraformaldehyde

Flight-grown biofilm samples will be fixed with paraformaldehyde (PFA) on-board the ISS and then returned for ground analysis via confocal microscopy and SEM. To minimize crew time and risk, samples cannot be fixed using the standard 20-minute fixation time, followed by washing and storage in PBS buffer. As such, it was necessary that fluorescence and biofilm structure stability with long-term storage in PFA was examined.

To determine loss of GFP and mCherry fluorescence during long-term storage of biofilms in PFA, biofilms were cultured for one week in mAUM-filled BioCells, then fixed with 4% PFA diluted in Dulbecco's PBS (D-PBS) (Gibco, cat no. 14190-144), or in D-PBS as a control, at 4°C for 20 minutes, 1 week, and 1 month. D-PBS was used for sample storage and microscopy to ensure that batch-to-batch variability in the concentration of each component will not affect sample integrity, and has only a slight change in formulation from PBS (KH_2PO_4 is reduced to 1.47 mM, from 1.8 mM, and Na_2HPO_4 is reduced to 8.06 mM from 10 mM). After fixing, the biofilms were washed 3 times with D-PBS, then the wells were filled with D-PBS and imaged using confocal microscopy at 60X. For wells where there was notable signal loss, supplemental staining with fluorophore-conjugated antibodies was tested. The wells were stained in one step in D-PBS buffer with anti-mCherry rat monoclonal antibody (clone 16D7) conjugated with Alexa Fluor 594 (5 $\mu\text{g}/\text{mL}$; Invitrogen M11240) and anti-GFP rabbit polyclonal antibody conjugated with Alexa Fluor 488 (5 $\mu\text{g}/\text{mL}$; Invitrogen A21311), then triple washed and stored in D-PBS. To assay loss of signal, the laser power and voltage of the respective lasers were set using the 20-minute fix control, and then held constant for the PFA-

treated biofilms. All views were taken as Z-stacks using sequential imaging and are presented as maximum intensity Z projections. There was no notable decrease in signal brightness between 20 minutes and 2 weeks of fixing; however, after 1 month the signal brightness was markedly lower. However, even after 1 month of storage in PFA, the signal level was detectable (**Figure 18 A**). Supplemental staining with fluorophore conjugated antibodies was able to augment the faded signal (**Figure 18 B**). Thus, storage in PFA for up to one month is practicable, and decreased signal intensity is recoverable by antibody staining.

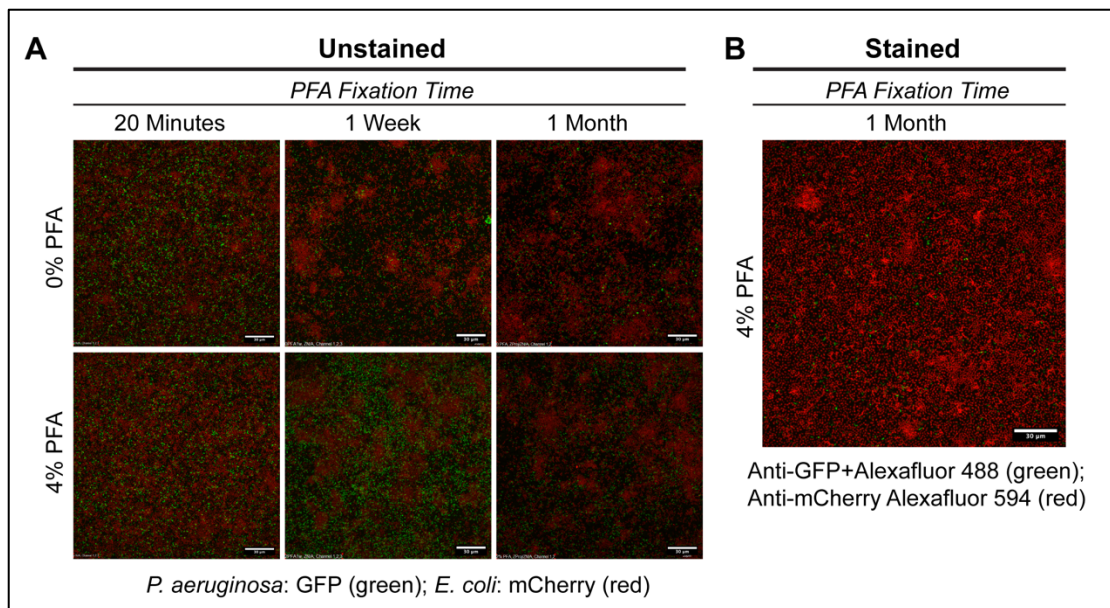


Figure 20. Fluorescence detection after fixing with PFA. GFP and mCherry fluorescence detected after incubation at 4°C with 0% and 4% PFA in D-PBS for 20 minutes, 1 week, and 1 month. **A**) Unstained *E. coli* and *P. aeruginosa* mixed culture biofilms grown 316L stainless steel showed a decrease in GFP and mCherry brightness that was most pronounced after 1 month’s fixation. **B**) Fluorescent signal from biofilms which were fixed for 1 month with PFA was recovered after staining with signal-boosting anti-mCherry and anti-GFP antibodies. Images were captured sequentially as Z-stacks and are maximum-intensity projections. Scale bars = 30 μm.

RNA Preservation for Transcriptomics

Samples for transcriptomic analysis via RNA-seq will be preserved with RNAlater II (ThermoFisher, cat no. B7024) in-flight and stored at -80°C for sample return. After the samples have been returned, they will be thawed, then RNA will be extracted using the Qiagen miRNeasy Mini kit (Qiagen, cat no. 217004). RNA will be quantified using a Nanodrop spectrophotometer and RNA integrity will be confirmed using an Agilent Bioanalyzer and then converted to cDNA using the Agilent Bravo liquid handler. The resulting cDNA will be sheared, checked for quality using a bioanalyzer, sequenced using Illumina NextSeq, and aligned to reference genomes. After analysis using EdgeR (Bioconductor), identified genes of interest will be confirmed by qPCR analysis. This work will be performed by a core facility at Arizona State University.

The RNA quality of mixed-species *E. coli* and *P. aeruginosa* biofilms grown in BioCells has been assessed by Bioanalyzer at Arizona State University, and the quality was found to be acceptable for downstream analysis.

Biofilm Matrix Staining

P. aeruginosa and *E. coli* produce different biofilm matrices. The polysaccharide component of *P. aeruginosa* biofilm matrix is primarily composed three polysaccharides: alginate, Pel, and Psl. Alginate-producing *P. aeruginosa* strains are typically mucoid and are often found in cystic fibrosis lung infections (170). Mucoid strains of *P. aeruginosa* have a mutation in *mucA*, the gene that codes for a repressor of alginate production, which leads to overproduction of alginate-based biofilm matrix (171). *P. aeruginosa* PAO1 is non-mucoid, thus alginate is not a major component of the PAO1 biofilm matrix (171). Pel is known to control *P. aeruginosa* pellicle formation and is essential for

attached biofilm maturation but is not required to initiate attached biofilm formation (172). Pel is composed of *N*-acetylgalactosamine and *N*-acetylglucosamine (173). The extracellular polysaccharide Psl is the primary biofilm matrix in *P. aeruginosa* PAO1 (174, 175). Psl is composed of mannose and galactose monomers (176, 177) and plays a role in biofilm initiation (178, 179) and adherence to biotic and abiotic surfaces (178). Psl is readily stained by the mannose-binding lectin, concanavalin A (180), which is commercially available as a conjugate to many different fluorophores.

The polysaccharide component of the *E. coli* biofilm matrix is composed of cellulose (181, 182), poly- β -1,6-*N*-acetyl-D-glucosamine (PGA) (181, 183), and colanic acid (181, 184). Cellulose is the major structural polysaccharide in *E. coli* biofilms (182, 185). PGA is an adhesin that is involved in cell-to-cell adhesion and abiotic surface attachment (183). Colanic acid plays a role in biofilm maturation (186–188) and has been implicated in stress response to desiccation (189, 190). The cellulose component of *E. coli* biofilm matrix can be stained with UV-fluorescent Calcofluor White (181, 191). While the matrices of both *P. aeruginosa* and *E. coli* have been well-studied in monoculture, an extensive search of the current literature did not yield any studies which investigated *E. coli* and *P. aeruginosa* matrix composition in mixed culture. Therefore, the mixed-species *E. coli* and *P. aeruginosa* biofilm matrix distribution will be investigated in flight and ground controls.

Biofilm matrix staining can reveal additional information about biofilm structure which cannot be revealed with cell staining alone, such as local distribution of matrix type and matrix thickness with and without disinfectant treatment. Concanavalin A (ConA) conjugated to Alexa Fluor 633 (ThermoFisher cat no. C21402), and Calcofluor

White (Biotium cat no. 29067) were tested in combination with anti-GFP conjugated with Alexa Fluor 488 and anti-mCherry conjugated with Alexa Fluor 594 for single-step staining. A single staining buffer was mixed in D-PBS with both antibodies (5 $\mu\text{g}/\text{mL}$ each), ConA (200 mg/mL) and Calcofluor White (0.8 mM). The wells of a BioCell containing 2-week old *E. coli* and *P. aeruginosa* mixed-species biofilms were filled with the staining buffer and incubated for 15 minutes at ambient temperature in a dark room, then triple rinsed and refilled with D-PBS. The stained wells were imaged by confocal microscopy with an Olympus FluoView FV-1000 confocal microscope, equipped with an Olympus UMPlanFL N 60X/1.00 water immersion lens, which has a 2 mm working distance. Micrographs were captured in a darkroom using a 488 nm argon laser for GFP, a 559 nm diode laser for mCherry, a 635 nm diode laser for ConA conjugated with Alexa Fluor 633, and a 405 nm diode laser for Calcofluor white. To capture all four fluorophores, each view was captured twice a z-stack. The first capture used the 488 nm laser to detect GFP and the 559 nm laser to capture mCherry using sequential imaging. The second capture used the 405 nm laser to capture Calcofluor white and the 633 nm laser to capture ConA using sequential imaging. ImageJ (192), accessed by Fiji (193), was used to make minor adjustments to brightness and contrast to the micrographs, then all four dyes were overlaid to create a composite image. The Z-stacks were Z-projected using maximum intensity projection, and rendered into 3-dimensional images using 3D-Viewer (194). Biofilms in the BioCell typically grow segregated, with *P. aeruginosa* colonizing the Teflon membrane and *E. coli* colonizing the stainless-steel surface. Thus, both surfaces were captured in a single well to show verify that calcofluor white selectively stained *E. coli* matrix and ConA selectively stained *P. aeruginosa* matrix.

Microscopy shows that Calcofluor White (blue) detected *E. coli* (red) biofilm matrix (Figure 21A), and ConA (yellow) was typically associated with *P. aeruginosa* biofilm matrix (Figure 21B). Moreover, the addition of anti-GFP and anti-mCherry antibodies did not prevent ConA or Calcofluor white staining, which showed that GFP and mCherry signal could be enhanced and the matrix could be stained in a single step.

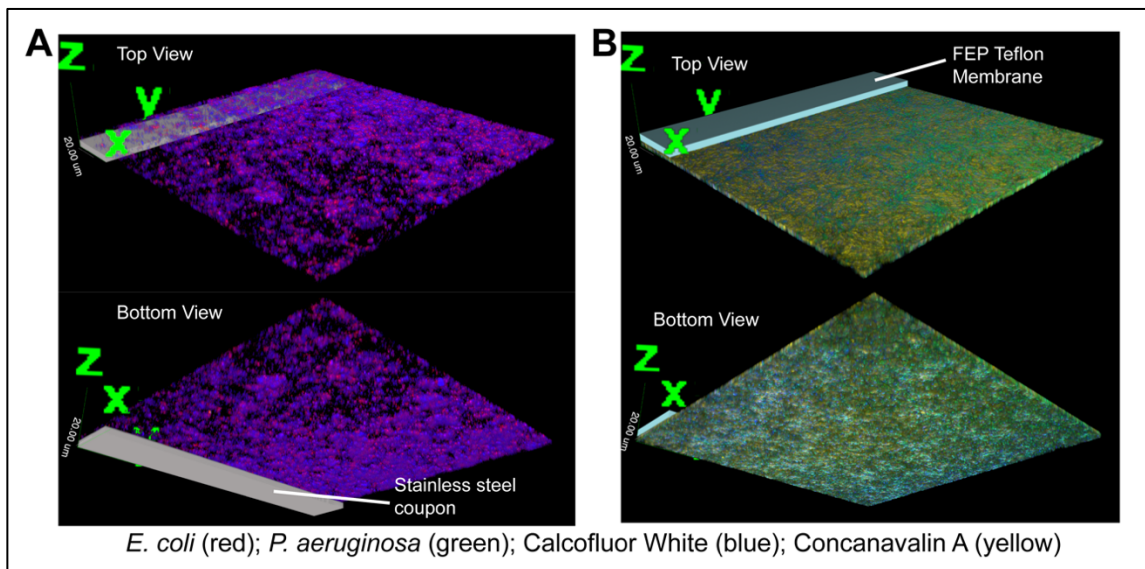


Figure 21. Biofilm matrix staining. Staining with ConA (yellow) and Calcofluor White (blue) of mixed-culture *E. coli* (red) and *P. aeruginosa* (green) biofilms allowed differentiation of matrix associated with each cell species. **A)** *E. coli* biofilm matrix on stainless-steel, which was primarily composed of cellulose, was stained blue with Calcofluor White. **B)** *P. aeruginosa* biofilm matrix on FEP Teflon, which was primarily composed of PSL, was stained yellow with concanavalin A. The addition of anti-GFP and anti-mCherry antibodies conjugated with the cognate fluorophores did not prevent ConA or Calcofluor White staining.

Experimental Timeline

Biosafety Level 2 organisms, such as *E. coli* and *P. aeruginosa*, must remain contained at all times in space flight. Changing the media in the BioCells during flight would greatly increase the likelihood that *E. coli* and *P. aeruginosa* containment would

not be maintained, posing a risk to astronauts on the ISS, so changing media in flight is not an option. However, sample integrity must also be considered. Therefore, the experimental timeline is limited by the amount of time that *E. coli* and *P. aeruginosa* biofilms can survive in the BioCell. To determine survival, BioCells were filled with mAUM.v4, inoculated with frozen and thawed *E. coli* and *P. aeruginosa* mixed inoculum, and incubated for 4, 14, 24, 42, and 56 days at Arizona State University. After incubation, the BioCells were fixed with 4% PFA, then cold-shipped to Texas State University. At Texas State, the BioCells were washed three times with cold D-PBS, then refilled with D-PBS and imaged by confocal microscopy.

At 4 and 14 days, biofilm growth was apparent on the stainless-steel surface (Figure 22). At 24 days, there was a notable loss of biofilm, but fluorescing bacterial cells were still present. At 42 and 56 days, no GFP or mCherry were detected. Thus, our early, middle, and late biofilm time points were set to 4 (+/- 1), 14 (+/- 1) and 24 (+/-3) days for flight.

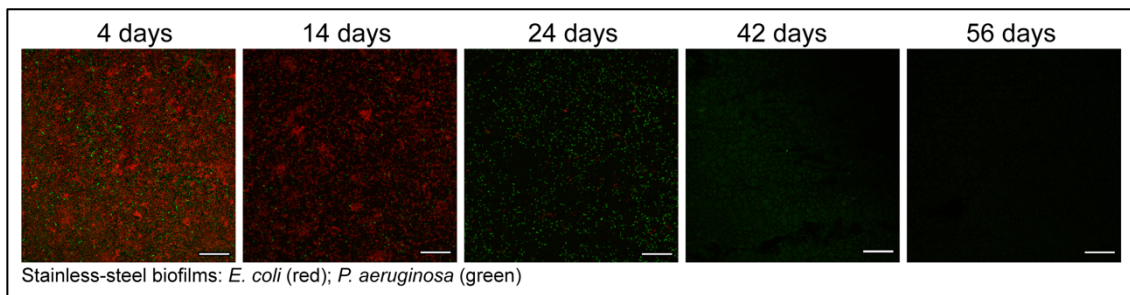


Figure 22. Biofilm survival on stainless steel in the BioCell. Mixed culture biofilm growth of *E. coli* (red) and *P. aeruginosa* (green) on the stainless-steel coupon in the BioCell for 4, 14, 24, 42, and 56 days showed that biofilm was only detectible at 4, 14, and 24 days, as determined by GFP and mCherry fluorescence. Images are maximum z projections. Scale bars = 30 μ m.

As was shown previously, GFP and mCherry fluorescence begins to degrade notably after approximately 1 month of storage in PFA. The expected time from sample packing to PI handover for the return flight from the ISS is approximately 1-2 weeks. Therefore, it is necessary that all samples are fixed as close as possible to the unberthing of SpaceX Cargo Dragon from the ISS, as this is the return mission for our samples. To facilitate this effort, the in-flight inoculation of our bacterial samples into the BioCells was scheduled using a staggered inoculation method (Figure 23), so that all samples could be fixed at approximately the same time. Although a staggered inoculation method will be used, all BioCell wells will be loaded with media at the same time before flight, from the same batch of media, to avoid unintended changes from batch-to-batch differences in concentration or media age.

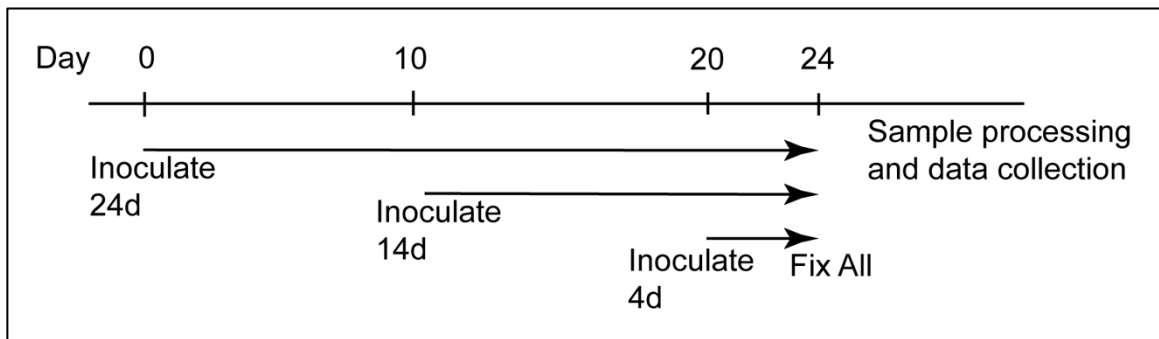


Figure 23. Inoculation and fixing timeline for the flight experiment. To minimize the exposure time to PFA, and thus prevent the loss of fluorophore brightness, the flight experiment will use a staggered bacterial inoculation and simultaneous fixing, the latter of which will occur as late as possible.

Statistical Analysis and Graphing

Statistical analysis and graphing were carried out using R (Version 3.5.1) (195), accessed by RStudio (Version 1.2.1335) (196) on macOS Catalina (Version 10.15.6). For

statistical analysis, the packages dplyr (197), scales (198), and broom (199) were used. All graphs were plotted using ggplot2 (200) with functions from reshape2 (201), tidyr (202), gridExtra (203), and plotrix (204) applied as needed.

Conclusion

Each of the individual parameters for the flight experiment have been optimized. To summarize the flight method, all BioCells will be filled with a single batch of mAUM.v4, with and without 400 ppb AgF, and loaded into P-HABs. In-flight, the BioCells will be inoculated with single-dose mixed-species inoculum suspended in FM using a staggered inoculation schedule (**Figure 21**). The mixing of FM and mAUM.v4 will result in the correct formulation of mAUM.v3. Inoculated BioCells will be returned to the P-HAB and incubated at ambient temperature for 4 (+/- 1), 14 (+/- 1) and 24 (+/-3) days, then all samples will be fixed with 4% PFA for microscopy or preserved with RNAlater II for transcriptomics as close to unberthing as possible. Upon sample return, PFA-fixed BioCells will be triple-washed with D-PBS and imaged via confocal microscopy, then the coupons will be removed from the BioCells and stored in HEPES for E-SEM imaging. The use of HEPES is discussed in Chapter 3. After E-SEM imaging, the biofilms will be removed from the coupons by sonication, and the coupons will be reanalyzed for corrosion using high-vacuum SEM and EDS analysis as needed. All imaging analysis will take place at Texas State University. The RNAlater II preserved BioCells will be returned to Arizona State University for RNA-seq and subsequent transcriptomic analysis.

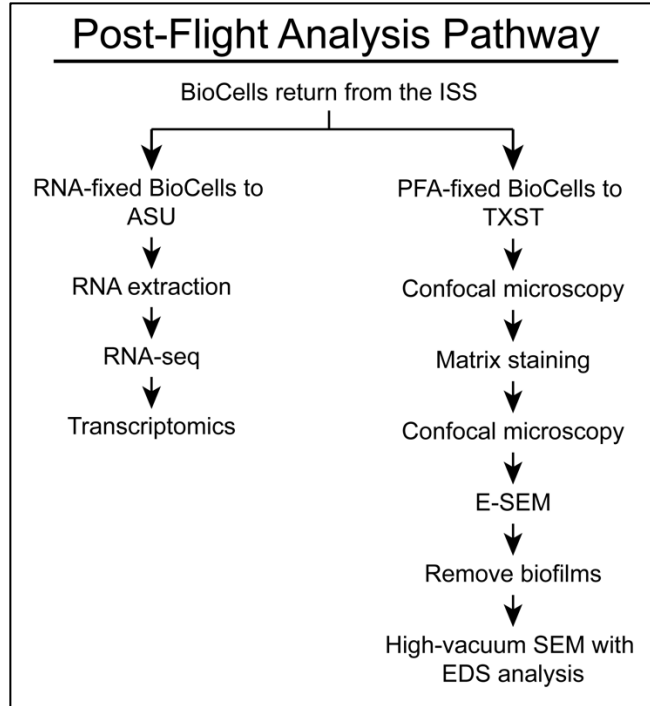


Figure 24. Post-flight analysis pathway. After the BioCells are returned to Earth from the ISS, the RNA-preserved BioCells (**left**) will be shipped to Arizona State University (ASU) for RNA extraction, RNA-seq, and transcriptomics analysis. PFA-fixed BioCells (**right**) will be returned to Texas State University (TXST) for confocal microscopy, matrix staining, environmental SEM, and high vacuum SEM with EDS analysis as needed.

III. GROUND-BASED BASELINE OF LONG-TERM DISINFECTION OF BIOFILMS BY SILVER FLUORIDE

Biofilm ECM confers increased antibiotic and disinfectant tolerance by serving as a diffusion barrier (205–207). Microorganisms in a biofilm community accumulate signaling molecules, metabolic byproducts, and bacteriocins which can contribute to microbial acclimation, resulting in enhanced antibiotic and disinfectant tolerance, which is conferred in part by the biofilm matrix (207–210). The term tolerance is used because microorganisms regain susceptibility to antimicrobial agents when they leave the sessile biofilm population and enter the unattached, planktonic population (211).

Biofilms represent a major risk to sustainable water filtration systems due to long-term persistence and difficulty of disinfection. Of note, biofilms can clog filtration substrate and cause material corrosion, damaging system function, integrity, and sustainability (6, 102). Due to persistence and increased tolerance to disinfectants, biofilms represent a major risk in supporting sustainability of water purification systems in various industries (212). The Water Recovery System (WRS) of the Environmental Control and Life Support System (ECLSS) on the International Space Station is one such system. WRS provides water to astronauts on the ISS by collecting waste water in the form of astronaut urine, sweat, and breath vapor and purifying it to potable water (17). In ECLSS, a persistent biofilm has formed that resists long-term disinfection (21). There is an urgent need to develop effective disinfection strategies against such biofilms because astronauts on board rely on ECLSS as their primary source of drinking water.

Current strategies in water treatment for biofilm control include prevention and disinfection. To prevent biofilm formation, anti-biofilm materials and finishes, which

have been precleaned, are used during construction of equipment (213). On ISS, iodine salts are used to disinfect water treated in ECLSS (16), and ionic silver is used to disinfect water treated by SRV-K, the Russian water recovery system (20). Prolonged exposure to iodine can cause hypothyroidism and sensitivity reactions (19). By contrast, ionic silver is safe for human consumption except at very high concentrations (214). Ionic silver has also been identified by NASA as a potential disinfectant to be used on future long-term space missions at concentrations up to 400 parts per billion (ppb) (146).

Silver-based disinfection has previously been found to be effective against biofilms in long-term studies (215, 216), although these studies primarily investigated cell viability through colony counts (215, 216), presence/absence detection of specific species through molecular techniques (216), or by detecting biomass using staining techniques (217). While some studies have used microscopy to observe biofilms which have been treated with silver, such studies have only investigated silver penetration and aggregation in the biofilm matrix (29, 218) and have not investigated biofilm structure with respect to distribution of specific cell types in biofilms formed on stainless steel.

Ionic silver is known to be toxic to bacterial cells in the +1 ionic form (140, 141). Both *P. aeruginosa* and *E. coli* display resistance to silver toxicity. *P. aeruginosa* is resistant to silver disinfection by production of the antimicrobial reducing agent, pyocyanin, which converts Ag^{1+} to the elemental form (Ag^0) in aerobic conditions (140). In *E. coli*, silver resistance is conferred by two point mutations that result in the loss of the porin, OmpF, resulting in decreased outer membrane permeability, and increased expression of the Cus efflux system, which allows silver ions to be transported out of the cell (219).

As of 2016, nine urinary tract infections (UTIs) have been reported in space flight (220). Space flight-associated risk factors, such as urinary retention due to incomplete voiding of the bladder in the low gravity environment, delayed access to facilities, and unclean urinary collection devices may increase the risk of UTI infection for astronauts in space flight (221). Thus, we have selected *E. coli* F11, which was isolated from a patient with clinical cystitis (125) and the *P. aeruginosa* standard strain, PAO1, which were grown in an artificial urine medium for this study. To investigate long-term disinfection on the presence of UTI pathogens in the ECLSS WRS, we developed a long-term study to investigate the formation, structure, disinfection tolerance, population composition, attachment substrate effects, and gene expression in mixed species *P. aeruginosa* and *E. coli* biofilms in the presence of Ag¹⁺.

Materials and Methods

Overview

This section utilizes samples which were prepared as described in Chapter 2. At Arizona State University, BioCells were filled with mAUM.v4 and stored at 4°C for 7 days to simulate the time between BioCell loading and experiment initiation after launch to the ISS. The BioCells were inoculated using frozen and thawed inoculum in FM, then incubated for 4, 14, and 24 days according to the schedule outlined in **Figure 23**. All BioCells were fixed simultaneously and then shipped to Texas State University for post-fix washing, microscopy, and analysis.

Bacterial Culture in BioCells

For confocal microscopy, three BioCells were used as the culturing vessels. The BioCells were filled, inoculated, and incubated at Arizona State University. All wells

were filled on the same day with 1.7 mL mAUM.v4 and stored at 4°C for 7 days (24-day BioCell), 17 days (14-day BioCell), or 27 days (4-day BioCell) to simulate handover, launch, and storage time during the flight experiment, as per the staggered inoculation schedule discussed in Chapter 2 (**Figure 21**). After storage, each BioCell was warmed and inoculated with 6.4×10^5 CFU *E. coli* F11 and 1.86×10^5 CFU *P. aeruginosa* PAO1 in frozen-thawed FM, as these are the cell numbers which are recovered from frozen FM after thawing. Ag¹⁺ treated wells contained AgF at 400 ppb. The BioCells were incubated for 4 days, 14 days, or 25 days at room temperature in the P-HAB. Of note, the BioCells were incubated in a vertical orientation as a result of the design of the P-HAB (**Figure 19 A, B**). During incubation, bacterial cell settling was noticed at the bottom edge of the wells. Thus, the 3.5 week BioCell was mixed once during incubation by briefly inverting the BioCell, and then returning the BioCell to the original orientation. After this initial mixing, it was decided that mixing was not necessary and may lead to artifacts in the data, so this mixing step was not repeated with the other BioCells. After incubation, biofilms were fixed with 4% PFA at 4°C for several days, then packed and cold-shipped to Texas State University. Upon receipt, the BioCells were unpacked and stored at 4°C overnight, then triple washed with D-PBS. Washed BioCell wells were filled with D-PBS for storage and microscopy.

E-SEM

After confocal analysis was complete, the coupons were removed from the BioCells for E-SEM and SEM analysis. D-PBS was removed from the wells, and the FEP Teflon membrane was cut with a sterile scalpel and discarded. The coupons were gently removed from the pedestal and submerged in D-PBS or 0.1 M HEPES (pH 7.4) (222) for

transport to the SEM lab. In the SEM lab, the coupons which were stored in D-PBS were directly loaded to the sample pin. Imaging with D-PBS showed that the high concentration of sodium ions may have altered the architecture of the biofilm (**Figure 25**), so the remaining coupons were stored in 0.1 M HEPES which did not appear to alter the biofilm structure. The coupons which were stored in 0.1 M HEPES were dipped once in deionized water before loading the sample pin, as residual HEPES blocked electrons from reaching the sample surface. All samples were attached to a sample pin using carbon tape. Environmental scanning electron microscopy (E-SEM) was carried out with a JEOL JSM-6010 PLUS/LA SEM using low vacuum (50 Pa) mode.

Results and Discussion

Characterization of Long-Term Biofilm Growth in BioCells

Population dynamics of biofilms grown in the BioCell were different depending on the surface on which the biofilm formed. Early biofilms on the stainless-steel coupons (**Figure 25 A**) were *E. coli* dominated, but at 14 days the *E. coli* (red) cell number dropped notably, and *P. aeruginosa* (green) was present in higher numbers. At 24 days, the biofilm on the stainless steel was nearly undetectable, which may have been due to loss of viability from lack of nutrients, or dispersion of bacterial cells from the biofilm into the liquid media. Dispersion can be induced by poor nutrient availability, as has been shown in *P. aeruginosa* (223). Biofilm formation on the gas permeable FEP Teflon membrane may alter the rate of gas diffusion through the membrane, changing the oxygenation level at the stainless steel surface. Thus, biofilms formed on FEP were also examined. FEP Teflon-associated biofilms (**Figure 25 C**) showed a different trend than biofilms formed on the stainless steel. At 14 days, *E. coli* had established growth on the

Teflon surface and *P. aeruginosa* biofilms were becoming patchy. At 24 days, the FEP Teflon was more predominantly colonized by *E. coli* and *P. aeruginosa* was present only as isolated cells. This change in the biofilm population may have been caused by the mixing of the 24 day BioCell as well as the vertical incubation orientation of all BioCells. It was noted in batch culture that *E. coli* in mAUM readily sedimented to the bottom of the culture. Incubating the BioCells in the vertical orientation, as well as mixing the 3.5 week BioCell during incubation may have increased *E. coli* access to the FEP Teflon membrane, which may be one method of *E. coli* introduction to the FEP Teflon surface.

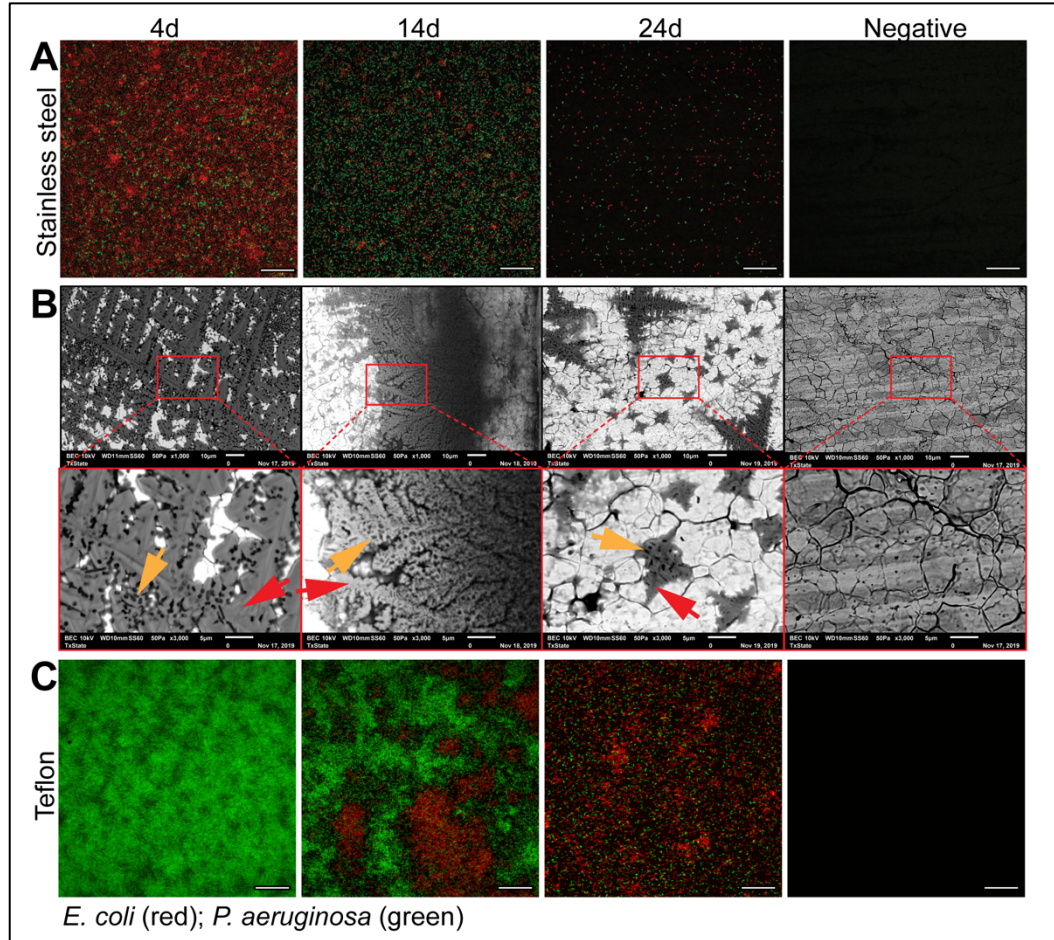


Figure 25. Mixed-culture biofilm growth in mAUM. **A)** Biofilm growth on stainless-steel coupons is *E. coli* (red) dominated, especially in 4-day biofilms. At 14 days, more *P. aeruginosa* (green) are present on the stainless steel. At 24 days, the stainless-steel associated biofilm is nearly undetectable. Negative refers to wells which were filled with mAUM, but not inoculated. **B)** E-SEM micrographs show that the loss in fluorescence is consistent with the loss of biofilm coverage. Yellow arrows indicate representative cells, seen as dark spots. Red arrows indicate possible sodium-disrupted biofilm matrix and sodium crystals, which had a “leafy” appearance. **C)** Biofilms associated with the FEP Teflon membrane are *P. aeruginosa* dominant in early growth. After 14 days, *E. coli* infiltrated the *P. aeruginosa* biofilm on the FEP Teflon surface. At 24 days, *P. aeruginosa* biofilm on the FEP Teflon surface was reduced relative to the earlier time points. Images are maximum z-projections. All scale bars = 30 μm.

As described in Chapter 2, the P-HAB design is limited to two small vents on the lid to allow air flow, and the only site of gas exchange in the BioCell is at the FEP-Teflon membrane. As a result, there was likely an oxygen gradient present between the gas

permeable FEP Teflon membrane and the stainless-steel surface, which may have contributed to the population differences seen in the stainless steel and Teflon associated biofilms. This hypothesis was supported by the observation of elongated *P. aeruginosa* cells on the stainless steel surface (**Figure 26 A**), which is a change in *P. aeruginosa* morphology known to be due to incomplete cellular division associated with biofilm growth in low-oxygen environments (224). *P. aeruginosa* cell elongation was seen in biofilms grown in the P-HAB (**Figure 26 B**), but not in biofilms formed in foil-wrapped BioCells (**Figure 26 A**), suggesting that the limited air flow in the P-HAB may have been due to a microaerobic or anaerobic growth condition at the stainless-steel surface. A reduced oxygen concentration may have caused a change in competition dynamics between *P. aeruginosa* and *E. coli* at the stainless-steel surface, as pyocyanin antimicrobial activity has been shown to be reduced in an anaerobic environment in minimal media (225).

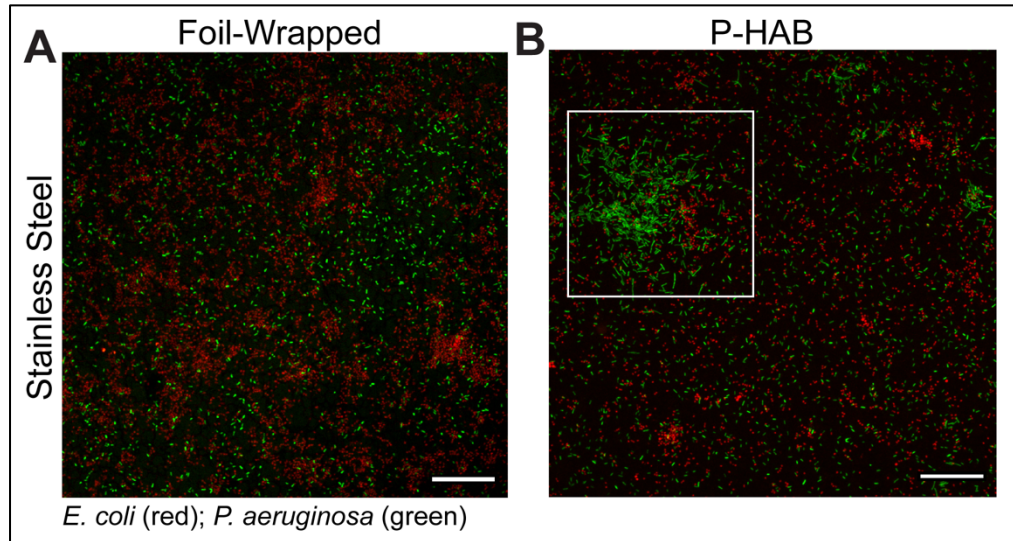


Figure 26. *P. aeruginosa* (green) cell elongation was seen in P-HAB-incubated BioCells, but not in foil-wrapped BioCells. **A)** *P. aeruginosa* in foil wrapped BioCells displayed normal cell length on the stainless-steel surface. **B)** *P. aeruginosa* cells were elongated on the stainless-steel surface of P-HAB incubated BioCells (white box). Images are maximum z projections. Scale bars = 30 μm .

In early biofilm growth, qualitative analysis showed more *P. aeruginosa* on the FEP Teflon membrane, where oxygen was entering the BioCell, than at the stainless-steel surface, where oxygen concentration may have been lower (**Figure 25 A, C**). Indole production by *E. coli* inhibits pyocyanin production in *P. aeruginosa* by inhibiting quorum signaling (112); thus, indole production promotes *E. coli* survival in long-term mixed culture with *P. aeruginosa* (112, 226). At 14 days, *E. coli* infiltration into the FEP Teflon membrane-associated biofilm was observed (**Figure 25 C**). Over long term culture, indole concentration may increase (112), which could cause a stronger suppression of *P. aeruginosa* quorum signaling, possibly inhibiting production of pyocyanin (112). In the absence of pyocyanin, *E. coli* survival may increase, which might allow infiltration of *E. coli* into the FEP Teflon membrane-associated *P. aeruginosa* biofilm, as seen at 14 days (**Figure 25 C**). Additionally, incubating the BioCell vertically

may have increased *E. coli* access to the FEP Teflon membrane, which could promote *E. coli* infiltration. One study that investigated *E. coli* retention to *P. aeruginosa* biofilms in glass-bead filters found that *E. coli* cells passed through the filter were retained by previously established *P. aeruginosa* PAO1 biofilms (227). *E. coli* has also been shown to induce dispersion in *P. aeruginosa* biofilms by binding cyclic-diguanylate (c-di-GMP), which reduces the amount of c-di-GMP signal in the immediate environment (228). The reduction in c-di-GMP signal was shown to induce *P. aeruginosa* to transition to the planktonic form (228). Vertical incubation of the BioCell may have increased *E. coli* to access to the *P. aeruginosa* biofilm, after which, *E. coli* mediated binding of c-di-GMP may have induced dispersion in *P. aeruginosa*.

On the stainless-steel surface, there appears to be a reduction of *E. coli* cell number seen at 14 days (**Figure 25 A**), which may indicate that *E. coli* have migrated from the stainless-steel surface to the FEP Teflon membrane, or that incubating the BioCell vertically promoted adherence to the *P. aeruginosa* biofilm. There also appears to be an increase in *P. aeruginosa* cell density on stainless steel from 4 to 14 days, which may indicate displaced bacterial cells from the FEP Teflon membrane induced by *E. coli* induced dispersion or as an artifact from incubating the BioCells vertically.

E-SEM imaging confirmed that the loss of fluorescence seen with biofilm age was associated with a loss in biofilm coverage (**Figure 25 B**), and was not the result of a loss of fluorescence. The coupons imaged in **Figure 25 B** were stored in D-PBS prior to loading to the E-SEM. The highly ordered leaf-like or star-like pattern seen has been associated with *E. coli* biofilms dried after treatment with saline (229). The formation of the leafy pattern in this experiment was potentially the result of storage in D-PBS

combined with biofilm drying while loading to the E-SEM. To prevent unintended damage to the biofilm structure, the 4- and 14-day AgF-treated biofilms were stored in HEPES and rinsed once with deionized water immediately before loading to the SEM.

Mixed Culture Biofilm Growth with Silver

When treated with 400 ppb AgF, *P. aeruginosa* is not detected at 4 or 14 days post inoculation (**Figure 27 A,C**). Resistance to ionic silver in *P. aeruginosa* is conferred by pyocyanin, which reduces the antimicrobial Ag¹⁺ to biologically inactive elemental Ag⁰ (140). In the presence of *E. coli*, pyocyanin production has been shown to be inhibited (112), thus *P. aeruginosa* may have lost the silver resistant phenotype in coculture with *E. coli*, resulting in no detection at these time points (**Figure 27 A, C**). E-SEM reveals the absence of biofilm coverage on the substrate, suggesting that the absence of fluorophore detection in confocal microscopy indicated the absence of biofilm, and not a loss of GFP and mCherry fluorescence (**Figure 27 B**). In *E. coli*, silver resistance has been shown to develop in 6 days (219). This is consistent with the finding here. In early biofilm growth, neither species was detected on either the stainless-steel coupon (**Figure 27 A**) or the FEP Teflon membrane (**Figure 27 C**). After 14 days incubation, *E. coli* biofilms were detected on both the stainless steel and the Teflon surfaces.

At 24 days, three distinct responses to AgF treatment were seen (Figure 27C). One response was characterized by primarily *E. coli* growth (N = 10, 47.6% of total wells) (**Figure 27 C, left; Figure 28 B**), the second was characterized by *P. aeruginosa* growth (N = 6, 28.6% of total wells) (**Figure 27 C, center; Figure 28 B**), and in the third, neither species was detected (N = 4, 19.0% of total wells) (**Figure 28 B**). In one instance,

both species survived in the presence of Ag^{1+} (N = 1, 4.8% of total wells). To determine if the different responses types were the same phenotypes reoccurring, the images from each well were classified as either *E. coli*-dominated (Ec), *P. aeruginosa*-dominated (Pa), no survival (None), or both species survived (Both), then analyzed by uCounter (<https://github.com/alistair-mclean/ucount.git>) to determine percent coverage of each species. Plotting the percent coverage showed that four distinct phenotypes arose repeatedly after long-term treatment with 400 ppb AgF (**Figure 28 A**). Each phenotype showed percent coverage that was tightly clustered across multiple replicates. *E. coli* coverage in *E. coli*-dominated wells on FEP Teflon was less tightly clustered, but since Teflon-associated *E. coli* biofilms tend to be patchy (**Figure 27 C**) this was not surprising.

Storage of the coupons in 0.1 M HEPES buffer with a deionized water rinse prevented sodium-associated damage to the biofilm structure in the 4- and 14-day biofilms (**Figure 27 B**). The 24-day biofilm, which was imaged first, was stored in D-PBS prior to imaging. Time constraints limited the number of coupons that could be analyzed by E-SEM, so the coupons for all three distinct phenotypes – *E. coli*-dominated, *P. aeruginosa*-dominated, and neither species present (**Figure 27D**) were not able to be imaged. The coupon shown in **Figure 27 B** was an *E. coli*-dominated well (**Figure 27 D**, left), which was chosen since the *E. coli*-dominated wells were seen the most frequently (Figure 28B).

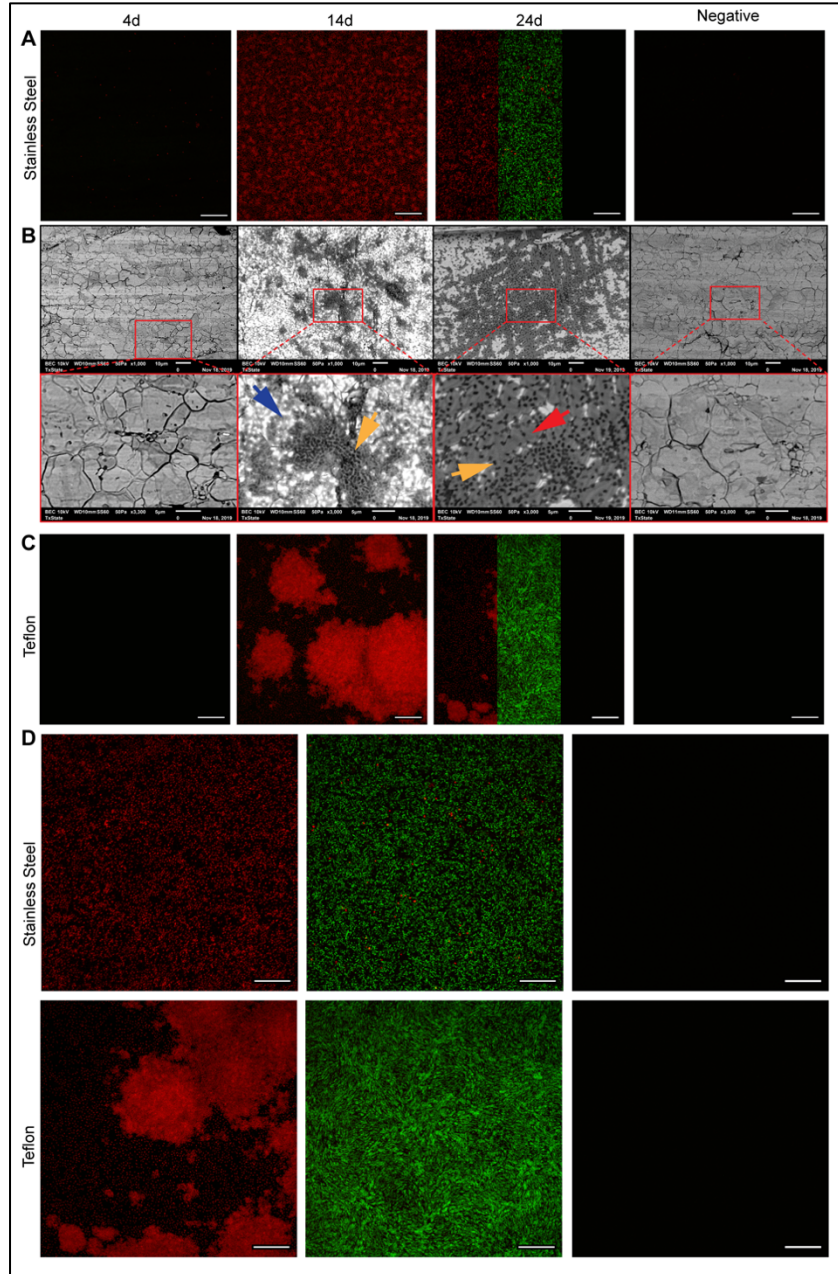


Figure 27. Mixed culture biofilm growth in mAUM with Ag¹⁺. Long-term biofilm growth with 400 ppb AgF on A) stainless steel coupon was delayed, with no growth apparent at 4 days and *E. coli* (red) growth at 14 days. At 14 days, *P. aeruginosa* (green) growth was not detected. B) SEM micrographs show that the absence of fluorescence at 4 days was consistent with a lack of biofilm coverage. Yellow arrows indicate representative cells, seen as dark spots. Red arrows indicate possible sodium-disrupted biofilm matrix and sodium crystals. Blue arrows indicate undisrupted biofilm matrix. C) Biofilms on the Teflon membrane show population dynamics that were consistent with biofilms on stainless steel. D) At 24 days, three distinct phenotypes were found. Note that the 24-day images in A) and B) are composites of the images in D). All scale bars = 30 μ m.

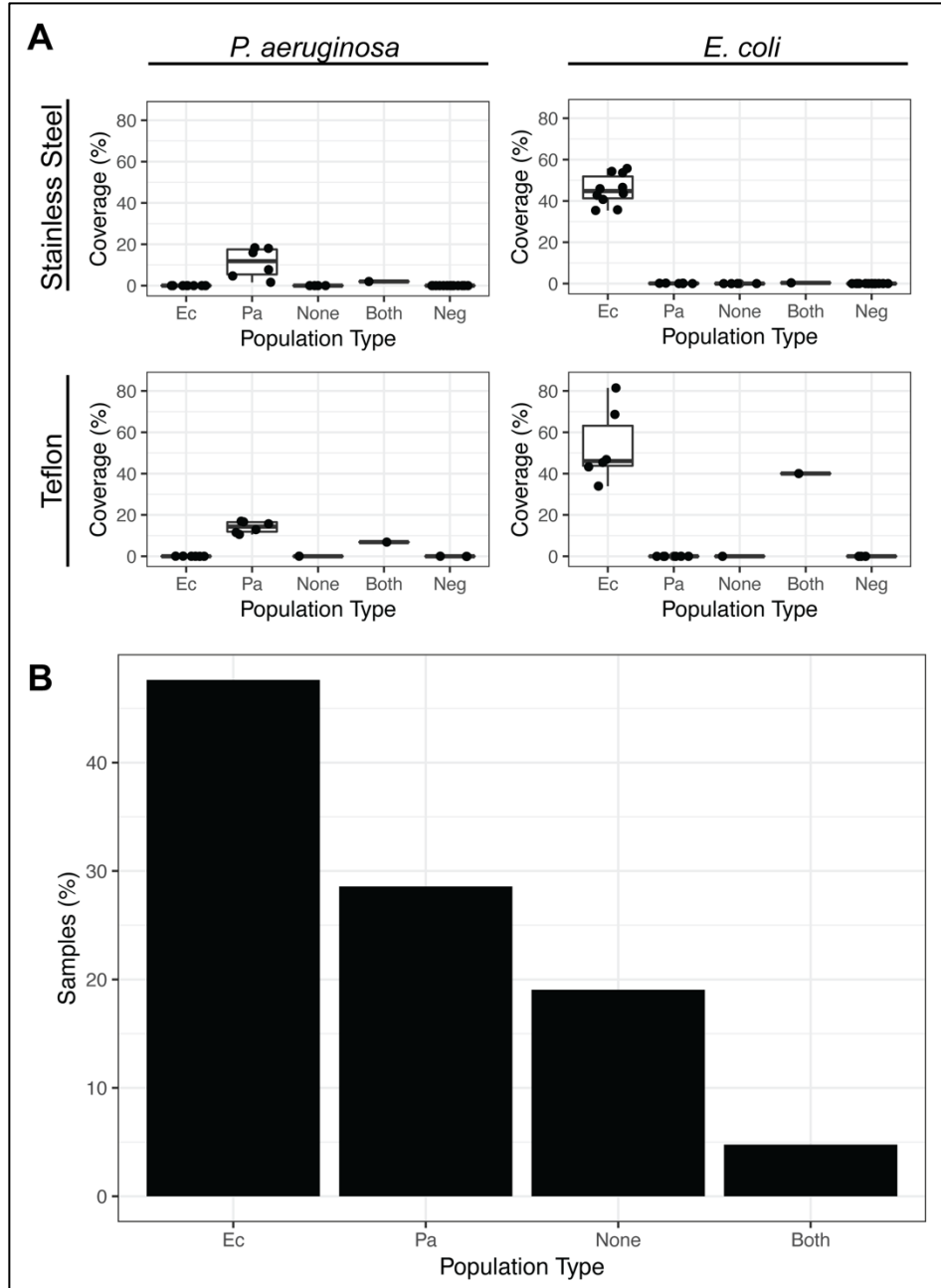


Figure 28. Effect of long-term treatment with 400 ppb AgF on phenotype. A) Coverage of *P. aeruginosa* (left) and *E. coli* (right), on stainless steel (top) and FEP Teflon (bottom) in 24-day mixed culture biofilms with 4 distinct population distributions in response to treatment with 400 ppb AgF. Population type describes the dominant species in each set of biofilms. **B)** Proportion of total 24-day AgF treated biofilms that display each population distribution. (Neg: Uninoculated control; Ec: *E. coli* dominated phenotype, N = 10; Pa: *P. aeruginosa* dominated phenotype, N = 6; None: Neither species detected, N = 4; Both: Both species detected with high proportion: N = 1).

Mixed culture biofilms of *E. coli* and *P. aeruginosa* cultured in artificial urine start off segregated, with the *P. aeruginosa* biofilm forming at the oxygenated FEP Teflon membrane, and the *E. coli* biofilm forming on the stainless steel. After 14 days incubation, *E. coli* penetration into the FEP Teflon-associated *P. aeruginosa* biofilm is apparent, and at 24 days, *P. aeruginosa* has begun to die off, which may be an artifact due to the vertical orientation or brief mixing of the BioCell during incubation. When 400 ppb AgF treatment is added, *E. coli* shows earlier recovery against AgF challenge, may be due to point mutations associated with porins in the *E. coli* cell envelope that remove Ag¹⁺ ions from the cell interior (219). In long-term treatment, silver disinfection results in three distinct populations which can be characterized by the dominant species. The coverage of these biofilms is highly replicable, indicating that the same populations are forming multiple times as a result of silver disinfection.

IV. CORROSION

A study released by the US Federal Highway Administration in 2002 estimates the cost of corrosion to have been \$276 billion, 3.1% of the United States' gross domestic product in 2002 (230). It is estimated that as much as 20% of corrosion is due to microbially induced corrosion (MIC) (231), which would put the cost of MIC at \$55.2 billion in 2002. MIC occurs due to biological processes such as biofilm formation (232) and can affect materials that are considered to be corrosion resistant (233, 234). Studies have shown that various species of bacteria, in both mono- and mixed-species biofilms, contribute to corrosion of various metals, including 316L stainless steel (6, 9, 10, 14, 231, 232, 235). As discussed in Chapter 1, pitting MIC arises when 1) the pH in the microenvironment below the biofilm is lowered as a result of microbial metabolism (9) and 2) an electrical potential difference is established across the surface of stainless steel due to differences in local redox potential (9).

MIC in the WRS on the ISS poses a risk to the resident crew. Long-term unchecked corrosion can cause leaks in the WRS piping, which can lead to water loss and potential equipment problems (i.e. electrical shorts). To date, only a few studies have been conducted to investigate the potential for corrosion in the life support systems on manned spacecraft, but those studies were limited to searching for the presence of microbes which are associated with high levels of MIC, rather than looking for corrosion in the life support systems (236, 237). Other studies, which investigate MIC on various materials found on board the ISS and other manned spacecraft, do not investigate MIC on stainless steel (238–240). The presence of a persistent biofilm which resists disinfection necessitates the study of the extent and severity of corrosion in the WRS. This research

aims to investigate MIC by looking directly at 316L stainless-steel coupons which have been used as an attachment surface for biofilm growth.

Materials and Methods

The stainless-steel examined here was inoculated and incubated as described in Chapters 2 and 3.

Sample Preparation

Following incubation, the 316L stainless-steel coupons were removed from the BioCells as described above, submerged in sterile deionized water and sonicated for 10 minutes to remove the biofilms. After sonication, the coupons were rinsed with fresh sterile deionized water and air-dried overnight, then imaged with a JEOL JSM-6010 PLUS/LA SEM using high vacuum mode.

SEM imaging of a greater sample size was planned, but shutdowns due to COVID-19 halted progress. The unexamined samples were stored in PBS for months. Saline has been shown to be corrosive to 316L stainless steel (241), so the remaining samples were not reliable. As a result, only one biological replicate of each treatment was examined.

Coverage Analysis

Corrosion coverage was determined by loading micrographs of each corroded area into ImageJ (192) accessed by Fiji (193) and using the free selection tool to outline contiguous areas of corrosion. Once each corrosion site was selected, the measurement tool was used to measure the area of the corrosion site. The individual area measurements on each coupon were combined to calculate the total corroded area for each treatment.

Linear regression analysis was used to look for correlations between average spot size, number of spots, and total corroded area.

Results and Discussion

Imaging by SEM showed no obvious relationship between corrosion and each incubation time for any treatment. Biofilm growth without and with 400 ppb silver resulted in corrosion at all biofilm ages (**Figure 29 A**; **Figure 30 A**). Corrosion was also seen on uninoculated steel for all incubation times, without and with AgF (**Figure 29 B**; **Figure 30 B**). The pattern of corrosion seen on both inoculated and uninoculated steel was consistent with pitting corrosion on 316L stainless steel found in previous studies (242, 243). **Figure 29 C** and **Figure 30 C** show uncorroded 316L stainless-steel for reference.

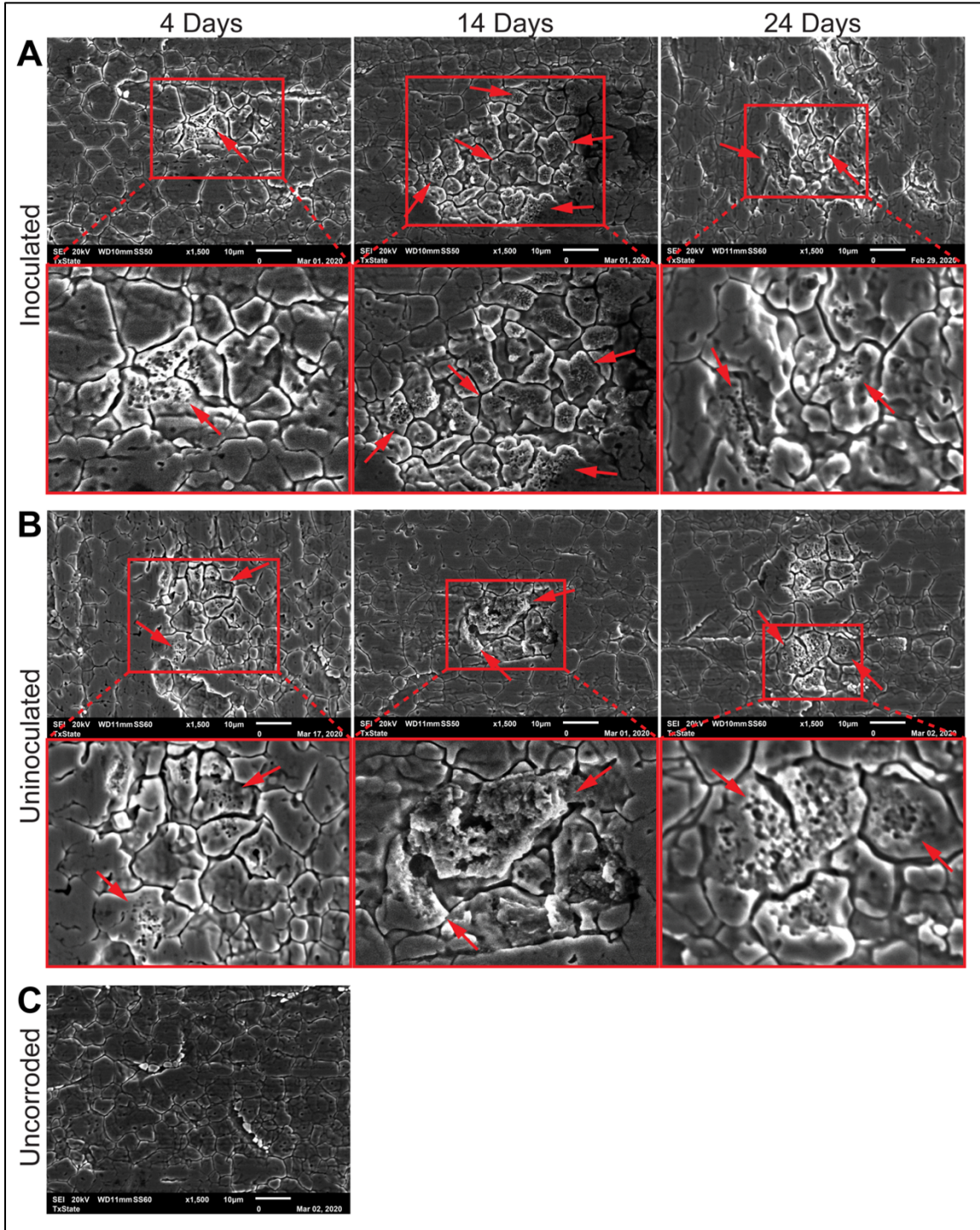


Figure 29. Corrosion on 316L stainless steel in A) inoculated and B) uninoculated mAUM. Top rows show the corrosion spot at 1500X, and the bottom rows show zoomed in views to highlight corrosion patterns, which appear as small pits in the stainless steel (red arrows). C) shows uncorroded 316L stainless steel for reference.

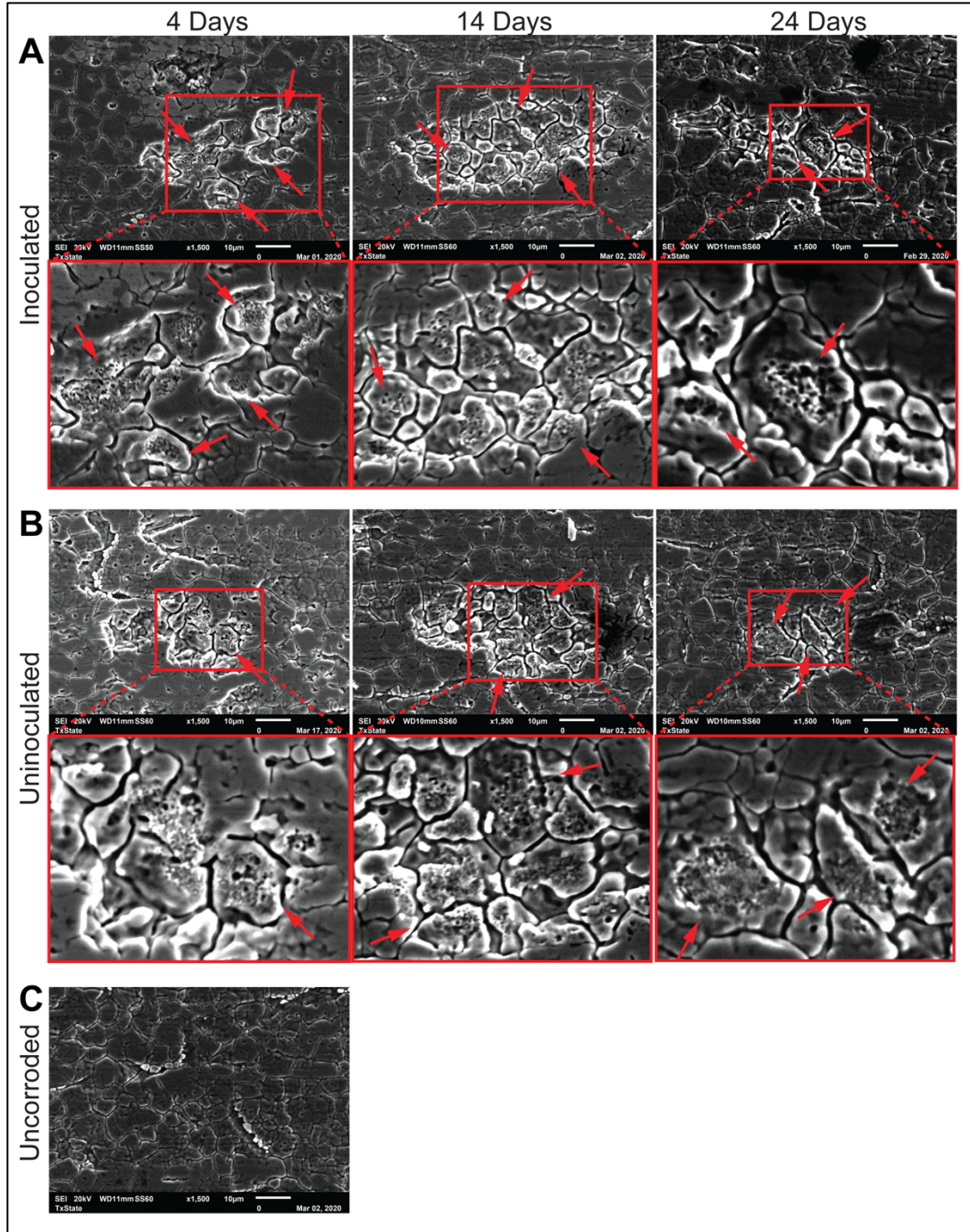


Figure 30. Corrosion on 316L stainless steel in A) inoculated and B) uninoculated mAUM with 400 ppb AgF disinfection treatment. Top rows show the corrosion spot at 1500X, and the bottom rows show zoomed in views to highlight corrosion patterns, which appear as small pits in the stainless steel (red arrows). C) shows uncorroded 316L stainless steel for reference, and is the same image in **Figure 29 C**.

Coverage analysis and spot counting showed that corrosion was highest in steel which had been incubated for 14 days, as measured by total corroded area (**Figure 32 C**). Steel which had been incubated for 14 days showed larger areas (**Figure 32 A**; three-way ANOVA with Tukey's HSD, $p < 0.001$) and more numerous spots (**Figure 32 B**) of corrosion, although it was expected that the 24-day biofilms would produce the most corrosion. This unexpected result may be due to a combined effect of the storage and incubation times and temperatures. The BioCells were loaded with mAUM.v4, then stored at 4°C for 7 days before the first inoculation to simulate the time needed to launch the BioCells to the ISS and initiate the experiment (**Figure 31**). After 7 days storage, the 24-day BioCell was removed from 4°C, inoculated, and incubated at ambient temperature. The filled 14- and 4-day BioCells remained in 4°C storage for 10 and 20 more days (17- and 27-days total, respectively) before inoculation.

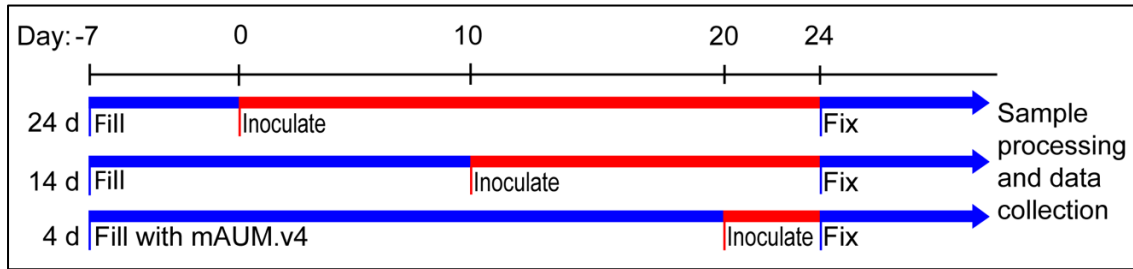


Figure 31. BioCell temperatures. This schematic shows the amount of time (in days) that the BioCells spent at each temperature over the course of the experiment. The time each sample spent at 4°C are indicated in blue, and at ambient temperature in red.

Previous studies showed that 316L stainless steel was susceptible to corrosion by artificial urine (241, 244), although it should be noted that these studies investigated corrosion on polished 316L stainless steel, which has been shown to be more resistant to

pitting than 316L stainless steel with a brushed finish, as used here (245). Based on previous reports (241, 244), it is conceivable that mAUM.4v was causing some corrosion on the stainless-steel surface during storage at 4°C. After inoculation, moving the BioCell to ambient temperature may have increased the corrosive activity of mAUM, leading to an increase in corrosion when compared to the 4-day samples, which were stored at 4°C for longer (**Figure 32 A**). This conclusion was supported by an increase in corrosion spot size on uninoculated steel which was incubated for 14 days as compared to 4 and 24 days. There was also an increase in corrosion spot size on the inoculated 14-day stainless steel, but the spot size increase was not significantly different from the uninoculated 14-day controls (three-way ANOVA with Tukey's HSD, $p = 0.96$), so we cannot conclude that the increase in corrosion area was due to MIC. However, it should be noted that there was an increase in the number of corrosion spots seen on the inoculated 14-day steel as compared to the uninoculated steel control (**Figure 32 B**).

At each incubation time, there was no significant difference in the size of the corrosion spots between inoculated and uninoculated samples (4 days: $p = 0.874$; 14 days: $p = 0.964$; 24 days: $p = 0.835$), indicating that the presence of biofilm may not contribute to corrosion spot size. At 24 days, corrosion spot size on stainless steel in silver-treated, inoculated mAUM appeared to trend to a larger spot size than on steel in uninoculated mAUM with silver fluoride; however, statistical analysis showed that there is no significant difference between corrosion spot size of the two samples (three-way ANOVA with Tukey's HSD, $p = 0.958$). There may have been an increase in total corrosion area on inoculated 24-day steel (**Figure 32 C**), but with only one biological replicate, the difference seen here was not conclusive. It may be that the corrosion seen

on 316L was electrochemical, rather than biological. Chloride ions are known to be corrosive (246) and may have been the cause of electrochemical pitting seen here.

Steel which was treated with 400 ppb AgF showed a trend of larger corrosion spots (**Figure 32 A**, blue) in both inoculated and uninoculated (negative) samples than samples without AgF (red), but this difference was not significant at any time point (Inoculated: 4 day: $p = 1.000$; 14 days: $p = 0.789$; 24 days: $p = 0.898$; Uninoculated: 4 day: $p = 0.999$; 14 day: 1.000 ; 24 day: 1.000 ; three-way ANOVA with Tukey's HSD), indicating that silver treatment may not have affected the size of corrosion spots. However, there did appear to be a smaller number of spots detected on the inoculated, silver treated steel at 14 days as compared to the inoculated steel without silver (**Figure 32 B**). The reduction in the number of corrosion spots was also consistent with a reduction in total corroded area in silver treated wells (**Figure 32 C**). Interestingly, silver treatment on uninoculated steel appeared to increase the number of corrosion spots (**Figure 32 B**) as well as the total corroded area (**Figure 32 C**), indicating that silver fluoride treatment may have resulted in electrochemical corrosion of steel in the absence of biofilm growth. This increase may have been caused by the addition of fluoride, as it is known to be corrosive (246) and has been shown to have a synergistic effect when combined with chloride, resulting in an increase in pitting potential on 316L stainless-steel (247).

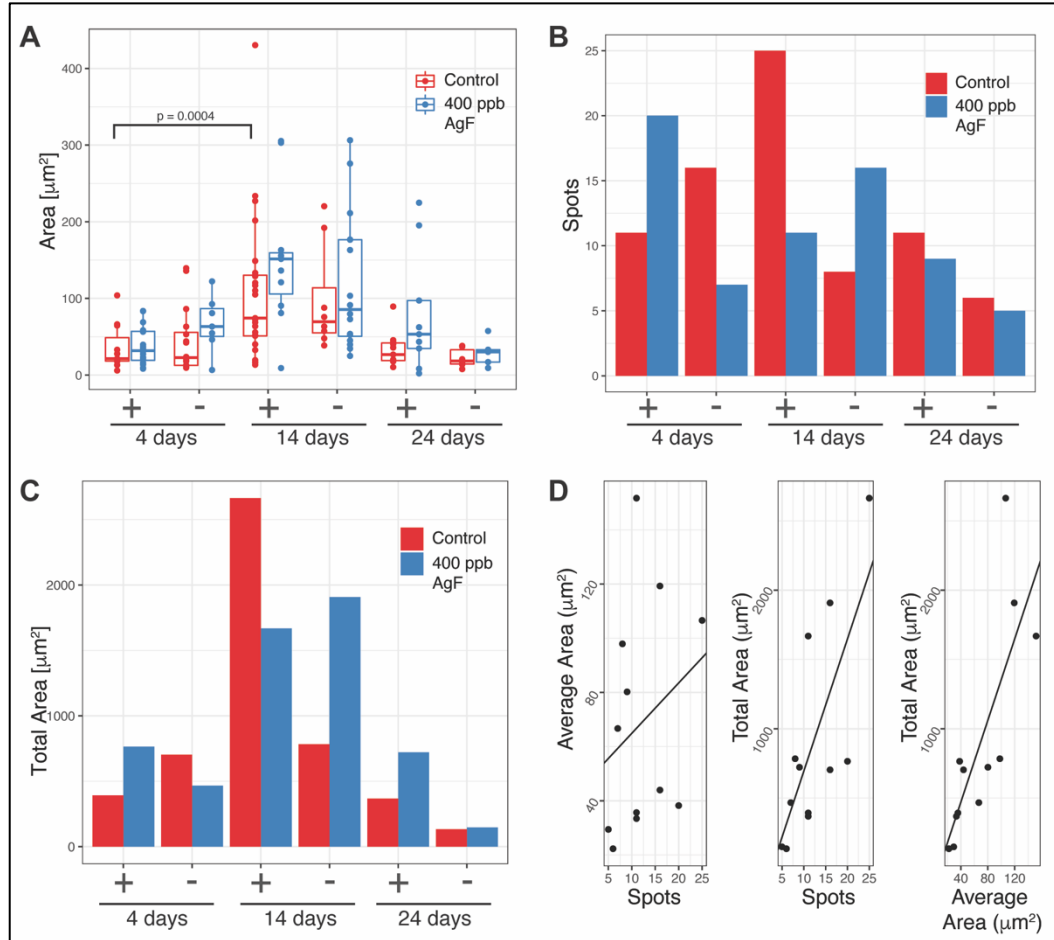


Figure 32. Coverage and quantity of corrosion spots on 316L stainless steel. A) Coverage of corrosion on stainless steel coupons incubated in mAUM without (red) and with (blue) 400 ppb AgF on inoculated (+) and uninoculated (-) steel. (Tukey’s HSD, 95% confidence interval). **B)** The number of discontinuous corrosion spots on 316L stainless steel incubated without (red) and with (blue) 400 ppb AgF on inoculated (+) and uninoculated (-) steel. **C)** Total corroded area after treatment without (red) and with (blue) 400 ppb AgF on inoculated (+) and uninoculated (-) steel. **D)** Simple linear regression analysis comparing the relationships between average spot size, number of spots, and total corroded area.

Linear regression analysis showed that the number of spots found on stainless steel did not have a strong correlation to the size of the corrosion spot (**Figure 32 D** (left), **Table 9**), but the total corrosion area had a moderate correlation to both the number of corrosion spots and the average spot size (**Figure 32 D** (center and right), **Table 9**). This

indicated that total corrosion area may be the best metric to quantify corrosion. Thus, it is recommended that for the flight experiment, where 6 biological replicates are examined, total corrosion is used as the metric to quantify and compare corrosion. However, in this experiment, where only a single biological replicate was examined, meaningful conclusions about the relationship between biofilm coverage and AgF treatment could not be drawn with this metric.

Table 9. Linear regression of corrosion measurements. β_1 describes the relationship of the response variable (Regression, first variable) to the predictor (Regression, second variable). ** $p < 0.01$.

<i>Regression</i>	<u>Coefficients</u>		<i>DF</i>	<i>R</i> ²
	β_1	<i>St. Error</i>		
Av. Spot Size~No. spots	1.859	2.117	10	0.072
Total Corr. Area~No. spots	95.34**	27.48	10	0.546
Total Corr. Area~Av. Spot Size	14.75**	3.57	10	0.631

Preliminary data indicates that electrochemical corrosion induced by urine may have induced more damage to 316L stainless steel than MIC. Additionally, preventative treatment of clean stainless-steel piping and storage tanks in the ISS WRS with 400 ppb AgF to inhibit biofilm formation may increase corrosive damage. However, the results of this study were not conclusive. The biggest caveat is that the analysis was performed with a single biological replicate. In the flight experiment post-flight analysis, where this experiment and analysis will be repeated, all 6 biological replicates should be imaged and analyzed to assess the findings described here.

V. EXPERIMENTAL VERIFICATION TEST AND CONCLUSIONS

The primary aims of this research were to 1) investigate and optimize the various experimental parameters that need to be controlled in-flight to ensure a successful experiment; 2) identify baselines for biofilm growth, disinfection, and corrosion; and 3) design post-flight data collection and analysis methods to efficiently process time-sensitive samples before they are degraded.

Chapter 2 described the optimization of each component of the flight experiment. The hardware design was optimized to provide uniformity to the 316L stainless-steel coupons, both in geometry and in surface composition. The long-term stability of the growth media and single-dose inoculum were optimized and verified, allowing for flexibility in the event of a delayed launch. The utilization of the amino acid solutions from mAUM.v3 as the cryopreservation buffer allowed for a single-dose inoculum which, when mixed into a BioCell which is pre-loaded with mAUM without amino acids, resulted in inoculated mAUM.v3 without additional reagents which may have been metabolized by the bacterial culture. The experimental timeline was defined to prevent loss of sample integrity during storage prior to the sample return. The work in Chapter 2 has resulted in a well-designed and optimized flight experiment.

Chapter 3 described the baseline for *E. coli* and *P. aeruginosa* biofilm growth on 316L stainless steel in artificial urine with and without silver fluoride disinfection. *E. coli* and *P. aeruginosa* biofilms were segregated in early-biofilm formation, but after 14 days, we saw infiltration of *E. coli* into *P. aeruginosa* FEP-Teflon associated biofilms, and at 24 days, *E. coli* was the dominant species on Teflon. Stainless steel-attached biofilms imaged at the same time points suggested that the infiltration and subsequent takeover by

E. coli of the FEP Teflon surface may have been caused, at least in part, by migration from the stainless-steel surface to the FEP Teflon surface. This migration may have been motivated by an oxygen gradient in the BioCell well which could not be prevented due to restrictions in equipment for space flight (Louis Stodieck, BioServe Technologies, personal communication), or it may have been an artifact caused by incubating the BioCells in the vertical orientation.

After 24 days incubation, we saw three reoccurring phenotypes in wells which had been treated with 400 ppb AgF. The phenotype which displayed predominately *E. coli* biofilms was seen the most frequently, at nearly 50% of all 24-day silver treated wells. This population may have arisen as a result of two point mutations, one which may cause loss of the OmpF porin, reducing outer membrane permeability, and the other which might have increased expression of the Cus efflux system, which effluxes silver ions (219). The second-most frequent population was dominated by *P. aeruginosa*. In this population, we still saw the presence of *E. coli*. *P. aeruginosa* produces pyocyanin, which may be used by *E. coli* to reduce biologically active Ag¹⁺ ions to biologically inactive elemental Ag⁰ (140, 141). This is a potential mechanism that may have caused the *P. aeruginosa*-dominated phenotype to arise.

The corrosion analysis in this research was inconclusive due to small sample size, but we were able to reliably detect corrosion. Additionally, data analysis methods to quantify and analyze corrosion in post-flight analysis were determined. Preliminary corrosion data suggested that electrochemical and temperature factors may play a bigger role in corrosive damage to 316L stainless-steel piping and storage tanks than microbiological corrosion.

Prior to flight, this experiment underwent a full, ground-based run-through of the experiment called an Experimental Verification Test (EVT). The purpose of the EVT was to ensure that the experiment had been designed such that there were no significant issues which could lead to failure in flight. Following the run-through of the experiment and subsequent data analysis, the research team met with a panel of NASA scientists to present the EVT results and determine whether the experiment passed EVT, based on a set of success criteria which was outlined by the experimental team prior to the initiation of the EVT run.

In EVT, we saw consistent growth of bacteria and reproducibility of data, high-resolution, good quality images by both confocal microscopy and SEM, and RNA of a sufficient quality and quantity which was suitable for downstream transcriptomic analysis. As a result, NASA determined that we had passed EVT, and our experiment is now qualified for flight. This experiment is scheduled to fly on SpaceX-21, which is currently expected to launch from NASA Kennedy Space Center in December 2020.

Two mechanisms for silver resistance which are proposed in this work but require future study to elucidate. In Chapter 3, I proposed two mechanisms by which distinct phenotypes of *E. coli* and *P. aeruginosa*-dominated biofilms might arise from silver fluoride treatment in mAUM. These hypothesized mechanisms are supported by literature (140, 141), but they have not yet been tested. We have received additional funding for the flight experiment which will be used for transcriptomic analysis, which may give clues as to the mechanism that results in different phenotypes.

One of the biggest limitations of this research is that we are unable to supply fresh media after inoculation due to issues regarding ISS crew safety. Ground-based studies

which investigate MIC are long-term experiments with frequent changing of media (9, 248, 249). mAUM is a minimal medium, so the nutrients will be used up rapidly. The untreated biofilm populations in this study show evidence of die-off by 24 days of culturing. As shown in Chapter 2, the 24-day biofilm cell number is reduced, which was confirmed by E-SEM in Chapter 3. Repeating this experiment with regular supplementation of fresh media may yield more meaningful results in both biofilm structure and corrosion.

This experiment was originally designed to be longitudinal. The ISS is equipped with a Light Microscopy Module (LMM) which allows for confocal and epifluorescent microscopy of specimens while on the ISS. However, preliminary data from Arizona State University showed that epifluorescent microscopy was not suitable for this experiment (unpublished), and the LMM confocal is equipped with only a single laser, which produces green light (532 nm). GFP requires blue light excitation (488 nm) and thus would not be detected by the LMM. As a result, the flight experiment had to be modified to allow for sample return prior to imaging, which has changed the type of data we can collect. Specimens which were incubated in flight must now be returned to Earth prior to imaging. During return, the spacecraft experiences shaking and extreme gravity forces which can alter biofilm structure. Since the samples must be fixed and returned prior to imaging, we also cannot conduct this study longitudinally. Each biofilm imaged will be a separate culture, instead of tracking changes in the same biofilm over time. A longitudinal study with more frequent observation would allow higher-resolution tracking of a biofilm as it develops and matures and would enable observation of how the distinct phenotypes seen in 24-day biofilms with silver treatment arise.

This study has produced an optimized flight experiment designed to model biofilm formation in the WRS on the ISS. The analysis of the pre-flight experiment presented here shows that there was a differential response to long-term silver treatment in mixed-species *E. coli* and *P. aeruginosa* biofilms, and suggested that corrosion on 316L stainless steel in the presence of such biofilms may have been the result of electrochemical processes, rather than by MIC. There were also indications that corrosion on uninoculated steel might be exacerbated by silver fluoride treatment. Characterizing the microbial response to, and corrosive potential of, silver disinfection will better inform NASA to make decisions regarding maintenance and disinfection of the WRS.

REFERENCES

1. Costerton JW, Cheng KJ, Geesey GG, Ladd TI, Nickel JC, Dasgupta M, Marrie TJ. 1987. Bacterial biofilms in nature and disease. *Ann Rev Microbiol* 41:435–464.
2. Stoodley P, Sauer K, Davies DG, Costerton JW. 2002. Biofilms as complex differentiated communities. *Annu Rev Microbiol*. 56:187–209.
3. Berlanga M, Guerrero R. 2016. Living together in biofilms: the microbial cell factory and its biotechnological implications. *Microb Cell Fact* 15:165.
4. Robertson SR, McLean RJC. 2015. Beneficial biofilms. *AIMS Bioeng* 2:437–448.
5. Chien C-C, Lin B-C, Wu C-H. 2013. Biofilm formation and heavy metal resistance by an environmental *Pseudomonas* sp. *Biochem Eng J* 78:132–137.
6. Beale DJ, Morrison PD, Key C, Palombo EA. 2014. Metabolic profiling of biofilm bacteria known to cause microbial influenced corrosion. *Water Sci Technol* 69:1–8.
7. Koechler S, Farasin J, Cleiss-Arnold J, Arsene-Ploetze F. 2015. Toxic metal resistance in biofilms: diversity of microbial responses and their evolution. *Res Microbiol* 166:764–773.
8. Donlan RM. 2002. Biofilms: Microbial life on surfaces. *Emerg Infect Dis* 8:881–890.
9. Hamzah E, Hussain MZ, Ibrahim Z, Abdolahi A. 2013. Influence of *Pseudomonas aeruginosa* bacteria on corrosion resistance of 304 stainless steel. *Corros Eng Sci Technol* 48:116–120.

10. Li S, Zhang Y, Liu J, Yu MEI. 2010. Influence of *Thiobacillus Ferroxidans* biofilm on the corrosion behavior of steel A3. *Int J Mod Phys B* 24:3083–3088.
11. Vega LM, Mathieu J, Yang Y, Pyle BH, McLean RJC, Alvarez PJJ. 2014. Nickel and cadmium ions inhibit quorum sensing and biofilm formation without affecting viability in *Burkholderia multivorans*. *Int Biodeterior Biodegrad* 91:82–87.
12. Mijndonckx K, Provoost A, Ott CM, Venkateswaran K, Mahillon J, Leys N, Van Houdt R. 2013. Characterization of the survival ability of *Cupriavidus metallidurans* and *Ralstonia pickettii* from space-related environments. *Microb Ecol* 65:347–360.
13. Chaitra TK. 2017. Synthesis and corrosion inhibition behavior of some new heterocyclic derivatives on mild steel in acid media. University of Mysore.
14. Shi X, Avci R, Geiser M, Lewandowski Z. 2003. Comparative study in chemistry of microbially and electrochemically induced pitting of 316L stainless steel. *Corros Sci* 45:2577–2595.
15. Jones HW. 2015. Estimating the life cycle cost of space systems. 45th Int Conf Environ Syst. Bellvue, Washington.
16. Shaw LA, Barreda JL. 2008. International Space Station USOS potable development water dispenser. SAE Tech Pap 1.
17. Carrasquillo RL. 2005. ISS ECLSS technology evolution for exploration. Am Inst Aeronaut Astronaut. 43rd AIAA Aerospace Sciences Meeting and Exhibit, Aerospace Sciences Meetings, Reno, Nevada.

18. Wong WC, Dudinsky LA, Garcia VM, Ott CM, Castro VA. 2010. Efficacy of various chemical disinfectants on biofilms formed in spacecraft potable water system components. *Biofouling* 26:583–586.
19. Zareba G, Cernichiari E, Goldsmith LA, Clarkson TW. 1995. Biological monitoring of iodine, a water disinfectant for long-term space missions. *Env Heal Perpsect* 103:1032–1035.
20. Straub II JE, Plumlee DK, Schultz JR. 2014. International Space Station potable water characterization, p. 20140005011. *In* 44th Int Conf on Env Systems. Tucson, AZ.
21. Pearson DL, Botkin DJ, Bruce RJ, Castro VA, Smith MJ, Oubre CM, Ott CM. 2012. Microbial monitoring of the International Space Station. *Environmental Monitoring: A Comprehensive Handbook*. DHI Publishing, River Grove, IL.
22. Mermel LA. 2013. Infection prevention and control during prolonged human space travel. *Clin Infect Dis* 56:123–130.
23. Bornemann G, Wasser K, Tonat T, Moeller R, Bohmeier M, Hauslage J. 2015. Natural microbial populations in a water-based biowaste management system for space life support. *Life Sci Sp Res* 7:39–52.
24. Zea L, McLean RJC, Rook TA, Angle G, Carter DL, Delegard A, Denvir A, Gerlach R, Gorti S, McIlwaine D, Nur M, Peyton BM, Stewart PS, Sturman P, Velez Justiniano YA. 2020. Potential biofilm control strategies for extended spaceflight missions. *Biofilm* 2:100026.
25. Hadrup N, Lam HR. 2014. Oral toxicity of silver ions, silver nanoparticles and colloidal silver--a review. *Regul Toxicol Pharmacol* 68:1–7.

26. Lansdown ABG. 2006. Silver in Health Care: Antimicrobial effects and safety in use, p. 17–34. *In* Biofunctional Textiles and the Skin. KARGER, Basel.
27. Silva E, M. Saraiva S, P. Miguel S, Correia IJ. 2014. PVP-coated silver nanoparticles showing antifungal improved activity against dermatophytes. *J Nanoparticle Res* 16.
28. Bryaskova R, Pencheva D, Nikolov S, Kantardjiev T. 2011. Synthesis and comparative study on the antimicrobial activity of hybrid materials based on silver nanoparticles (AgNps) stabilized by polyvinylpyrrolidone (PVP). *J Chem Biol* 4:185–191.
29. Sheng Z, Van Nostrand JD, Zhou J, Liu Y. 2015. The effects of silver nanoparticles on intact wastewater biofilms. *Front Microbiol* 6.
30. Benoit MR, Klaus DM. 2007. Microgravity, bacteria, and the influence of motility. *Adv Sp Res* 39:1225–1232.
31. Klaus D, Simske S, Todd P, Stodieck L. 1997. Investigation of space flight effects on *Escherichia coli* and a proposed model of underlying physical mechanisms. *Microbiol* 143:449–455.
32. Kacena MA, Leonard PE, Todd P, Luttgies MW. 1997. Low gravity and inertial effects on the growth of *E. coli* and *B. subtilis* in semi-solid media. *Aviat Sp Env Med* 68:1104–1108.
33. Zea L, Larsen M, Estante F, Qvortrup K, Moeller R, Dias de Oliveira S, Stodieck L, Klaus D. 2017. Phenotypic Changes Exhibited by *E. coli* Cultured in Space. *Front Microbiol* 8.

34. Kim W, Tengra FK, Young Z, Shong J, Marchand N, Chan HK, Pangule RC, Parra M, Dordick JS, Plawsky JL, Collins CH. 2013. Spaceflight promotes biofilm formation by *Pseudomonas aeruginosa*. PLoS One 8:e62437.
35. Kim W, Tengra FK, Shong J, Marchand N, Chan H, Young Z, Pangule RC, Parra M, Dordick JS, Plawsky JL, Collins CH. 2013. Effect of spaceflight on *Pseudomonas aeruginosa* final cell density is modulated by nutrient and oxygen availability. BMC Microbiol 13:241.
36. Kacena M, Todd P. 1997. Growth characteristics of *E. coli* and *B. subtilis* cultured on an agar substrate in microgravity. Microgravity Sch Technol 10:58–62.
37. Fajardo-Cavazos P, Nicholson WL. 2016. Cultivation of *Staphylococcus epidermidis* in the human spaceflight environment leads to alterations in the frequency and spectrum of spontaneous rifampicin-resistance mutations in the *rpoB* gene. Front Microbiol 7.
38. Su L, Zhou L, Liu J, Cen Z, Wu C, Wang T, Zhou T, Chang D, Guo Y, Fang X, Wang J, Li T, Yin S, Dai W, Zhou Y, Zhao J, Fang C, Yang R, Liu C. 2014. Phenotypic, genomic, transcriptomic and proteomic changes in *Bacillus cereus* after a short-term space flight. Adv Sp Res 53:18–29.
39. Blount P. 2003. Molecular mechanisms of mechanosensation. Neuron 37:731–734.
40. Martinac B, Buechner M, Delcour AH, Adler J, Kung C. 1987. Pressure-sensitive ion channel in *Escherichia coli*. Proc Natl Acad Sci USA 84:2297–2301.
41. Peng Z, Pak OS, Feng Z, Liu AP, Young YN. 2016. On the gating of mechanosensitive channels by fluid shear stress. Acta Mech Sin 32:1012–1022.

42. Thomas WE, Trintchina E, Forero M, Vogel V, Sokurenko E V. 2002. Bacterial adhesion to target cells enhanced by shear force. *Cell* 109:913–923.
43. Persat A, Inclan YF, Engel JN, Stone HA, Gitai Z. 2015. Type IV pili mechanochemically regulate virulence factors in *Pseudomonas aeruginosa*. *Proc Natl Acad Sci USA* 112:7563–7568.
44. Rodesney CA, Roman B, Dhamani N, Cooley BJ, Katira P, Touhami A, Gordon VD. 2017. Mechanosensing of shear by *Pseudomonas aeruginosa* leads to increased levels of the cyclic-di-GMP signal initiating biofilm development. *Proc Natl Acad Sci USA* 114:5906–5911.
45. Hou J, Veeregowda DH, van de Belt-Gritter B, Busscher HJ, van der Mei HC. 2017. Extracellular polymeric matrix production and relaxation under fluid shear and mechanical pressure in *Staphylococcus aureus* biofilms. *Appl Environ Microbiol* 84.
46. Hammond TG, Hammond JM. 2001. Optimized suspension culture: the rotating-wall vessel. *Am J Physiol Ren Physiol* 281:F12–F25.
47. Nickerson CA, Ott CM, Wilson JW, Ramamurthy R, Pierson DL. 2004. Microbial responses to microgravity and other low-shear environments. *Microbiol Mol Biol Rev* 68:345–361.
48. Sukharev S, Betanzos M, Chiang CS, Guy HR. 2001. The gating mechanism of the large mechanosensitive channel MscL. *Nature* 409:720–724.
49. Sukharev S, Sigurdson WJ, Kung C, Sachs F. 1999. Energetic and spatial parameters for gating of the bacterial large conductance mechanosensitive channel, MscL. *J Gen Physiol* 113:525–40.

50. Ingber D. 1999. How cells (might) sense microgravity. *FASEB J* 13.
51. Pivetti CD, Yen MR, Miller S, Busch W, Tseng YH, Booth IR, Saier MH. 2003. Two families of mechanosensitive channel proteins. *Microbiol Mol Biol Rev* 67:66–85.
52. Martinac B, Adler J, Kung C. 1990. Mechanosensitive ion channels of *E. coli* activated by amphipaths. *Nature* 348:261–263.
53. Sukharev SI, Martinac B, Arshavsky VY, Kung C. 1993. Two types of mechanosensitive channels in the *Escherichia coli* cell envelope: solubilization and functional reconstitution. *Biophys J* 65:177–183.
54. Le Roux AL, Quiroga X, Walani N, Arroyo M, Roca-Cusachs P. 2019. The plasma membrane as a mechanochemical transducer. *Philos Trans R Soc L B Biol Sci* 374:20180221.
55. Sukharev S, Durell SR, Guy HR. 2001. Structural models of the MscL gating mechanism. *Biophys J* 81:917–936.
56. Elmore DE, Dougherty DA. 2001. Molecular dynamics simulations of wild-type and mutant forms of the *Mycobacterium tuberculosis* MscL channel. *Biophys J* 81:1345–1359.
57. Sawada Y, Sokabe M. 2015. Molecular dynamics study on protein–water interplay in the mechanogating of the bacterial mechanosensitive channel MscL. *Eur Biophys J* 44:531–543.
58. Ingber D. 1997. Integrins, tensegrity, and mechanotransduction. *Gravit Sp Biol Bull* 10:49–55.

59. Jones LJF, Carballido-López R, Errington J. 2001. Control of cell shape in bacteria. *Cell* 104:913–922.
60. Shih YL, Rothfield L. 2006. The bacterial cytoskeleton. *Microbiol Mol Biol Rev* 70:729–754.
61. Levin PA, Margolis PS, Setlow P, Losick R, Sun D. 1992. Identification of *Bacillus subtilis* genes for septum placement and shape determination. *J Bacteriol* 174:6717–6728.
62. de Boer P, Crossley R, Rothfield L. 1992. The essential bacterial cell-division protein FtsZ is a GTPase. *Nature* 359:254–256.
63. RayChaudhuri D, Park JT. 1992. *Escherichia coli* cell-division gene *ftsZ* encodes a novel GTP-binding protein. *Nature* 359:251–254.
64. Mukherjee A, Dai K, Lutkenhaus J. 1993. *Escherichia coli* cell division protein FtsZ is a guanine nucleotide binding protein. *Proc Natl Acad Sci USA* 90:1053–1057.
65. Figge RM, Divakaruni A V, Gober JW. 2004. MreB, the cell shape-determining bacterial actin homologue, co-ordinates cell wall morphogenesis in *Caulobacter crescentus*. *Mol Microbiol* 51:1321–1332.
66. Kruse T, Bork-Jensen J, Gerdes K. 2004. The morphogenetic MreBCD proteins of *Escherichia coli* form an essential membrane-bound complex. *Mol Microbiol* 55:78–89.
67. Robertson GT, Doyle TB, Du Q, Duncan L, Mdluli KE, Lynch AS. 2007. A novel indole compound that inhibits *Pseudomonas aeruginosa* growth by targeting MreB is a substrate for MexAB-OprM. *J Bacteriol* 189:6870–6881.

68. Komeili A. 2006. Magnetosomes are cell membrane invaginations organized by the actin-like protein MamK. *Science* (80) 311:242–245.
69. Singhi D, Srivastava P. 2020. Role of bacterial cytoskeleton and other apparatuses in cell communication. *Front Mol Biosci* 7:158.
70. Shih YL, Kawagishi I, Rothfield L. 2005. The MreB and Min cytoskeletal-like systems play independent roles in prokaryotic polar differentiation. *Mol Microbiol* 58:917–928.
71. Rothfield L, Taghbalout A, Shih YL. 2005. Spatial control of bacterial division-site placement. *Nat Rev Microbiol* 3:959–968.
72. Schwarz RP, Goodwin TJ, Wolf DA. 1992. Cell culture for three-dimensional modeling in rotating-wall vessels: An Application of Simulated Microgravity. *J Tiss Cult Meth* 14:51–58.
73. Wolf DA, Sams CF, Schwarz RP. 1992. High aspect reactor vessel and method of use. The United States of America as represented by the Administrator of the National Aeronautics and Space Administration, Washington, D. C., United States.
74. Klaus DM. 2001. Clinostats and bioreactors. *Gravit Sp Biol Bull* 14:55–64.
75. Nickerson CA, Ott CM, Wilson JW, Ramamurthy R, LeBlanc CL, Höner zu Bentrup K, Hammond T, Pierson DL. 2003. Low-shear modeled microgravity: a global environmental regulatory signal affecting bacterial gene expression, physiology, and pathogenesis. *J Microbiol Methods* 54:1–11.
76. Demain AL, Fang A. 2001. Secondary metabolism in simulated microgravity. *Chem Rec* 1:333–346.

77. Fang A, Pierson DL, Mishra SK, Koenig DW, Demain AL. 1997. Secondary metabolism in simulated microgravity: beta-lactam production by *Streptomyces clavuligerus*. *J Ind Microbiol Biotechnol* 18:22–25.
78. Fang A, Pierson DL, Koenig DW, Mishra SK, Demain AL. 1997. Effect of simulated microgravity and shear stress on microcin B17 production by *Escherichia coli* and on its excretion into the medium. *Appl Env Microbiol* 63:4090–4092.
79. Wilson JW, Ott CM, Ramamurthy R, Porwollik S, McClelland M, Pierson DL, Nickerson CA. 2002. Low-shear modeled microgravity alters the *Salmonella enterica* serovar Typhimurium stress response in an RpoS-independent manner. *Appl Env Microbiol* 68:5408–5416.
80. Arunasri K, Adil M, Venu Charan K, Suvro C, Himabindu Reddy S, Shivaji S. 2013. Effect of simulated microgravity on *E. coli* K12 MG1655 growth and gene expression. *PLoS One* 8:e57860.
81. Tucker DL, Ott CM, Huff S, Fofanov Y, Pierson DL, Willson RC, Fox GE. 2007. Characterization of *Escherichia coli* MG1655 grown in a low-shear modeled microgravity environment. *BMC Microbiol* 7:15.

82. Wilson JW, Ott CM, Honer zu Bentrup K, Ramamurthy R, Quick L, Porwollik S, Cheng P, McClelland M, Tsapralis G, Radabaugh T, Hunt A, Fernandez D, Richter E, Shah M, Kilcoyne M, Joshi L, Nelman-Gonzalez M, Hing S, Parra M, Dumars P, Norwood K, Bober R, Devich J, Ruggles A, Goulart C, Rupert M, Stodieck L, Stafford P, Catella L, Schurr MJ, Buchanan K, Morici L, McCracken J, Allen P, Baker-Coleman C, Hammond T, Vogel J, Nelson R, Pierson DL, Stefanyshyn-Piper HM, Nickerson CA. 2007. Space flight alters bacterial gene expression and virulence and reveals a role for global regulator Hfq. *Proc Natl Acad Sci USA* 104:16299–16304.
83. Crabbe A, Pycke B, Van Houdt R, Monsieurs P, Nickerson C, Leys N, Cornelis P. 2010. Response of *Pseudomonas aeruginosa* PAO1 to low shear modelled microgravity involves AlgU regulation. *Env Microbiol* 12:1545–1564.
84. Orsini SS, Lewis AM, Rice KC. 2017. Investigation of simulated microgravity effects on *Streptococcus mutans* physiology and global gene expression. *npj Microgravity* 3:4.
85. Aunins TR, Erickson KE, Prasad N, Levy SE, Jones A, Shrestha S, Mastracchio R, Stodieck L, Klaus D, Zea L, Chatterjee A. 2018. Spaceflight modifies *Escherichia coli* gene expression in response to antibiotic exposure and reveals role of oxidative stress response. *Front Microbiol* 9.
86. Duscher AA, Conesa A, Bishop M, Vroom MM, Zubizarreta SD, Foster JS. 2018. Transcriptional profiling of the mutualistic bacterium *Vibrio fischeri* and an *hfq* mutant under modeled microgravity. *npj Microgravity* 4:25.

87. Zea L, Prasad N, Levy SE, Stodieck L, Jones A, Shrestha S, Klaus D. 2016. A molecular genetic basis explaining altered bacterial behavior in space. *PLoS One* 11.
88. Castro SL, Nelman-Gonzalez M, Nickerson CA, Ott CM. 2011. Induction of attachment-independent biofilm formation and repression of Hfq expression by low-fluid-shear culture of *Staphylococcus aureus*. *Appl Env Microbiol* 77:6368–6378.
89. Yang J, Barrila J, Roland KL, Ott CM, Nickerson CA. 2016. Physiological fluid shear alters the virulence potential of invasive multidrug-resistant non-typhoidal *Salmonella* Typhimurium D23580. *NPJ Microgravity* 2:16021.
90. Nickerson CA, Ott CM, Mister SJ, Morrow BJ, Burns-Keliher L, Pierson DL. 2000. Microgravity as a novel environmental signal affecting *Salmonella enterica* serovar Typhimurium virulence. *Infect Immun* 68:3147–3152.
91. Hammond TG, Stodieck L, Birdsall HH, Becker JL, Koenig P, Hammond JS, Gunter MA, Allen PL. 2013. Effects of microgravity on the virulence of *Listeria monocytogenes*, *Enterococcus faecalis*, *Candida albicans*, and methicillin-resistant *Staphylococcus aureus*. *Astrobiol* 13:1081–1090.
92. Rosado H, Doyle M, Hinds J, Taylor PW. 2010. Low-shear modelled microgravity alters expression of virulence determinants of *Staphylococcus aureus*. *Acta Astronaut* 66:408–413.
93. Kalpana D, Im C, Lee YS. 2016. Comparative growth, cross stress resistance, transcriptomics of *Streptococcus pyogenes* cultured under low shear modeled microgravity and normal gravity. *Saudi J Bacteriol Sci* 23:24–33.

94. Crabbe A, Schurr MJ, Monsieurs P, Morici L, Schurr J, Wilson JW, Ott CM, Tsaprailis G, Pierson DL, Stefanyshyn-Piper H, Nickerson CA. 2011. Transcriptional and proteomic responses of *Pseudomonas aeruginosa* PAO1 to spaceflight conditions involve Hfq regulation and reveal a role for oxygen. *Appl Env Microbiol* 77:1221–1230.
95. Grant KC, Khodadad CLM, Foster JS. 2013. Role of Hfq in an animal–microbe symbiosis under simulated microgravity conditions. *Int J Astrobiol* 13:53–61.
96. Wilson JW, Ott CM, Quick L, Davis R, Honer zu Bentrup K, Crabbe A, Richter E, Sarker S, Barrila J, Porwollik S, Cheng P, McClelland M, Tsaprailis G, Radabaugh T, Hunt A, Shah M, Nelman-Gonzalez M, Hing S, Parra M, Dumars P, Norwood K, Bober R, Devich J, Ruggles A, CdeBaca A, Narayan S, Benjamin J, Goulart C, Rupert M, Catella L, Schurr MJ, Buchanan K, Morici L, McCracken J, Porter MD, Pierson DL, Smith SM, Mergeay M, Leys N, Stefanyshyn-Piper HM, Gorie D, Nickerson CA. 2008. Media ion composition controls regulatory and virulence response of *Salmonella* in spaceflight. *PLoS One* 3:e3923.
97. Roy R, Shilpa PP, Bagh S. 2016. A systems biology analysis unfolds the molecular pathways and networks of two proteobacteria in spaceflight and simulated microgravity conditions. *Astrobiology* 16:677–689.
98. McLean RJC, Cassanto JM, Barnes MB, Koo JH. 2001. Bacterial biofilm formation under microgravity conditions. *FEMS Microbiol Let* 195:115–119.
99. Lynch S V, Mukundakrishnan K, Benoit MR, Ayyaswamy PS, Matin A. 2006. *Escherichia coli* biofilms formed under low-shear modeled microgravity in a ground-based system. *Appl Env Microbiol* 72:7701–7710.

100. Wang H, Yan Y, Rong D, Wang J, Wang H, Liu Z, Wang J, Yang R, Han Y. 2016. Increased biofilm formation ability in *Klebsiella pneumoniae* after short-term exposure to a simulated microgravity environment. *Microbiologyopen* 5.
101. Morrison MD, Fajardo-Cavazos P, Nicholson WL. 2019. Comparison of *Bacillus subtilis* transcriptome profiles from two separate missions to the International Space Station. *npj Microgravity* 5:1.
102. Carter DL. 2017. Impact of biofilms on the design and operation of ISS life support systems. Huntsville, AL.
103. Krohn DD. 1992. Long-term corrosion evaluation of stainless steels in space shuttle iodinated resin and water. Houston, TX.
104. Verostko C. 2009. Development of ersatz formulations of wastewater streams generated in spacecraft closed life support systems. *Bioastronautics Transm Memo* TM No.: LM.
105. Brooks T, Keevil CW. 1997. A simple artificial urine for the growth of urinary pathogens. *Let Appl Microbiol* 24:203–206.
106. Hryckowian AJ, Baisa GA, Schwartz KJ, Welch RA. 2015. *dsdA* does not affect colonization of the murine urinary tract by *Escherichia coli* CFT073. *PLoS One* 10:e0138121.
107. Hull RA, Gill RE, Hsu P, Minshew BH, Falkow S. 1981. Construction and expression of recombinant plasmids encoding Type 1 or D-mannose-resistant pili from a urinary tract infection *Escherichia coli* isolate. *Infect Immun* 33:933–938.
108. Taylor GR. 1974. Recovery of medically important microorganisms from Apollo astronauts. *Aerosp Med* 45:824–828.

109. Hawkins WR, Ziegelschmid JF. 1975. Clinical aspects of crew health. Biomedical results Apollo NASA Spec:43–81.
110. Johnston RS, Dietlein LF, Berry CA. 1975. Biomedical results of Apollo. Washington D.C.
111. Lee J, Jayaraman A, Wood TK. 2007. Indole is an inter-species biofilm signal mediated by SdiA. BMC Microbiol 7:42.
112. Chu W, Zere TR, Weber MM, Wood TK, Whiteley M, Hidalgo-Romano B, Valenzuela Jr. E, McLean RJ, Zere TR, Hidalgo-Romano B, Valenzuela Jr. E, McLean RJ, Chu W, Weber MM, Wood TK, Whiteley M. 2012. Indole production promotes *Escherichia coli* mixed-culture growth with *Pseudomonas aeruginosa* by inhibiting quorum signaling. Appl Env Microbiol 78:411–419.
113. Holloway BW. 1955. Genetic recombination in *Pseudomonas aeruginosa*. Microbiol 13:572–581.
114. Cole SJ, Records AR, Orr MW, Linden SB, Lee VT. 2014. Catheter-associated urinary tract infection by *Pseudomonas aeruginosa* is mediated by exopolysaccharide-independent biofilms. Infect Immun 82:2048–2058.
115. Gupta RK, Harjai K, Chhibber S. 2016. Rhl quorum sensing affects the virulence potential of *Pseudomonas aeruginosa* in an experimental urinary tract infection. Antonie Van Leeuwenhoek 109:1535–1544.
116. Trøstrup H, Thomsen K, Christophersen LJ, Hougen HP, Bjarnsholt T, Jensen PØ, Kirkby N, Calum H, Høiby N, Moser C. 2013. *Pseudomonas aeruginosa* biofilm aggravates skin inflammatory response in BALB/c mice in a novel chronic wound model. Wound Repair Regen 21:292–299.

117. Rumbaugh KP, Colmer JA, Griswold JA, Hamood AN. 2001. The effects of infection of thermal injury by *Pseudomonas aeruginosa* PAO1 on the murine cytokine response. *Cytokine* 16:160–168.
118. Rumbaugh KP, Griswold JA, Iglewski BH, Hamood AN. 1999. Contribution of quorum sensing to the virulence of *Pseudomonas aeruginosa* in burn wound infections. *Infect Immun* 67:5854–5862.
119. Wu H, Song Z, Givskov M, Döring G, Worlitzsch D, Mathee K, Rygaard J, Høiby N. 2001. *Pseudomonas aeruginosa* mutations in lasI and rhlII quorum sensing systems result in milder chronic lung infection. *Microbiol* 147:1105–1113.
120. Ryu JC, Kim MJ, Kwon Y, Oh JH, Yoon SS, Shin SJ, Yoon JH, Ryu JH. 2017. Neutrophil pyroptosis mediates pathology of *P. aeruginosa* lung infection in the absence of the NADPH oxidase NOX2. *Mucosal Immunol* 10:757–774.
121. Bragonzi A, Worlitzsch D, Pier GB, Timpert P, Ulrich M, Hentzer M, Andersen JB, Givskov M, Conese M, Döring G. 2005. Nonmucoid *Pseudomonas aeruginosa* expresses alginate in the lungs of patients with cystic fibrosis and in a mouse model. *J Infect Dis* 192:410–419.
122. Heydorn A, Ersbøll BK, Hentzer M, Parsek MR, Givskov M, Molin S. 2000. Experimental reproducibility in flow-chamber biofilms. *Microbiol* 146:2409–2415.
123. Svanborg-Edén C, Hull R, Falkow S, Leffler H. 1983. Target cell specificity of wild-type *E. coli* and mutants and clones with genetically defined adhesins. *Prog Food Nutr Sci* 7:75–89.

124. Jantusch BA, Hull SI. 1996. Restriction fragment length polymorphism of PCR amplified *papE* gene products is correlated with complete serotype among uropathogenic *Escherichia coli* isolates. *Microb Pathog* 20:351–360.
125. Stapleton A, Moseley S, Stamm WE. 1991. Urovirulence determinants in *Escherichia coli* isolates causing first-episode and recurrent cystitis in women. *J Infect Dis* 163:773–779.
126. Welch RA, Burland V, Plunkett 3rd G, Redford P, Roesch P, Rasko D, Buckles EL, Liou SR, Boutin A, Hackett J, Stroud D, Mayhew GF, Rose DJ, Zhou S, Schwartz DC, Perna NT, Mobley HL, Donnenberg MS, Blattner FR. 2002. Extensive mosaic structure revealed by the complete genome sequence of uropathogenic *Escherichia coli*. *Proc Natl Acad Sci USA* 99:17020–17024.
127. Berger H, Hacker J, Juarez A, Hughes C, Goebel W. 1982. Cloning of the chromosomal determinants encoding hemolysin production and mannose-Resistant hemagglutination in *Escherichia coli*. *J Bacteriol* 152:1241–1247.
128. Datsenko KA, Wanner BL. 2000. One-step inactivation of chromosomal genes in *Escherichia coli* K-12 using PCR products. *Proc Natl Acad Sci USA* 97:6640–6645.
129. Beynon LM, Dumanski AJ, McLean RJ, MacLean LL, Richards JC, Perry MB. 1992. Capsule structure of *Proteus mirabilis* (ATCC 49565). *J Bacteriol* 174:2172–2177.
130. Davis JH, Rubin AJ, Sauer RT. 2011. Design, construction and characterization of a set of insulated bacterial promoters. *Nucleic Acids Res* 39:1131–1141.

131. Pringle SL, Palmer KL, McLean RJ. 2017. Indole production provides limited benefit to *Escherichia coli* during co-culture with *Enterococcus faecalis*. Arch Microbiol 199:145–153.
132. Verostko CE, Carrier C, Finger BW. 2004. Ersatz wastewater formulations for testing water recovery systems. SAE Technical Paper.
133. Shaw WHR, Bordeaux JJ. 1955. The decomposition of urea in aqueous media. J Am Chem Soc 77:4729–4733.
134. Luque-Almagro VM, Cabello P, Sáez LP, Olaya-Abril A, Moreno-Vivián C, Roldán MD. 2018. Exploring anaerobic environments for cyanide and cyano-derivatives microbial degradation. Appl Microbiol Biotechnol 102:1067–1074.
135. Cook AR. 1975. Urease activity in the rumen of sheep and the isolation of ureolytic bacteria. J Gen Microbiol 92:32–48.
136. Weatherburn MW. 1967. Phenol-hypochlorite reaction for determination of ammonia. Anal Chem 39:971–974.
137. Settimio L, McLaughlin MJ, Kirby JK, Langdon KA, Janik L, Smith S. 2015. Complexation of silver and dissolved organic matter in soil water extracts. Environ Pollut 199:174–184.
138. Chen Z, Yang P, Yuan Z, Guo J. 2017. Aerobic condition enhances bacteriostatic effects of silver nanoparticles in aquatic environment: an antimicrobial study on *Pseudomonas aeruginosa*. Sci Rep 7:7398.

139. Hassett DJ, Charniga L, Bean K, Ohman DE, Cohen MS. 1992. Response of *Pseudomonas aeruginosa* to pyocyanin: mechanisms of resistance, antioxidant defenses, and demonstration of a manganese-cofactored superoxide dismutase. *Infect Immun* 60:328–36.
140. Muller M, Merrett ND. 2014. Pyocyanin production by *Pseudomonas aeruginosa* confers resistance to ionic silver. *Antimicrob Agents Chemother*. 58:5492–5499.
141. Muller M. 2018. Bacterial silver resistance gained by cooperative interspecies redox behavior. *Antimicrob Agents Chemother*. 62.
142. Whooley MA, McLoughlin AJ. 1982. The regulation of pyocyanin production in *Pseudomonas aeruginosa*. *Eur J Appl Microbiol Biotechnol* 15:161–166.
143. Cole SJ, Hall CL, Schniederberend M, Farrow III JM, Goodson JR, Pesci EC, Kazmierczak BI, Lee VT. 2018. Host suppression of quorum sensing during catheter-associated urinary tract infections. *Nat Commun* 9:4436.
144. Baron SS, Row JJ. 1981. Antibiotic action of pyocyanin. *Antimicrob Agents Chemother* 20:814–820.
145. Prabhu S, Poulouse EK. 2012. Silver nanoparticles: mechanism of antimicrobial action, synthesis, medical applications, and toxicity effects. *Int Nano Lett* 2:32.
146. Wallace WT, Castro-Wallace SL, Kui CKM, Loh LJ, Hudson E, Gazda DB, Lewis JF. 2016. Effects of material choice on biocide loss in Orion water storage tanks, p. 1–10. *In* 46th International Conference on Environmental Systems. Vienna, Austria.
147. Marquis RE. 1995. Antimicrobial actions of fluoride for oral bacteria. *Can J Microbiol* 41:955–964.

148. Ji C, Stockbridge RB, Miller C. 2014. Bacterial fluoride resistance, Fluc channels, and the weak acid accumulation effect. *J Gen Physiol* 144:257–261.
149. Baker JL, Sudarsan N, Weinberg Z, Roth A, Stockbridge RB, Breaker RR. 2012. Widespread genetic switches and toxicity resistance proteins for fluoride. *Science* (80) 335:233–235.
150. Bala WA, Benitha VS, Jeyasubramanian K, Hikku GS, Sankar P, Kumar S V. 2017. Investigation of anti-bacterial activity and cytotoxicity of calcium fluoride nanoparticles. *J Fluor Chem* 193:38–44.
151. Schweizer HP, Po C. 1996. Regulation of glycerol metabolism in *Pseudomonas aeruginosa*: characterization of the glpR repressor gene. *J Bacteriol* 178:5215–5221.
152. Young G. 1947. Pigment production and antibiotic activity in cultures of *Pseudomonas aeruginosa*. *J Bacteriol* 54:109–117.
153. Patil S, Nikam M, Patil H, Anokhina T, Kochetkov V, Chaudhari A. 2017. Bioactive pigment production by *Pseudomonas* spp. MCC 3145: Statistical media optimization, biochemical characterization, fungicidal and DNA intercalation-based cytostatic activity. *Process Biochem* 58:298–305.
154. Jayaseelan S, Ramaswamy D, Dharmaraj S. 2014. Pyocyanin: production, applications, challenges and new insights. *World J Microbiol Biotechnol* 30:1159–1168.

155. Dantas P V, Peres S, Campos-Takaki GM, La Rotta CE. 2013. Utilization of raw glycerol for pyocyanin production from *Pseudomonas aeruginosa* in half-microbial fuel cells: Evaluation of two electrochemical approaches. *J Electrochem Soc* 160:G142–G148.
156. Peng L, Shimizu K. 2003. Global metabolic regulation analysis for *Escherichia coli* K12 based on protein expression by 2-dimensional electrophoresis and enzyme activity measurement. *Appl Microbiol Biotechnol* 61:163–178.
157. Oh MK, Liao JC. 2000. Gene expression profiling by DNA microarrays and metabolic fluxes in *Escherichia coli*. *Biotechnol Prog* 16:278–286.
158. Iuchi S, Cole ST, Lin EC. 1990. Multiple regulatory elements for the *glpA* operon encoding anaerobic glycerol-3-phosphate dehydrogenase and the *glpD* operon encoding aerobic glycerol-3-phosphate dehydrogenase in *Escherichia coli*: further characterization of respiratory control. *J Bacteriol* 172:179–184.
159. Weissenborn DL, Wittekindt N, Larson TJ. 1992. Structure and regulation of the *glpFK* operon encoding glycerol diffusion facilitator and glycerol kinase of *Escherichia coli* K-12. *J Biol Chem* 267:6122–31.
160. Durnin G, Clomburg J, Yeates Z, Alvarez PJJ, Zygorakis K, Campbell P, Gonzalez R. 2009. Understanding and harnessing the microaerobic metabolism of glycerol in *Escherichia coli*. *Biotechnol Bioeng* 103:148–161.
161. Martínez-Gómez K, Flores N, Castañeda HM, Martínez-Batallar G, Hernández-Chávez G, Ramírez OT, Gosset G, Encarnación S, Bolívar F. 2012. New insights into *Escherichia coli* metabolism: carbon scavenging, acetate metabolism and carbon recycling responses during growth on glycerol. *Microb Cell Fact* 11:46.

162. Hua Q, Yang C, Oshima T, Mori H, Shimizu K. 2004. Analysis of gene expression in *Escherichia coli* in response to changes of growth-limiting nutrient in chemostat cultures. *Appl Env Microbiol* 70:2354–2366.
163. Notley L, Ferenci T. 1996. Induction of RpoS-dependent functions in glucose-limited continuous culture: what level of nutrient limitation induces the stationary phase of *Escherichia coli*. *J Bacteriol* 178:1465–1468.
164. Hardiman T, Lemuth K, Keller MA, Reuss M, Siemann-Herzberg M. 2007. Topology of the global regulatory network of carbon limitation in *Escherichia coli*. *J Biotechnol* 132:359–374.
165. Hubálek Z. 2003. Protectants used in the cryopreservation of microorganisms. *Cryobiol* 46:205–229.
166. Daily WA, Higgens CE. 1973. Preservation and storage of microorganisms in the gas phase of liquid nitrogen. *Cryobiol* 10:364–367.
167. Takano M, Sado JI, Ogawa T, Terui G. 1973. Freezing and freeze-drying of *Spirulina platensis*. *Cryobiol* 10:440–444.
168. Zhao G, Zhang G. 2005. Effect of protective agents, freezing temperature, rehydration media on viability of malolactic bacteria subjected to freeze-drying. *J Appl Microbiol* 99:333–338.
169. Zea L, Nisar Z, Rubin P, Cortesão M, Luo J, McBride SA, Moeller R, Klaus D, Müller D, Varanasi KK, Muecklich F, Stodieck L. 2018. Design of a spaceflight biofilm experiment. *Acta Astronaut* 148:294–300.

170. Martin DW, Schurr MJ, Mudd MH, Govan JR, Holloway BW, Deretic V. 1993. Mechanism of conversion to mucoidy in *Pseudomonas aeruginosa* infecting cystic fibrosis patients. *Proc Natl Acad Sci USA* 90:8377–8381.
171. Wozniak DJ, Wyckoff TJO, Starkey M, Keyser R, Azadi P, O’Toole GA, Parsek MR. 2003. Alginate is not a significant component of the extracellular polysaccharide matrix of PA14 and PAO1 *Pseudomonas aeruginosa* biofilms. *Proc Natl Acad Sci USA* 100:7907–7912.
172. Friedman L, Kolter R. 2003. Genes involved in matrix formation in *Pseudomonas aeruginosa* PA14 biofilms. *Mol Microbiol* 51:675–690.
173. Jennings LK, Storek KM, Ledvina HE, Coulon C, Marmont LS, Sadovskaya I, Secor PR, Tseng BS, Scian M, Filloux A, Wozniak DJ, Howell PL, Parsek MR. 2015. Pel is a cationic exopolysaccharide that cross-links extracellular DNA in the *Pseudomonas aeruginosa* biofilm matrix. *Proc Natl Acad Sci USA* 112:11353–11358.
174. Colvin KM, Irie Y, Tart CS, Urbano R, Whitney JC, Ryder C, Howell PL, Wozniak DJ, Parsek MR. 2012. The Pel and Psl polysaccharides provide *Pseudomonas aeruginosa* structural redundancy within the biofilm matrix. *Env Microbiol* 14:1913–1928.
175. Jackson KD, Starkey M, Kremer S, Parsek MR, Wozniak DJ. 2004. Identification of *psl*, a locus encoding a potential exopolysaccharide that is essential for *Pseudomonas aeruginosa* PAO1 biofilm formation. *J Bacteriol* 186:4466–4475.

176. Friedman L, Kolter R. 2004. Two genetic loci produce distinct carbohydrate-rich structural components of the *Pseudomonas aeruginosa* biofilm matrix. *J Bacteriol* 186:4457–4465.
177. Ma L, Lu H, Sprinkle A, Parsek MR, Wozniak DJ. 2007. *Pseudomonas aeruginosa* Psl is a galactose- and mannose-rich exopolysaccharide. *J Bacteriol* 189:8353–8356.
178. Ma L, Jackson KD, Landry RM, Parsek MR, Wozniak DJ. 2006. Analysis of *Pseudomonas aeruginosa* conditional Psl variants reveals roles for the Psl polysaccharide in adhesion and maintaining biofilm structure postattachment. *J Bacteriol* 188:8213–8221.
179. Jones CJ, Wozniak DJ. 2017. Psl produced by mucoid *Pseudomonas aeruginosa* contributes to the establishment of biofilms and immune evasion. *MBio* 8.
180. Strathmann M, Wingender J, Flemming HC. 2002. Application of fluorescently labelled lectins for the visualization and biochemical characterization of polysaccharides in biofilms of *Pseudomonas aeruginosa*. *J Microbiol Methods* 50:237–248.
181. Beloin C, Roux A, Ghigo JM. 2008. *Escherichia coli* biofilms. *Curr Top Microbiol Immunol* 322:249–89.
182. Zogaj X, Nimtz M, Rohde M, Bokranz W, Romling U. 2001. The multicellular morphotypes of *Salmonella Typhimurium* and *Escherichia coli* produce cellulose as the second component of the extracellular matrix. *Mol Microbiol* 39:1452–1463.

183. Wang X, Preston JF, Romeo T. 2004. The pgaABCD locus of *Escherichia coli* promotes the synthesis of a polysaccharide adhesin required for biofilm formation. *J Bacteriol* 186:2724–2734.
184. Stevenson G, Andrianopoulos K, Hobbs M, Reeves PR. 1996. Organization of the *Escherichia coli* K-12 gene cluster responsible for production of the extracellular polysaccharide colanic acid. *J Bacteriol* 178:4885–4893.
185. Serra DO, Richter AM, Hengge R. 2013. Cellulose as an architectural element in spatially structured *Escherichia coli* biofilms. *J Bacteriol* 195:5540–5554.
186. Prigent-Combaret C, Vidal O, Dorel C, Lejeune P. 1999. Abiotic surface sensing and biofilm-dependent regulation of gene expression in *Escherichia coli*. *J Bacteriol* 181:5993–6002.
187. Danese PN, Pratt LA, Kolter R. 2000. Exopolysaccharide production is required for development of *Escherichia coli* K-12 biofilm architecture. *J Bacteriol* 182:3593–3596.
188. Hanna A, Berg M, Stout V, Razatos A. 2003. Role of capsular colanic acid in adhesion of uropathogenic *Escherichia coli*. *Appl Env Microbiol* 69:4474–4481.
189. Ophir T, Gutnick DL. 1994. A role for exopolysaccharides in the protection of microorganisms from desiccation. *Appl Env Microbiol* 60:740–745.
190. Sledjeski DD, Gottesman S. 1996. Osmotic shock induction of capsule synthesis in *Escherichia coli* K-12. *J Bacteriol* 178:1204–1206.
191. Hughes J, McCully ME. 1975. The use of an optical brightener in the study of plant structure. *Stain Technol* 50:319–329.

192. Schneider CA, Rasband WS. 2012. NIH Image to ImageJ: 25 years of image analysis. *Nat Methods* 9:671–675.
193. Schindelin J, Arganda-Carreras I, Frise E, Kaynig V, Longair M, Pietzsch T, Preibisch S, Rueden C, Saalfeld S, Schmid B, Tinevez JY, White DJ, Hartenstein V, Eliceiri K, Tomancak P, Cardona A. 2012. Fiji: an open-source platform for biological-image analysis. *Nat Methods* 9:676–82.
194. Schmid B, Schindelin J, Cardona A, Longair M, Heisenberg M. 2010. A high-level 3D visualization API for Java and ImageJ. *BMC Bioinformatics* 11:274.
195. R Core Team. 2020. R: A language and environment for statistical computing. 3.5.1. R Foundation for Statistical Computing, Vienna, Austria.
196. RStudio Team. 2020. RStudio: Integrated Development for R. 1.2.1335. RStudio PBC, Boston, MA.
197. Wickham H, François R, Henry L, Müller K. 2018. dplyr: A grammar of data manipulation. R package version 0.7.6.
198. Wickham H. 2018. scales: Scale functions for visualization. R package version 1.0.0.
199. Robinson D, Hayes A. 2019. broom: Convert statistical analysis objects into tidy tibbles. R package version 0.5.2.
200. Wickham H. 2016. ggplot2: Elegant graphics for data analysis. Springer-Verlag New York.
201. Wickham H. 2007. Reshaping data with the reshape package. *J Stat Softw* 21:1–20.

202. Wickham H, Henry L. 2018. tidy: Easily tidy data with “spread()” and “gather()” functions. R package version 0.8.1.
203. Augue B. 2017. gridExtra: Miscellaneous functions for “Grid” graphics. R package version 2.3.
204. Lemon J. 2006. Plotrix: a package in the red light district of R. R-News 6:8–12.
205. Lewis K. 2010. Persister cells. *Annu Rev Microbiol* 64:357–372.
206. Mah TFC, O’Toole GA. 2001. Mechanisms of biofilm resistance to antimicrobial agents. *Trends Microbiol* 9:34–39.
207. Bridier A, Briandet R, Thomas V, Dubois-Brissonnet F. 2011. Resistance of bacterial biofilms to disinfectants: a review. *Biofouling* 27:1017–1032.
208. Fux CA, Costerton JW, Stewart PS, Stoodley P. 2005. Survival strategies of infectious biofilms. *Trends Microbiol* 13:34–40.
209. Hall CW, Mah TF. 2017. Molecular mechanisms of biofilm-based antibiotic resistance and tolerance in pathogenic bacteria. *FEMS Microbiol Rev* 41:276–301.
210. Yan J, Bassler BL. 2019. Surviving as a community: antibiotic tolerance and persistence in bacterial biofilms. *Cell Host Microbe* 26:15–21.
211. Petrova OE, Sauer K. 2016. Escaping the biofilm in more than one way: desorption, detachment or dispersion. *Curr Opin Microbiol* 30:67–78.
212. Boltz JP, Smets BF, Rittmann BE, van Loosdrecht MCM, Morgenroth E, Daigger GT. 2017. From biofilm ecology to reactors: a focused review. *Water Sci Technol* 75:1753–1760.
213. Simões M, Simões LC, Vieira MJ. 2010. A review of current and emergent biofilm control strategies. *LWT - Food Sci Technol* 43:573–583.

214. Birmele MN, McCoy LE, Roberts MS. 2011. Disinfection of spacecraft potable water systems by passivation with ionic silver, p. 1–8. *In* 41st International Conference of Environmental Systems. Portland, OR, USA.
215. Silvestry-Rodriguez N, Bright KR, Slack DC, Uhlmann DR, Gerba CP. 2008. Silver as a residual disinfectant to prevent biofilm formation in water distribution Systems. *Appl Env Microbiol* 74:1639–1641.
216. Budeli P, Moropeng RC, Mpenyana-Monyatsi L, Momba MNB. 2018. Inhibition of biofilm formation on the surface of water storage containers using biosand zeolite silver-impregnated clay granular and silver impregnated porous pot filtration systems. *PLoS One* 13:e0194715.
217. Kalishwaralal K, BarathManiKanth S, Pandian SRK, Deepak V, Gurunathan S. 2010. Silver nanoparticles impede the biofilm formation by *Pseudomonas aeruginosa* and *Staphylococcus epidermidis*. *Colloids Surf B* 79:340–344.
218. Wu J, Li F, Hu X, Lu J, Sun X, Gao J, Ling D. 2019. Responsive assembly of silver nanoclusters with a biofilm locally amplified bactericidal effect to enhance treatments against multi-drug-resistant bacterial infections. *ACS Cent Sci* 5:1366–1376.
219. Randall CP, Gupta A, Jackson N, Busse D, O’Neill AJ. 2015. Silver resistance in Gram-negative bacteria: a dissection of endogenous and exogenous mechanisms. *J Antimicrob Chemother* 70:1037–1046.
220. Law J, Cole R, Young MH, Mason S. 2016. NASA astronaut urinary conditions associated with spaceflight, p. JSC-CN-24668. *In* Annual Scientific Meeting of the Aerospace Medical Association.

221. Jones JA, Jennings R, Pietryzk R, Ciftcioglu N, Stepaniak P. 2005. Genitourinary issues during spaceflight: A review. *Int J Impot Res* 17:S64–S67.
222. Martin NL, Beveridge TJ. 1986. Gentamicin interaction with *Pseudomonas aeruginosa* cell envelope. *Antimicrob Agents Chemother* 29:1079–1087.
223. Hunt SM, Werner EM, Huang B, Hamilton MA, Stewart PS. 2004. Hypothesis for the role of nutrient starvation in biofilm detachment. *Appl Env Microbiol* 70:7418–7425.
224. Yoon MY, Lee KM, Park Y, Yoon SS. 2011. Contribution of cell elongation to the biofilm formation of *Pseudomonas aeruginosa* during anaerobic respiration. *PLoS One* 6:e16105.
225. Hassan HM, Fridovich I. 1980. Mechanism of the antibiotic action pyocyanine. *J Bacteriol* 141:156–63.
226. Adhikary NRD. 2011. Long term co-culture in *Escherichia coli* and *Pseudomonas aeruginosa*. Texas State University.
227. Liu Y, Li J. 2008. Role of *Pseudomonas aeruginosa* biofilm in the initial adhesion, growth and detachment of *Escherichia coli* in porous media. *Env Sci Technol* 42:443–449.
228. Ma Q, Zhang G, Wood TK. 2011. *Escherichia coli* BdcA controls biofilm dispersal in *Pseudomonas aeruginosa* and *Rhizobium meliloti*. *BMC Res Notes* 4:447.

229. Gómez Gómez JM, Medina J, Hochberg D, Mateo-Martí E, Martínez-Frías J, Rull F. 2014. Drying bacterial biosaline patterns capable of vital reanimation upon rehydration: Novel hibernating biomineralogical life formations. *Astrobiol* 14:589–602.
230. Koch GHEA. Corrosion cost and prevention strategies in the United States. CC Technol NACE Int Coop with U S Dep Transp Fed Highw Adm.
231. Li H, Zhou E, Zhang D, Xu D, Xia J, Yang C, Feng H, Jiang Z, Li X, Gu T, Yang K. 2016. Microbiologically influenced corrosion of 2707 hyper-duplex stainless steel by marine *Pseudomonas aeruginosa* biofilm. *Sci Rep* 6:20190.
232. Videla HA, Herrera LK. 2005. Microbiologically influenced corrosion: looking to the future. *Int Microbiol* 8:169–180.
233. İlhan-Sungur E, Cansever N, Cotuk A. 2007. Microbial corrosion of galvanized steel by a freshwater strain of sulphate reducing bacteria (*Desulfovibrio* sp.). *Corros Sci* 49:1097–1109.
234. Inaba Y, West AC, Banta S. 2020. Enhanced microbial corrosion of stainless steel by *Acidithiobacillus ferrooxidans* through the manipulation of substrate oxidation and overexpression of *rus*. *Biotechnol Bioeng* bit.27509.
235. Zhang P, Xu D, Li Y, Yang K, Gu T. 2015. Electron mediators accelerate the microbiologically influenced corrosion of 304 stainless steel by the *Desulfovibrio vulgaris* biofilm. *Bioelectrochemistry* 101:14–21.
236. Obenhuber DC, Rodgers EB, L HT. 1991. Microbial Biofilm Studies of the Environmental Control and Life Support System Water Recovery Test for Space Station Freedom. *SAE Trans* 100:888–892.

237. Roman MC, Weir NE, Wilson ME, Pyle BH. 2006. Microbial characterization of Internal Active Thermal Control System (IATCS) hardware surfaces after five years of operation in the International Space Station. *SAE Trans* 115:369–402.
238. Gu JD. 2007. Microbial colonization of polymeric materials for space applications and mechanisms of biodeterioration: A review. *Int Biodeterior Biodegrad* 59:170–179.
239. Gu JD, Roman M, Esselman T, Mitchell R. 1998. The role of microbial biofilms in deterioration of space station candidate materials. *Int Biodeterior Biodegrad* 41:25–33.
240. Alekhova TA, Aleksandrova AA, Novozhilova TI, Lysak L V, Zagustina NA, Bezborodov AM. [Monitoring of microbial degraders in manned space stations]. *Prikl Biokhim Mikrobiol* 41:435–43.
241. Kajer W, Krauze A, Walke W, Marciniak J. 2008. Corrosion behavior of AISI 316L steel in artificial body fluids. *J Achiev Mater Manuf Eng* 31:247–253.
242. Gupta S, Anand S. 2018. Induction of pitting corrosion on stainless steel (grades 304 and 316) used in dairy industry by biofilms of common sporeformers. *Int J Dairy Technol* 71:519–531.
243. Li K, Whitfield M, Van Vliet KJ. 2013. Beating the bugs: roles of microbial biofilms in corrosion. *Corros Rev* 31:73–84.
244. Nagalakshmi R, Nagarajan L, Rathish RJ, Prabha SS, Vijaya N, Jeyasundari J, Ragendran S. 2014. Corrosion resistance of SS316L in artificial urine in presence of D-glucose. *Int J Nano Corr Sci Eng* 1:39–49.

245. Rhouma AB, Braham C, Fitzpatrick ME, Leidion J, Sidhom H. 2001. Effects of surface preparation on pitting resistance, residual stress, and stress corrosion cracking in austenitic stainless steels. *J Mat Eng Perform* 10:507–514.
246. Revie RW, Uhlig HH. 2008. *Corrosion and corrosion control*. Fourth Edi. John Wiley & Sons, Hoboken, NJ.
247. Wang ZB, Hu HX, Zheng YG. 2018. Synergistic effects of fluoride and chloride on general corrosion behavior of AISI 316 stainless steel and pure titanium in H₂SO₄ solutions. *Corr Sci* 130:203–217.
248. Jia R, Yang D, Xu J, Xu D, Gu T. 2017. Microbiologically influenced corrosion of C1018 carbon steel by nitrate reducing *Pseudomonas aeruginosa* biofilm under organic carbon starvation. *Corros Sci* 127:1–9.
249. Nan L, Xu D, Gu T, Song X, Yang K. 2015. Microbiological influenced corrosion resistance characteristics of a 304L-Cu stainless steel against *Escherichia coli*. *Mater Sci Eng C* 48:228–234.